Impact of the Agulhas Current on storm development

Jason O'Connor

Supervisor: Prof. Mathieu Rouault

University of Cape Town

Faculty of Science

Department of Oceanography

SEA5012W Applied Ocean Sciences Minor Dissertation (M.Sc.)

February 2020

Acknowledgements

- I would like to thank my supervisor, Prof. Mathieu Rouault, for his continued support and guidance throughout my time completing this project. I greatly appreciate his assistance with helping me choose a topic as well as with the editing of the final submission. I would also like to thank him for organising and managing my bursary for this year.
- I would like to thank Arielle Nkwinkwa Njouodo for her assistance in providing me with the model output data as well as helping me with MATLAB. I greatly appreciate her wisdom and availability to my numerous queries.
- I would like to thank the Nansen-Tutu Institute for providing me with the funding for this study
- I would like to thank John Field for helping me with the editing of my final draft
- I would like to thank Ramontsheng Rapolaki for his assistance with MATLAB
- I would like to thank my fellow Master's classmates for their continued support throughout the year
- Lastly, I would like to thank my family for believing that I could finish this thesis on time

ABSTRACT

A high-resolution atmospheric model (WRF) is used to investigate the impact of the Agulhas Current on synoptic storm development. A sensitivity experiment is conducted to analyse the influence of the Agulhas Current's sea surface temperature (SST) on rain producing, synoptic scale weather features. Two model configurations: Control (CTL) and Smooth (SMTH) are analysed to understand the effect of the Agulhas Current's SST and high latent heat fluxes on storms that develop or track over the Current. The two configurations are identical except that the SMTH simulation has the SST signature of the Agulhas reduced by smoothing out the strong SST gradients associated with the Current. This results in the Agulhas Current core having SSTs reduced by roughly 1.5°C in the SMTH configuration. Consequently, lower (100 – 150 $W.m^{-2}$) latent heat fluxes are also simulated at the Current core's location in the SMTH run. Using daily South Africa Weather Service synoptic charts from 2001 – 2005, when the model output is available, two hundred (200) synoptic scale storms are found to track over the Current. Using the TRMM 3B42 3-hourly 0.25 x 0.25° precipitation rain rate product, 70 (of the 200) are found to have produced rainfall. Five model variables are used as proxies for the storm intensity of these 70 storms. Ten storms are found to show storm intensification when passing over the Current. In the CTL simulation, of these ten storms, ten show lower 850mb geopotential heights (m), nine show higher surface wind speeds ($m.s^{-1}$), seven show higher rain rates ($mm.hr^{-1}$), eight show higher Eddy Kinetic Energy (EKE) ($m^2.s^{-2}$) and nine show greater upward moisture flux at the surface ($g.m^{-2}.s^{-1}$) compared to the SMTH run once each storm has propagated over the Current. Model output analysis shows sustained or dissipating storm intensity of the other 60 storms while passing over the Current. Nonetheless, these results provide a strong case for the influence of the Agulhas Current on the intensification of synoptic scale, rain producing events.

Table of Contents

Chapter 1: Introduction

1.1 Research outline

Much of the current available research done on the impact of the Agulhas Current on the overlying atmosphere has focused on either wind changes (Rouault et al. 2016; Chelton & Xie 2010), rainfall (Rouault et al. 2013; Jury et al. 1993; Nkwinkwa Njoiodo et al. 2018) or modifications to the atmospheric boundary layer (Jury et al. 1997; Jury & Walker 1998; Rouault et al. 2000; O'Neill et al. 2005). Only one study (Rouault et al. 2002) has been dedicated to investigating the evolution of a specific weather event and how the Agulhas Current could have impacted that storm. This study aims to contribute to the observations already made on the impact of Agulhas Current by investigating multiple storm events.

As the strongest Western Boundary Current (WBC) in the Southern Hemisphere (Stramma & Lutjeharms 1997), the Agulhas Current plays a pivotal role in the climate system of Southern Africa by transporting heat poleward and releasing it into the atmosphere. Observations made during the Agulhas Current Air-Sea Exchange Experiment found increases in sensible and latent heat at the locations corresponding to an increase in sea temperature (Rouault et. al 1995). Latent heat losses from WBCs have been observed to be much larger during extreme weather events. Latent heat fluxes up to 1000 $W.m^{-2}$ during a storm passage across the Gulf Stream (Xue et. al 1995) and 500 $W.m^{-2}$ over an Agulhas eddy (Rouault & Lutjeharms 2000) have been recorded.

Rouault et al. (2002) has stated that " … many of the rain-producing weather systems over southern South Africa track across these strong SST gradients, it is likely that the existence of this current may play a significant role in regional weather and climate" (Rouault et al. 2002, pp. 655). Reason (2001) also informs us that " … South Africa is relatively prone to large-scale devastating flood and drought events and has a significant rural population dependent on subsistence agriculture, there is great local interest in better understanding of this rainfall variability" (Reason 2001, pp. 2770). These two points of concern serve as the main motivation for this study.

1.2 Basic overview of the Agulhas System

The Agulhas Current transports 73 Sv (1 Sv = 10^6m³.s^{-1}) of warm tropical water into the Southern Hemisphere mid-latitudes along the southeast coast of Africa (Beal & Bryden 1999; Stramma & Lutjeharms 1997). It receives most of its water from a large recirculation gyre in the South-West Indian Ocean that extends towards 60°S (Tyson & Preston-Whyte 2000). Found to extend to roughly 1000m deep, the Current flows closely to the continental shelf until the latitude of Port Elizabeth (34°S) whereby the shelf widens to form the Agulhas bank therefore taking the Current further away from the coast (Lutjeharms 1981). Further south, the Current retroflects back into the mid-latitude South Indian Ocean as the Agulhas Return Current (ARC) (Lutjeharms & van Ballegooyen 1988). Unlike its Northern Hemisphere WBC counterparts, the Agulhas Current experiences little interannual variability with few seasonal perturbations along its track (Rouault & Penven 2011). Figure 1.1 gives a basic view of the Agulhas Current and its oceanography. This study however will focus only on the part of the Agulhas Current found between approximately 20 - 40°S and 20 - 40°E. In other words, this study excludes the retroflection and Agulhas Return Current regions.

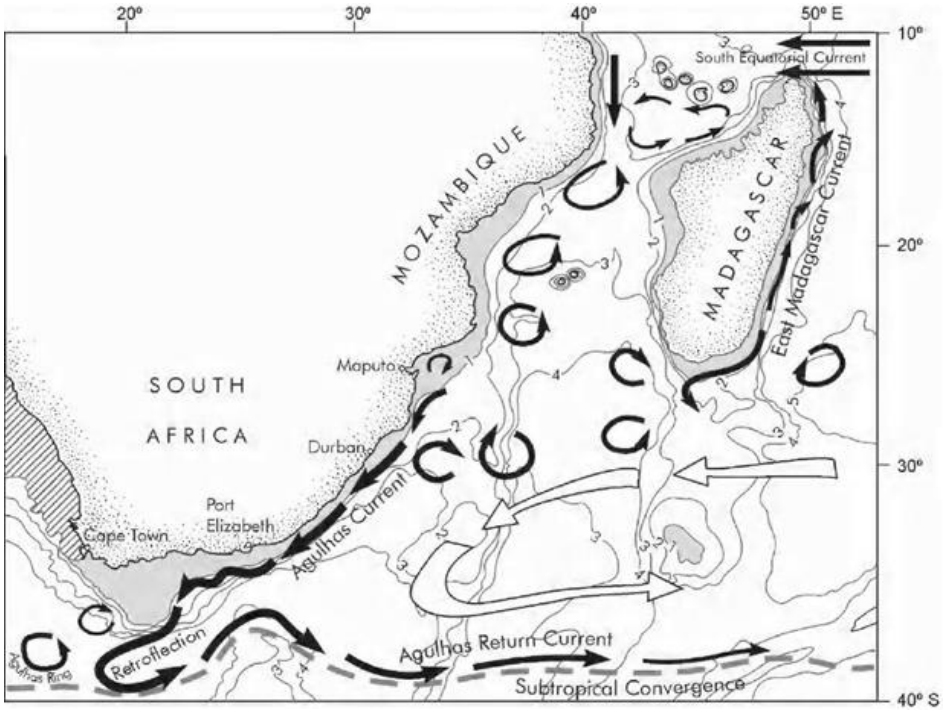

Figure 1.1: Greater Agulhas System and its connection to the Indian Ocean. Shaded areas indicate 200m bathymetry. Bathymetry contour intervals every 1km.

The Agulhas Current is approximately 90 – 100 km wide, with the core of the Current being situated 20 km offshore at the surface moving further offshore with increasing depth (Beal & Bryden 1999). Local upwelling mechanisms allow for an intrusion of cold water from depths of around 200 – 600 m allowing for extreme horizontal sea surface temperature (SST) gradients of about 10°C.40 km^{-1} to occur (Rouault et al. 1995). Similar strong SST gradients are found in the North Pacific (Kuroshio Current) and the North Atlantic (Gulf Stream).

Large heat fluxes are common features of WBCs due to large air-sea temperature differences. During ACASEX (Agulhas Air-Sea Exchange Experiment) in 1995, it was found that latent heat fluxes increase fivefold (to 270 $W.m^{-2}$) over the Agulhas compared to the surrounding waters (160 $W.m^{-2}$ at the seaward border and 40 $W.m^{-2}$ over the cool shelf waters). An increase in wind speed, wind stress, sensible and latent heat flux as well as a negative stability parameter were all found at the location of an increase in sea temperature (Rouault et al. 1995; Lee-Thorp et al. 1999). Lee-Thorp et al. (1999) found that latent heat makes up the majority (80 – 90%) of the total surface heat flux over the Current and thus indicates a substantial injection of moisture into the overlying atmosphere. This coincides with observations made during ACASEX (Rouault et al. 1995) and Lutjeharms et al. (1986) of semi-permanent clouds anchored over the Current during fair-weather conditions.

Modification to the Marine Boundary Layer (MBL) is another key characteristic associated with sharp SST gradients. Both Jury & Walker (1988) and Rouault et al. (1995) found an increase of 400m of the height of the MBL over the Current. These results are attributed to the significant increase in sensible and latent fluxes over the Current that consequently result in vigorous convective mixing. Rouault et al. (2002) has suggested that these high latent heat fluxes may lead to increased onshore advection of low-level moisture which in turn could significantly impact storm evolution. Jury et al. (1997) found surface heat fluxes of magnitude 100 $W.m^{-2}.km^{-1}$ across a transition zone of part of the South African coastline.

In order to place the storms this study will investigate into context, the typical weather experienced along South Africa's east coast needs to be detailed. South Africa experiences a subtropical climate which is also impacted by tropical and temperate rain-bearing weather systems (Tyson & Preston-White 2000). The country is influenced by the South Atlantic High Pressure system to the west and the South Indian High Pressure system to the east and during summer a heat low dominates the interior. Rainfall along the east coast is enhanced by the

presence of the Agulhas Current as coastal summer rainfall averages around 100 mm.month^{-1} with westerly waves, ridging highs, tropical temperature troughs and east coast lows accounting for 80% of the rainfall that occurs along the coastline boarding the Current (Preston-White & Tyson 1988).

1.3 Gulf Stream and Kuroshio Current

Much of current literature on WBCs has focused on the two Northern Hemisphere currents namely the Kuroshio Extension (Xu et al. 2011; Xu et al. 2010; Kelly et al. 2010) in the North Pacific and the Gulf Stream (Kelly et al. 2010; Minobe et al. 2008; Parfitt & Czaja 2016; Parfitt et al. 2016; Sheldon et al. 2017; Vanniere et al. 2017; Chelton & Xie 2010) in the North Atlantic. However, few studies have studied the effect of the Agulhas Current on climate and local weather. Nonetheless, understanding how these Northern Hemisphere WBCs alter their overlying atmosphere is crucial when examining the Agulhas Current.

One of the main findings by Kelly et al. (2010) was that both the Gulf Stream and the Kuroshio current "… have large impacts on the local and regional structures of the marine boundary layer and on the lower atmosphere" and that " … WBCs intensify cyclogenesis and anchor storm-track locations." (Kelly et al. 2010; pp. 5664). The study also put forward a recommendation (for future studies) by posing the question: "Is preconditioning by the WBCs a critical factor in storm intensification?" (pp. 5664). This also serves as one of the motivations for this study.

Minobe et al. (2008) concluded that " … the Gulf Stream affects the entire troposphere" and that " … upward motion and cloud formation extend into the upper troposphere … " (pp. 1). In addition, Sheldon et al. (2017) concluded that the warm section of the Gulf Stream creates a conducive environment for increased vertical motion in cyclones. The extreme heat fluxes measured over the Gulf Stream have been attributed to the relatively colder and drier continental air masses moving offshore creating large air-sea temperature differences (Kelly et. al 2010). Although Josey et. al (1999) has measured lower (100 – 150 W.m^{-2}) climatological latent heat fluxes over the Agulhas Current compared to the Gulf Stream and Kuroshio

Current, the Agulhas Current experiences less seasonal variability in its heat losses to the overlying atmosphere.

Meanwhile, Parfitt et al. (2016), who conducted a similar model experiment preformed in this study, found increased (± 30 %) atmospheric frontal frequency in their control experiment, with the cold frontal response being the majority contributor. The strengthening of the cold fronts was attributed to the greater cross-frontal surface sensible heat flux gradient associated with the control experiment (Parfitt et al. 2016). In a similar study done by Vanniere et al. (2017), it was found that on the warm edge of the front for their control configuration, " … shallow convection develops earlier and the amount of convective rain increases". Finally, this study showed that over the warm ocean, the lower troposphere is vertically well mixed due to the surface turbulent fluxes forcing moist convection (Vanniere et al. 2017).

Very similar results were found by studies focusing on the Kuroshio Current in the North Pacific. Xu et al. (2011), using the same atmospheric model with similar configurations. A clear SST – surface wind speed relationship with high (low) speeds observed over the warm (cold) sections of the Kuroshio Extension were found. Deep convection, enhanced convective precipitation, increased cloud tops and frequent cumulus convection were all observed over the warm tongue as well as wind convergence (Xu et al. 2011). Similar to the Gulf Stream, the anchoring of a narrow rain band due to enhanced upward heat fluxes and convective instability found in the lower atmosphere were also observed.

A related study focusing on a cool water pool associated with a large Kuroshio meander done by Xu et al. (2010), found comparable results. Over the cool section, local reductions in wind speeds, cloud liquid water (CLW) and precipitation were all observed and are suggested to be linked to the large meander-induced SST cooling. Both Xu et al. (2010) and Xu et al. (2011) found a positive SST – wind speed correlation and thus concluded that the ocean was forcing the atmosphere. However, Chelton & Xie (2010) do add however that surface wind stress associated with SST-induced perturbations can feed back into the ocean via wind-driven upwelling and upper-ocean mixing.

Similarities and differences between the Gulf Stream and Kuroshio Current are summarised in Kelly et al. (2010). The two most important conclusions from this study is that 1) both currents intensity cyclogenesis and anchor storm tracks and 2) both have large impacts on

local weather and the MBL. Sharp SST fronts associated with these WBCs enhance low-level baroclinicity and thus are likely to impact synoptic scale weather activity. Kelly et. al. (2010) did however recognise the bias of using SST anomalies in climate studies as Sutton & Mathieu (2002) have argued that SST is more a result of ocean-atmosphere interaction rather than ocean dynamics.

1.4 This study

This study makes use of the Advanced Research version of the Weather Research and Forecast model (WRF-ARW) to run two simulations: Control (CNTL) and Smooth (SMTH) whereby the latter has the signature of the Agulhas Current reduced. In other words, the CNTL simulation has the observed SST gradient whereas the SMTH simulation has this sharp gradient reduced. By taking the difference *(CTL – SMTH)* between the two configurations, the impact of the Agulhas Current on atmospheric variables can be studied. Five atmospheric variables are used as proxies for storm intensity. The 850mb geopotential height (m), surface wind ($m.s^{-1}$), surface rain rate ($mm.hr^{-1}$), eddy kinetic energy (EKE) up to the 850mb level ($m^2.s^{-2}$) and turbulent moisture flux at the surface ($g.m^{-2}.s^{-1}$) are the five variables used. Each individual storm event is analysed individually by examining the evolution of these atmospheric variables in the two simulations.

This study has two main objectives: 1) to analyse the evolution of specific storm events over the Agulhas Current and 2) to quantify the effect of the Current on the atmospheric variables listed above. This research aims will provide greater insight into how the intensity of surface low pressure systems changes over a specific region of the Agulhas region as well as attempting to measure the influence this warm ocean region has on the atmospheric above it with regards to such weather events.

Following this, chapter 2 will detail the data used and methods followed in this report. Chapter 3 will show the results of the WRF model analysis of the ten intensifying storms identified in the WRF model output. The influence of the Agulhas Current will also be quantified in chapter 3. In chapter 4, these results as well as the developed storm statistics will be discussed. Finally, chapter 5 will outline the main conclusions of this study.

Chapter 2: Data and Methods

2.1 Weather Research and Forecast Model

The Advanced Research version of the Weather Research and Forecast model (WRF-ARW) version 3.7.1 (Skamarock & Klemp 2008) was used in this study to explore the impact the Agulhas Current has on storm development. WRF is arguably the most popular (± 36000 registrations) atmospheric model due to it being provided without cost, restrictions on modifications or copyright encumbrance (Powers et al. 2017). Previous papers such as Rouault et al. (2003) have stated the need for high resolution models in order to accurately capture the sharp SST gradients associated with WBCs. It is said that at least a 25 km spatial resolution would be required to properly resolve the steep SST fronts between the Agulhas and surrounding waters as well as the associated surface heat fluxes. Nkwinkwa Njouodo et al. (2018) made use of the same model to explore coastal rainfall on South Africa's east coast.

Developed by the National Centre for Atmospheric Research (NCAR), WRF is a non-hydrostatic, fully compressible, sigma coordinate model operating on a Arakawa-C grid (Skamarock et al. 2005). WRF is freely available and has numerous applications. From conducting idealised simulations to running as a global atmospheric model, the WRF model provides special capabilities to various Earth system prediction applications (i.e. hydrology or air chemistry) (Powers et al. 2017). Data assimilation, parameterisation research and real-time numerical weather prediction are just some of the functions WRF is designed to achieve (Skamarock et al. 2008).

Model Specifications

The specifications set to the WRF model were as follows. Spatial resolution was 25 x 25 km^2 with 56 vertical eta-coordinate levels. The domain was set to 17- 43°S and 8- 52°E. Simulations were set to run from 1st December 2000 to 1st January 2006 with the first month dedicated to the spin-up period. Lateral boundary conditions were provided by 6-hourly ERA-Interim reanalysis data (0.75°, Simmons et al. 2007, Dee et al. 2011). Daily surface data was supplied by Optimum Interpolated Sea Surface Temperature (OISST, 0.25°x 0.25°, Reynolds et al.

2007). In order to avoid discontinuity between the model and the forcing data, a relaxation zone was applied to the first four lateral grid points. Temporal resolution of the output data is 3-hourly.

Model Physics

The WRF Single Moment (WSM) 6 class model was used for the microphysics scheme (Hong & Lim 2006) and the Yonsei University parameterisation for the Planetary Boundary Layer (Hong et al. 2006). The Rapid Radiative Transfer Model was employed to force the short and longwave radiation (Mlawer et al. 1997; Dudhia 1989). The 4-layer NOAH land surface model (Chen & Dudhia 2001) was applied as well as the Kain-Fritch scheme (Kain 2004) for the cumulus convection parameterisation.

2.2 Two model simulations

Two WRF model configurations were set up in this sensitivity experiment: Control (CTL) and Smooth (SMTH). Both are identical except that the latter has smoothed SST boundary conditions. In this configuration (SMTH), a spatial filter based on a 9-neighbour grid method allows for this smoothing. This involves each grid point receiving a weighted average of that grid point plus the surrounding 8 points. The centre point has a weighting of 1, whereas the points directly to the west, east, south and north receive a weight of 0.5. Corner points receive a weight of 0.3. All 9 points are then multiplied by their weights, summed and then divided by the total weight to acquire a smooth value (Nkwinkwa Njouodo et al. 2018).

This smoothing was applied to the proper Agulhas region (24 °- 37° S & 21° - 38° E) resulting in a lowering of the core SST by approximately 1.0 – 1.5°C and surrounding waters by 0.25 – 1.0°C in the SMTH configuration. The difference in SST between the two configurations remains virtually zero for the Retroflection and Return Current due to this smoothing method. However, due to this smoothing method, slightly warmer (0.5 - 1°C) SSTs were simulated for a small area of ocean near Port Elizabeth in the SMTH run *(Figure 2.2).*

An example of this smoothening technique is demonstrated below in Figure 2.1. In the CLT panel *(left),* the warm, narrow Agulhas core is simulated close to the South African east

coastline with its sharp SST gradients whereas in the SMTH panel *(right)* the core and sharp SST gradients are absent and instead a normal gradual latitudinal change in SST is simulated.

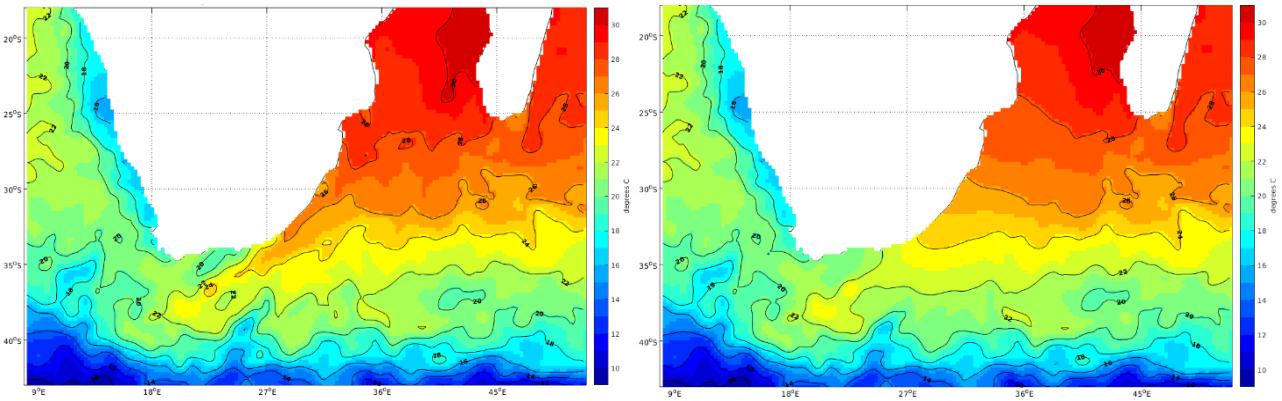

Figure 2.1: WRF model Sea Surface Temperature (SST) for *(left)* CNTL and *(right)* SMTH simulations for 12h00 UTC 11 April 2005. Measured in °C. Contour intervals given at 2°C starting at 9°C.

The difference between the CTL and SMTH runs is the main focus in the experiment. All plots showing the difference between the two configurations illustrate the effect the Agulhas Current. Figure 2.2 shows the area of Agulhas region where the smoothing method has resulted in warmer SSTs in the CTL simulation.

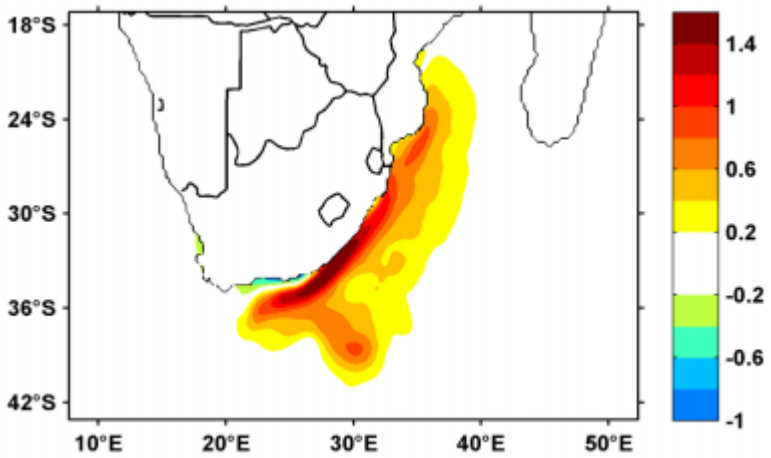

Figure 2.2*:* ~~Absolute~~ Difference between Control (CTL) and Smooth (SMTH) sea surface temperature WRF model simulations. Measured in °C. Warm (cold) colours indicate warmer (colder) SSTs in the CTL simulation.

As stated, Rouault et al. (1995) found that the latent heat flux over the Agulhas Current increases fivefold at the location of the east Agulhas Bank. As a result of the decrease in SST due to the smoothing method applied in the SMTH run, lower (150 – 100 $W.m^{-2}$) latent heat fluxes were modelled in this run. An example of this is shown in Figure 2.3. In the same region where the smoothing technique is applied, larger latent heat fluxes are simulated in the CTL configuration. Similar with the SST plots, the difference in latent heat flux remains virtually zero in the Retroflection and Return Current regions.

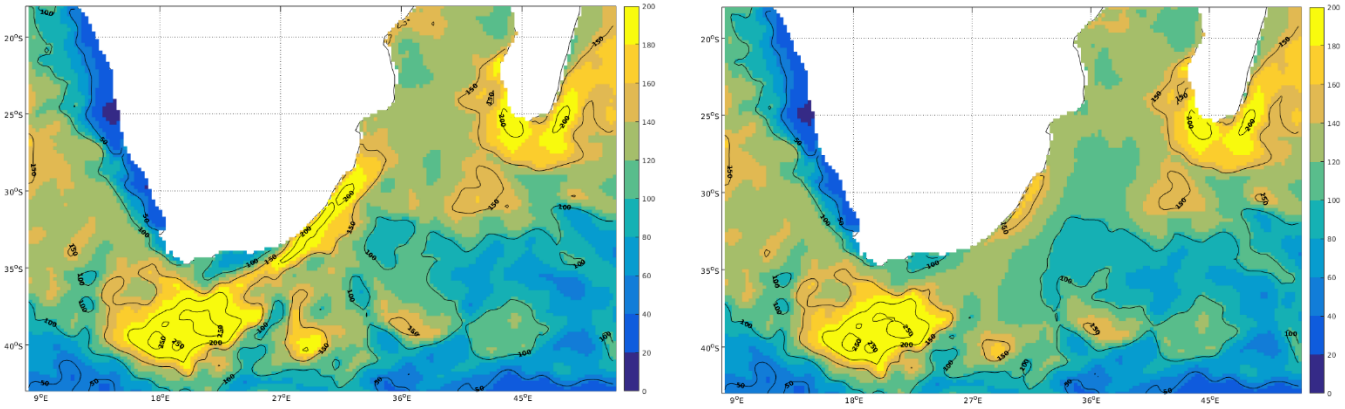

***Figure 2.3**:* March 2003 monthly average WRF model Latent Heat flux output for *(left)* CNTL and *(right)* SMTH simulations. Measured in $W.m^{-2}$. Contour intervals at 50 $W.m^{-2}$.

2.3 Storm Identification

The key focus of this study is exploring the evolution of storms over the Agulhas region. It was decided that a 'storm' would be defined as a synoptic scale, rain producing low pressure system. From 2001 to 2005, when model output is available every 3 hours, all storms propagating directly over or within the vicinity of the Agulhas Current were systematically identified. This was done using the South African Weather Service (SAWS) daily synoptic charts and the Tropical Rainfall Measuring Mission (TRMM) 3B42 v7 3 hourly precipitation reanalysis product. Once a list of the dates of these storms was complied, the WRF output for these dates was analysed.

SAWS daily weather charts

The first step in compiling a list of all the synoptic scale, rain producing low pressure systems moving over the Agulhas region involved the daily synoptic weather charts provided by the SAWS. All daily charts from 2001 to 2005 were examined. Any low pressure system, indicated by an 'L' on the chart, with at least one closed isobar that developed or moved over the Agulhas region had been selected. In this step, the 'Agulhas region' refers to the area of ocean with warmer SSTs in the CTL configuration (24 - 37° S & 21 - 38° E) *(Figure 2.2).* Two hundred (200) of these storm systems were found and their dates recorded.

An example of such method of identification is shown below in Figure 2.4. In this example, a low-pressure system existing over the western half of South Africa *(Top left)* moves eastward towards Port Elizabeth *(Top right)* and then offshore over the Agulhas region *(Bottom).*

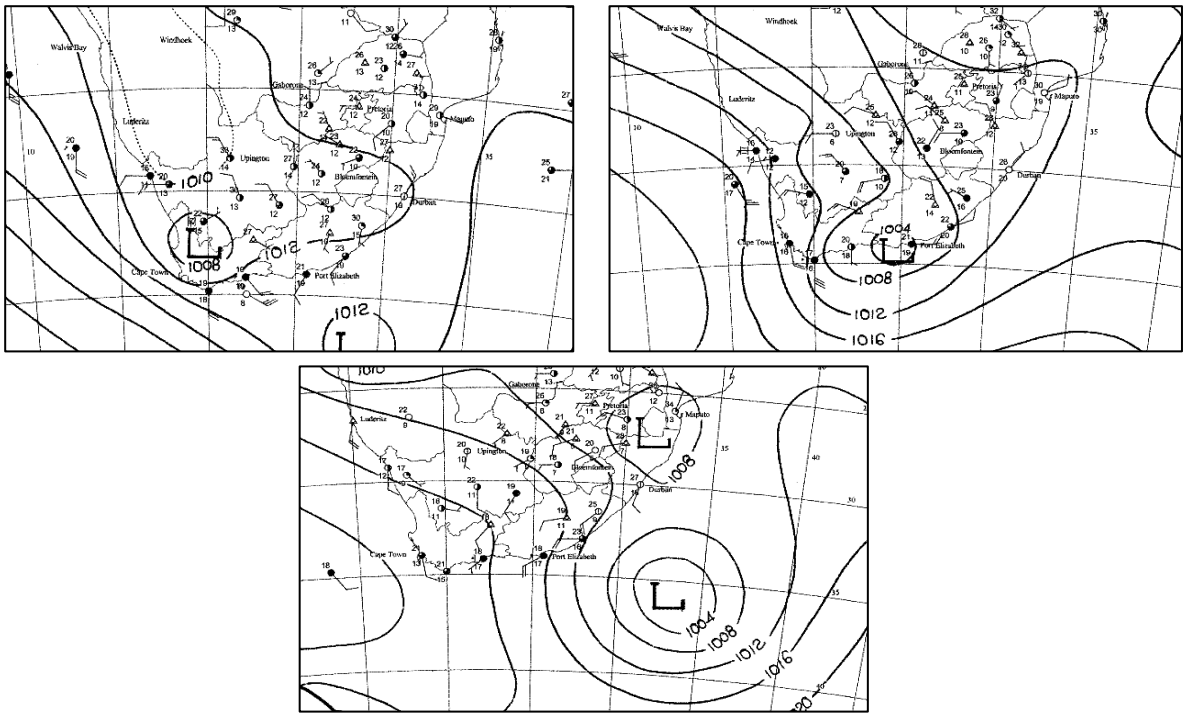

Figure 2.4*:* Synoptic surface conditions for *(Top left)* 10 April 2005, *(Top right)* 11 April 2005 and *(Bottom)* 12 April 2005. Charts are generated at 12h00 UTC.

TRMM 3B42 3 hourly precipitation reanalysis product

Once all the synoptic scale low pressure systems passing over the Agulhas region were identified, those that produced rainfall were selected. A high-resolution precipitation reanalysis product was used for this step. For 17 years (1997 – 2015) the TRMM satellite has

acquired valuable information relating to global tropical rainfall. The satellite had five onboard instruments, three of which were rainfall sensors (PR, TMI & VIRS). The Precipitation Radar (PR) was the first spaceborne radar instrument designed to measure rainfall and the reanalysis product used in this study is derived from this instrument (Huffman et al. 2012).

The TRMM dataset used in this study contains the output of the TRMM 3B42 algorithm, which is a 3-hourly merged rainfall product. The output is available on a 0.25 x 0.25° grid box every three hours. The output has four variables: high quality precipitation ($mm.hr^{-1}$), IR precipitation ($mm.hr^{-1}$), precipitation ($mm.hr^{-1}$) and relative error ($mm.hr^{-1}$) (Huffman et al 2012). Due to the swath gaps in the high-quality precipitation variable, the precipitation variable was used to determine which storms produced rain. This dataset can be access at: https://doi.org/10.5067/TRMM/TMPA/3H/7. The regions where rainfall was required to occur are the same regions enclosed by the outermost closed surface isobar of the identified synoptic low illustrated on the corresponding SAWS synoptic map. All 200 synoptic low-pressure systems were checked and 70 were found to have produced rainfall.

The product rainfall for the same dates and times (10 – 12 April 2005) as in Figure 2.4 are shown in Figure 2.5. The figure shows heavy rainfall over the southwest region of South Africa where the storm is centred on the 10th April *(Top left).* Rainfall can then be observed to move southeast offshore the next day *(Top right)* and then further out to sea *(Bottom).*

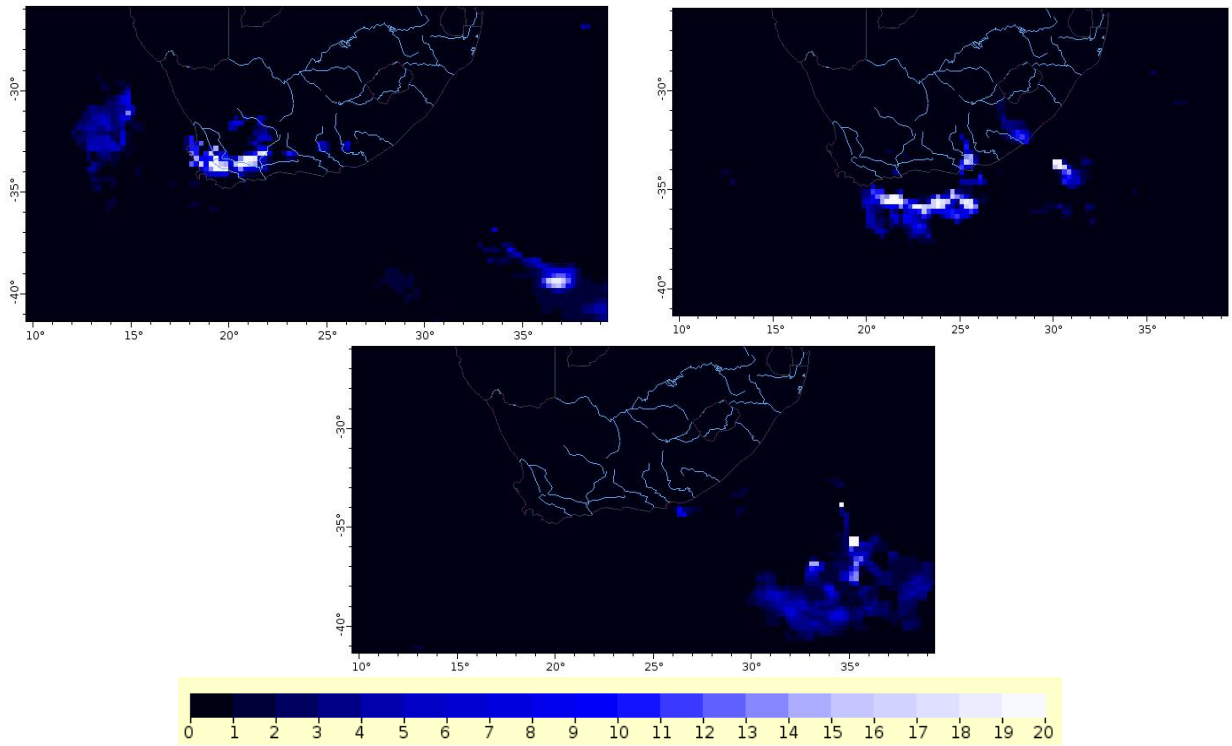

***Figure 2.5**:* TRMM PR 3B42 v7 3-hourly precipitation for *(Top left)* 10 Apr 2005, *(Top right)* 11 Apr 2005 and *(Bottom)* 12 Apr 2005. Rainfall is measured in mm.hr^{-1}. Maps were generated at 12h00 UTC.

WRF model analysis

After all the synoptic storms were checked with the TRMM precipitation product, the next step was to analyse these storms with the atmospheric model output *(WRF).* At this stage ~~we had~~ 70 synoptic scale, rain producing low pressure systems propagating over the Agulhas region from 2001 to 2005 had been identified. The study aimed to focus on the intensity of these storms and how that intensity changed once the storm moved over the Agulhas Current. The impact of the Agulhas Current on the atmospheric variables chosen was analysed by plotting the difference between the CTL and SMTH simulations.

The five atmospheric variables were chosen as proxies to study the intensity of each storm were then plotted. The geopotential height variable has been referenced at the 850 mb level to show the contraction/expansion of the atmospheric air column. This pressure level is most commonly associated with the top of the marine boundary layer (MBL) which is roughly 1500m. The EKE variable was calculated by simply adding the EKE at each vertical level between the surface and the 850 mb level rather than vertically integrating the pressure levels. The wind and turbulent moisture flux variables were plotted at the surface to show the potential movement of moisture inland from the Current. The evolution of these five variables

for each storm in the CTL and SMTH simulations was plotted along with the difference between the two for each of the five variables. All calculations and analyses were conducted using the numerical computing programme MATLAB.

An example of such plots is shown below in Figure 2.6. It illustrates the evolution of the 850mb geopotential height of the 10 – 12 April 2005 storm in both simulations. The difference between the two runs is plotted on the right to show the impact of the Current on this atmospheric variable for this storm. The area enclosed by the orange boundary indicates the Agulhas region where the SST is between 0.25 – 1.0°C warmer in the CTL simulation. The area enclosed by the red boundary indicates where SSTs are warmer than 1°C in the CTL simulation (a.k.a. Agulhas core).

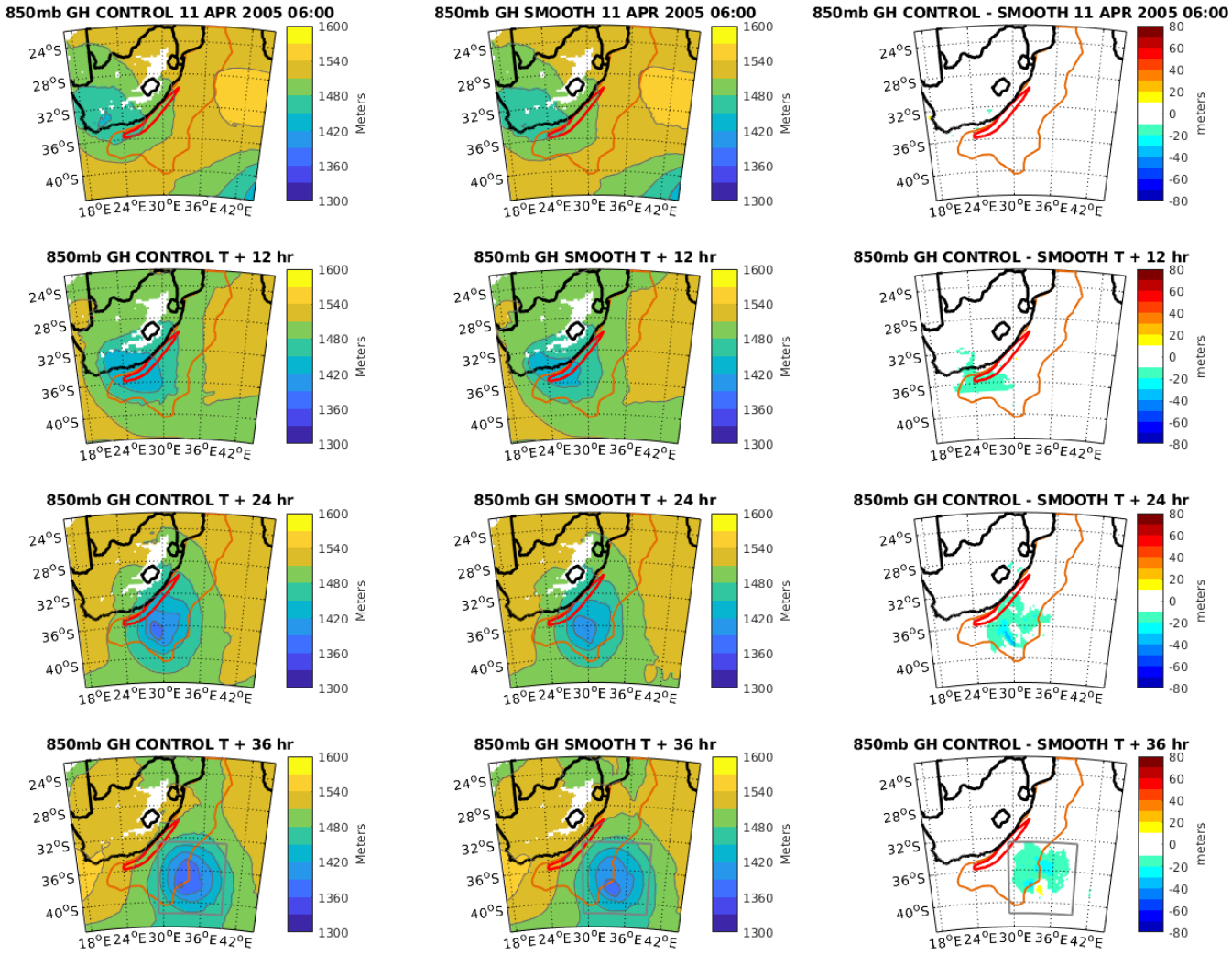

Figure 2.6: WRF 850mb geopotential height for 10 – 12 April 2005 storm measured in meters above sea level (m). From top to bottom: 11 April 06:00; 11 April 18:00; 12 April 06:00 & 12 April 18:00. *(Left)* Control simulation *(Middle)* Smooth simulation & *(Right)* Difference (CTL – SMTH). Orange boundary encloses area where SSTs are 0.25 - 1°C warmer in CTL simulation. Red boundary encloses area where SSTs are > 1°C warmer in CTL simulation Grey box *(Bottom)* encloses developed storm.

Quantifying the impact of the Agulhas Current

The final step of this analysis process involved statistically measuring the impact of the Agulhas Current on these storms. Once each storm had developed over the Current region, indicated by the orange and red boundary areas, a grey box was then plotted around the developed storm. The outermost closed 850mb geopotential height contour, in the CTL run, was chosen as a suitable boundary for each storm. The location of each storm's grey box is the same for all five variables, not just the 850mb geopotential height.

The bottom panel of each variable plot shows a grey box enclosing the developed storm. Values for the grey box in the difference plot (bottom right panel) were then averaged to show if there was a stronger or weaker storm in the CTL run. Standard deviations were also calculated to show the variability between the two configurations. For example, in Figure 2.6, within the grey box in the difference (CTL – SMTH) plot, there is a large 'blue' area as well as a much smaller 'orange/red' area. Cool colours in these difference plots indicate lower 850mb geopotential heights in the CTL simulation and thus a more intense storm. Warm colours in these difference plots indicate higher 850mb geopotential height in the CTL simulation and thus a less intense storm. In this case, the larger blue area within the grey box suggests that this storm is more intense in the CTL simulation once situated over the Agulhas Current.

Chapter 3: Results

3.1 Storm events

The first step in identifying the storms of interest involved checking the synoptic weather charts between 2001 and 2005 provided by the SAWS. 200 synoptic scale low pressure systems were found during the five-year period. These storms included coastal low pressure systems, mid-latitude cyclones, interior low pressures as well as tropical lows originating from the Mozambique channel. The dates of these storm events were recorded. The next step involved determining which of these 200 storms produced rainfall. After using the TRMM 3B42 v7 precipitation reanalysis product, 70 were found to have produced ~~significant~~ rainfall. At this point, the dates of all 70 of the synoptic scale, rain producing low pressure systems tracking over the Agulhas region from 2001 to 2005 were identified.

3.2 WRF model analysis

The next step was analysing the Weather Research and Forecast model output of these 70 storms. After analysing the five atmospheric model variables *(Chapter 2.3: WRF model analysis)* of these storms, ten were found to have intensified whilst moving over the Current region. The variable plots of these ten storms are presented in the following sub-sections. The other 60 storms showed either sustained or dissipating storm intensity whilst propagating over the Current region. Many of the storm systems that showed sustained storm intensity were large mid-latitude cyclones moving west to east. There were roughly 28 (out of 60) instances of these mid-latitude cyclones. The rest (32) were small low-pressure systems, namely coastal and interior lows, that dissipated over the Agulhas Current.

From the ten that showed patterns of intensification, three different types (or categories) of weather events were identified. Three were small low pressure systems that originated directly over the Agulhas region *(Category A).* Three were mid-latitude cyclones, originating southwest of the domain region, moving eastward over the Agulhas Current *(Category B).* Four were interior low pressure systems that originated over land and then moved offshore

over the Agulhas region *(Category C).* All these synoptic-scale, rain producing low pressure systems propagated over the Agulhas Current during their evolution.

When interpreting the WRF variable plots, it is important to note how the variable changes as the storm tracks over the orange *(outer Agulhas region)* and the red *(Agulhas core)* areas. The differences between the two configurations have been included in these plots to show the impact of the Agulhas Current by subtracting the SMTH values from the CTL values. However, the evolution of each of these storms in *both* simulations needs to be carefully examined. The quantitative effect of the Agulhas Current on each storm will be shown with the WRF model plots of the atmospheric variables.

Quantifying the effect of the Agulhas Current

As outlined in Chapter 2.3*,* the average of the difference *(CTL – SMTH)* values were calculated along with the standard deviations within the grey box of each storm. Interpretation of these results should be done bearing in mind that five different atmospheric variables were used as proxies for storm intensity as opposed to one single variable defining storm strength. The WRF model configurations have been set up to show whether the difference in storm evolution between the two runs, is attributable to the Agulhas Current. The average values for the grey box within the difference plots will be interpreted as follows:

Negative (positive) average 850mb geopotential height difference values indicate a deeper (weaker) developed storm in the CTL simulation. Positive (negative) average surface rain rate difference values indicate more (less) rainfall produced by the developed storm in the CTL simulation. Positive (negative) average surface wind speed difference values indicate a stronger (weaker) developed storm in the CTL simulation. Positive (negative) average eddy kinetic energy difference values indicate a stronger (weaker) developed storm in the CTL simulation. Positive (negative) average surface turbulent moisture flux difference values indicate more (less) moisture at the location of the storm in the CTL simulation. Standard deviation values were calculated to quantify the variability between the CTL and SMTH runs for each developed storm. 'Developed storm' refers to when the system has evolved over the Agulhas Current and has started to track away from the Current region.

3.3 Category A storms

Storm A1: 19 – 21 July 2002

The first category A storm was a small offshore low pressure located at approximately 30°S & 35°E. As indicated by Figure 3.3.1, this system tracks very slowly southwest down South Africa's east coast. The storm remains mainly offshore whilst moving southwest. Over the first 48 hours, the centre storm pressure is sustained at 1016 hPa *(Top left, Top right)* however on the 21st July, the system deepens as the centre isobar decreases from 1016 hPa to 1012 hPa *(Bottom).*

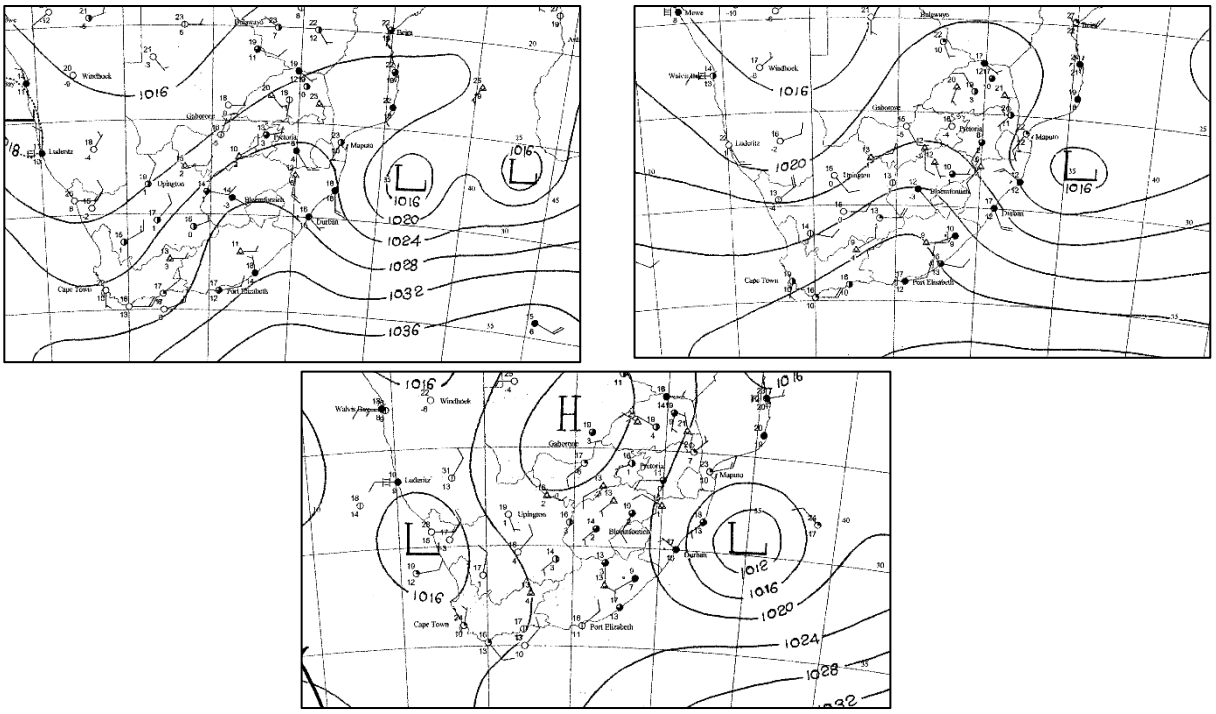

Figure 3.3.1 : Storm A1. Surface synoptic conditions for *(Top left)* 19 July 2002 *(Top right) 20* July 2002 & *(Bottom)* 21 July 2002. Charts were generated at 12h00 UTC.

Figure 3.3.2 shows a deepening of the storm in both simulations as the geopotential height contours decreased as the system tracks southwest over the Agulhas Current. The storm centre is modelled closer to the coastline in the SMTH run however a slightly deeper developed system is found in the CTL run.

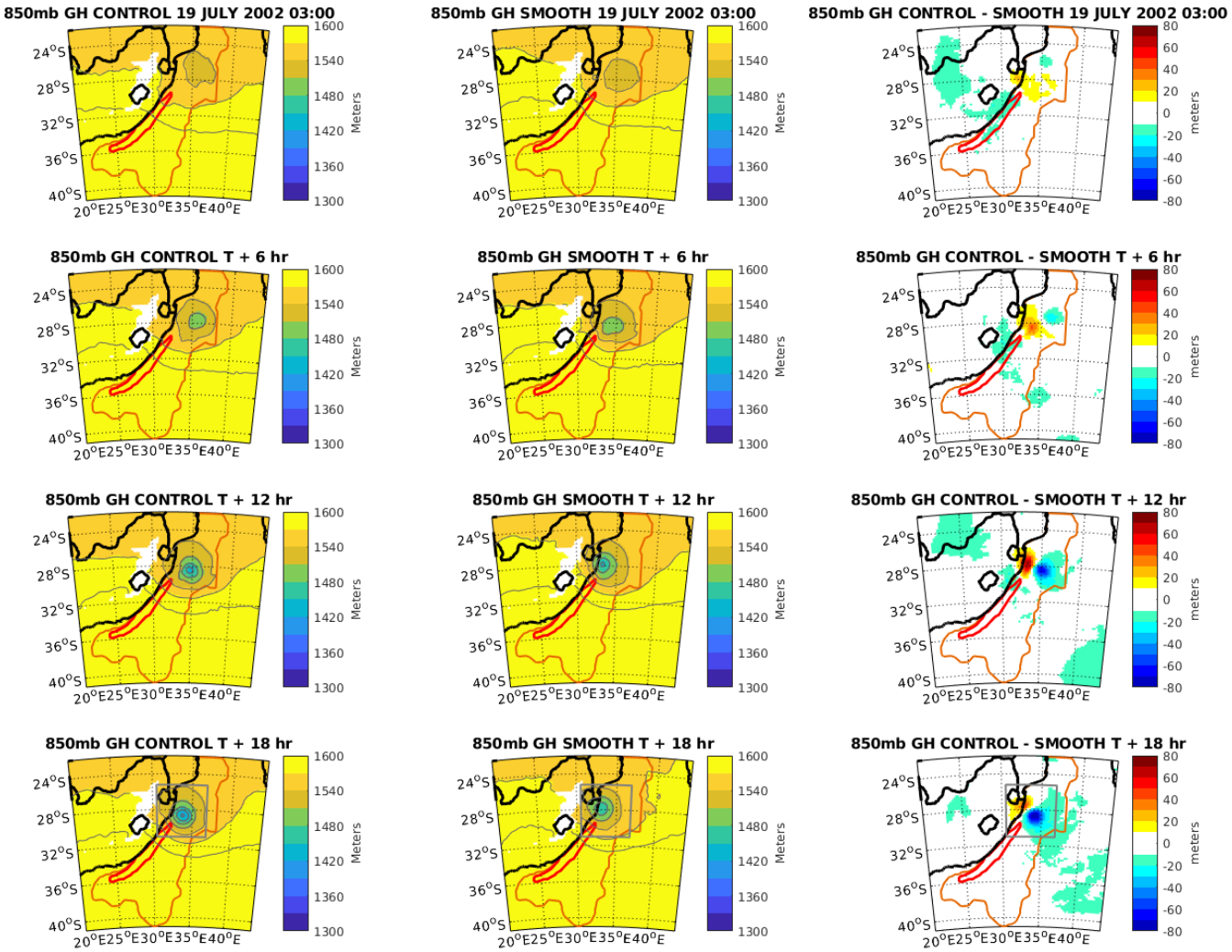

Figure 3.3.2: Storm A1. WRF model 850mb geopotential height (m). From top to bottom: 19 July 03:00; 19 July 09:00; 19 July 15:00 & 19 July 21:00. *(Left)* CTL simulation *(middle)* SMTH simulation & *(right)* Difference (CTL – SMTH). Orange boundary encloses area where SSTs are 0.25 - 1°C warmer in CTL simulation. Red boundary encloses area where SSTs are > 1°C warmer in CTL simulation. *(Bottom)* Grey box encloses developed storm.

Figure 3.3.3 shows modelled rainfall moving closer to land as the storm tracks southwest. There is no obvious increase in overall rainfall during the storm's evolution in either simulation, however rainfall does increase directly on the coastline between Durban and Maputo. Minimal difference between the two configurations is found.

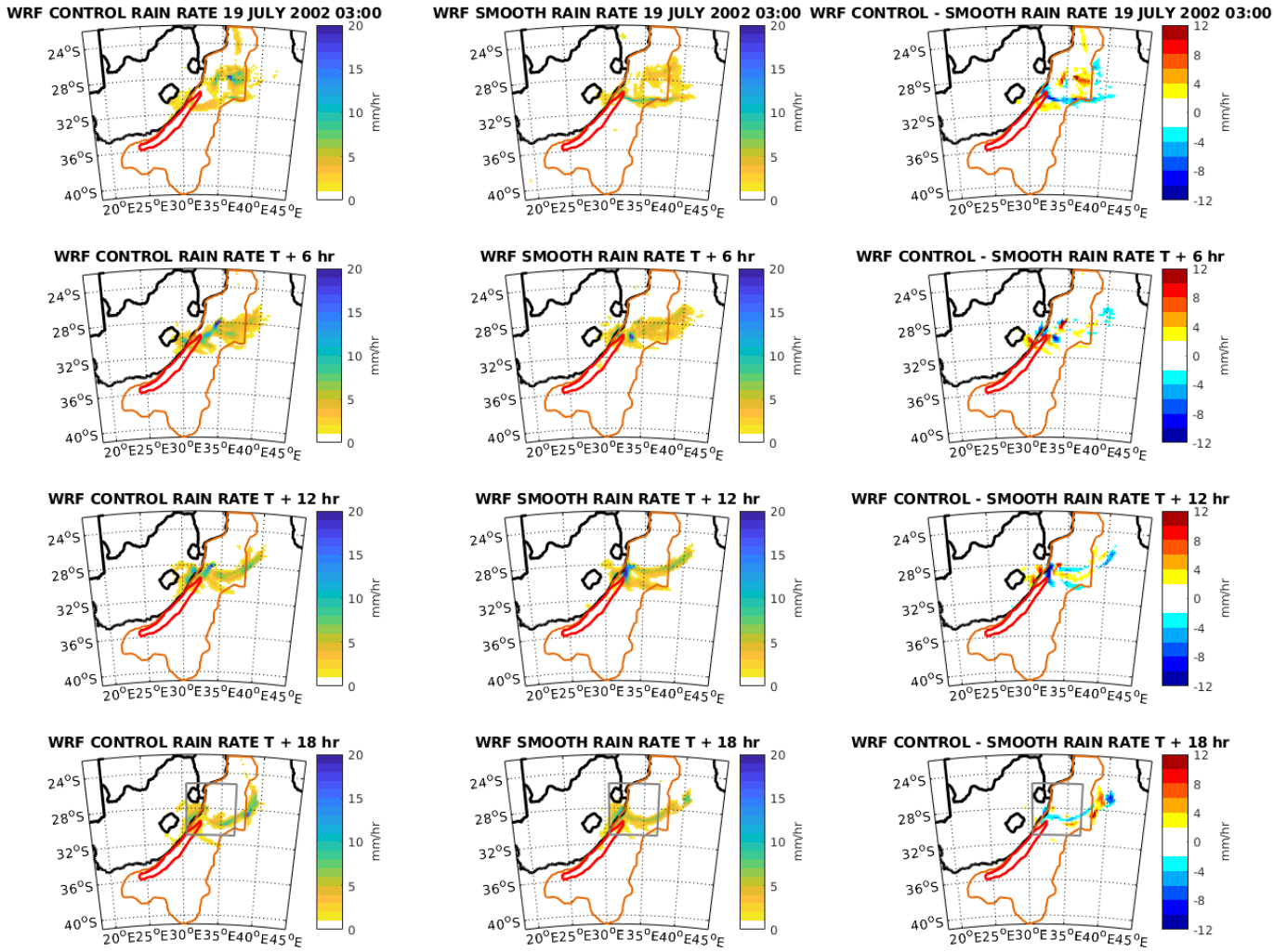

Figure 3.3.3: Storm A1. WRF model surface rain rate (mm.hr^{-1}). From top to bottom: 19 July 03:00; 19 July 09:00; 19 July 15:00 & 19 July 21:00. *(Left)* CTL simulation *(middle)* SMTH simulation & *(right)* Difference (CTL – SMTH). Orange boundary encloses area where SSTs are 0.25 - 1°C warmer in CTL simulation. Red boundary encloses area where SSTs are > 1°C warmer in CTL simulation. *(Bottom)* Grey box encloses developed storm.

Figure 3.3.4 indicates surface wind speeds increase considerably in both simulations. Maximum wind speeds are found closer to the coastline as the storm propagates over the Agulhas Current. There is virtually no difference between the CTL and SMTH simulations.

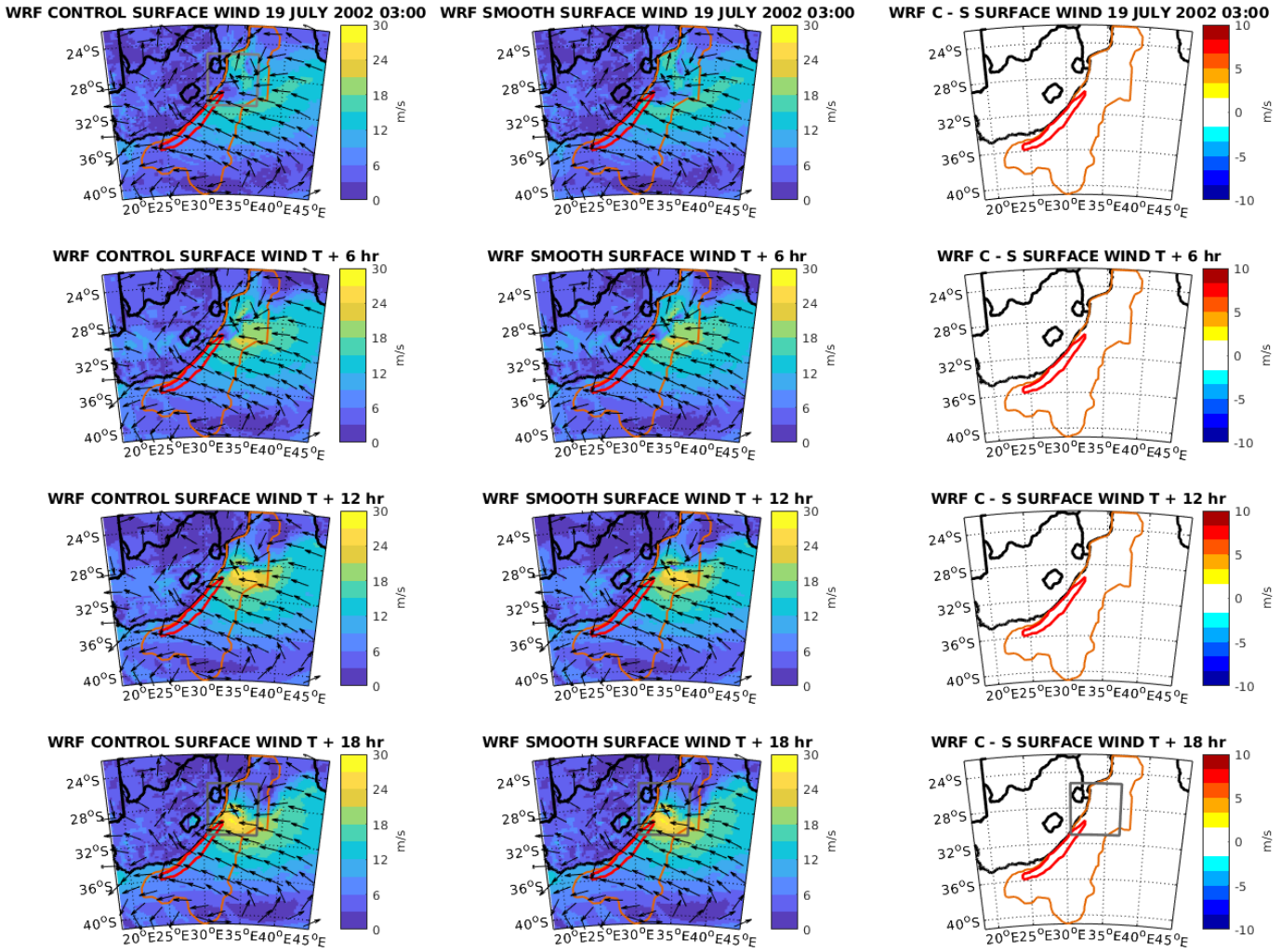

Figure 3.3.4: Storm A1. WRF model surface wind ($m.s^{-1}$). From top to bottom: 19 July 03:00; 19 July 09:00; 19 July 15:00 & 19 July 21:00. *(Left)* CTL simulation *(middle)* SMTH simulation & *(right)* Difference (CTL – SMTH). Black arrows indicate normalised surface wind vectors. Orange boundary encloses area where SSTs are 0.25 - 1°C warmer in CTL simulation. Red boundary encloses area where SSTs are > 1°C warmer in CTL simulation. *(Bottom)* Grey box encloses developed storm.

The eddy kinetic energy (EKE) up to the 850mb height of the storm is shown in Figure 3.3.5. This figure indicates that the storm becomes dramatically more energetic in both simulations as the system tracks over the Agulhas region. The increased vorticity of the storm can be observed in both configurations.

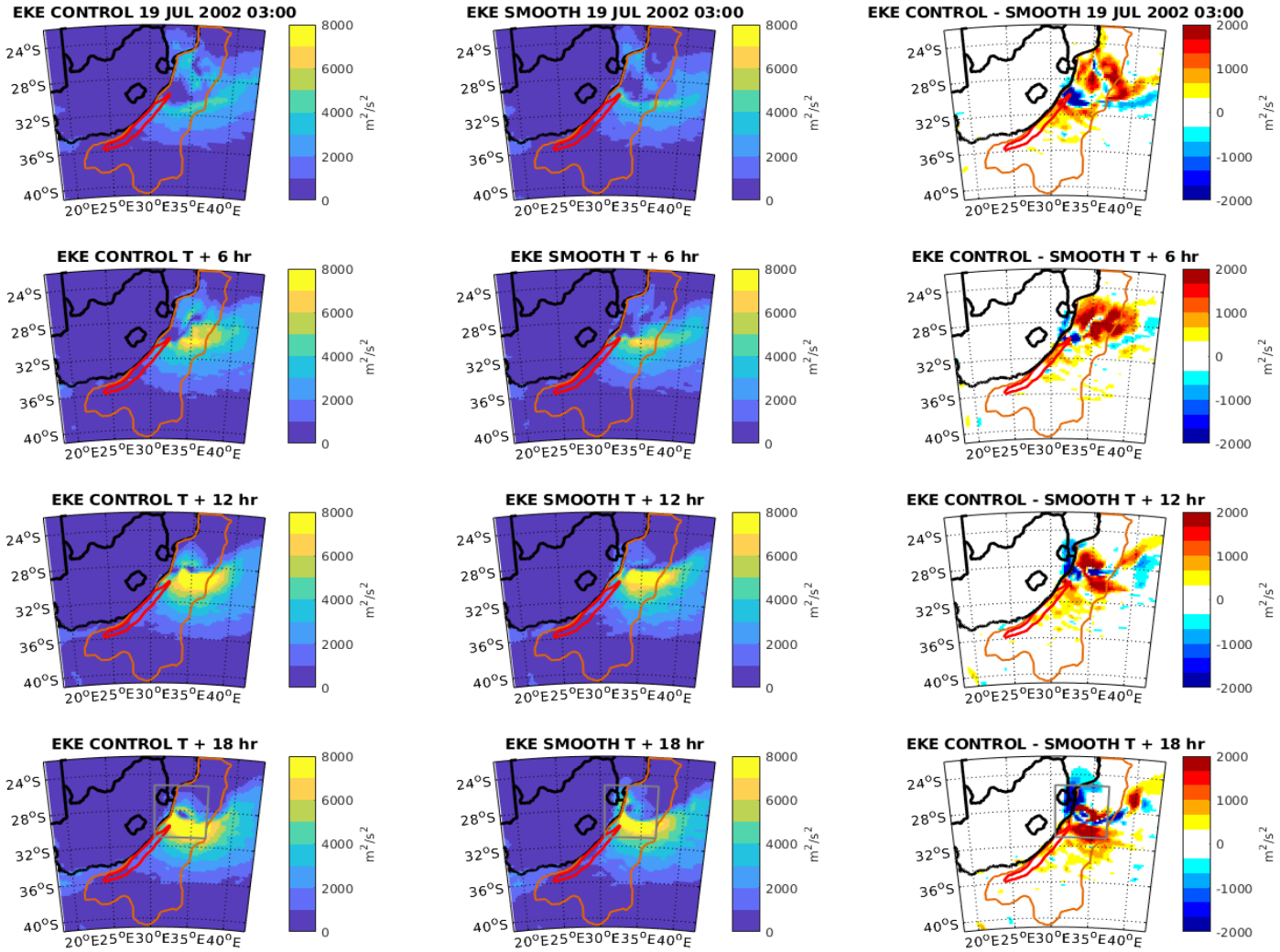

Figure 3.3.5: Storm A1. WRF model eddy kinetic energy up to the 850mb level ($m^2.s^{-2}$). From top to bottom: 19 July 03:00; 19 July 09:00; 19 July 15:00 & 19 July 21:00. *(Left)* CTL simulation *(middle)* SMTH simulation & *(right)* Difference (CTL – SMTH). Orange boundary encloses area where SSTs are 0.25 - 1°C warmer in CTL simulation. Red boundary encloses area where SSTs are > 1°C warmer in CTL simulation. *(Bottom)* Grey box encloses developed storm.

Figure 3.3.6 shows the surface turbulent moisture flux over the Current region and surrounding waters. High fluxes are found consistently throughout the storm's evolution over the Current region in both configurations. The vorticity of the storm can be observed in both simulations

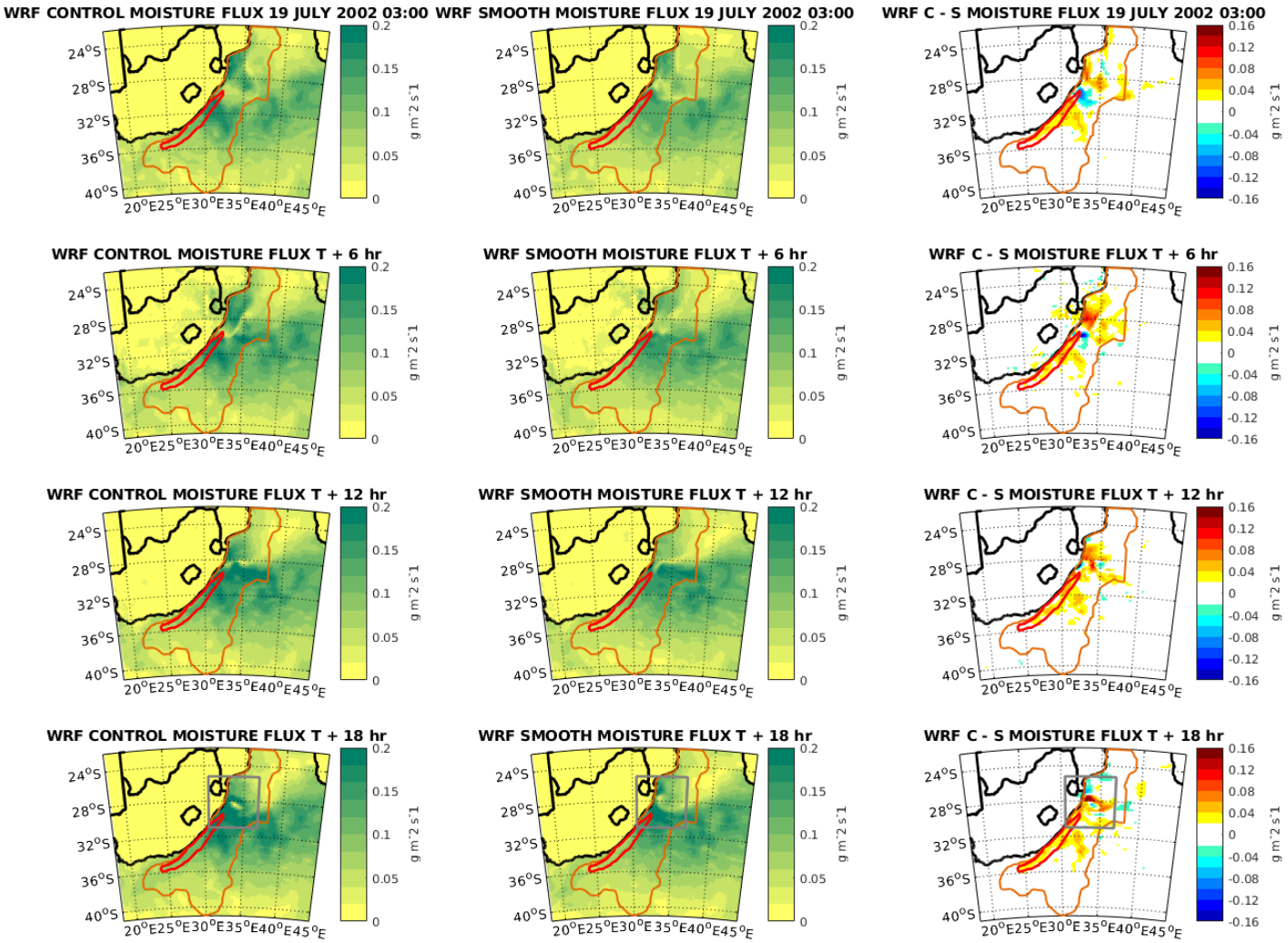

Figure 3.3.6: Storm A1. WRF model surface turbulent moisture flux ($g.m^{-2}.s^{-1}$). From top to bottom: 19 July 03:00; 19 July 09:00; 19 July 15:00 & 19 July 21:00. *(Left)* CTL simulation *(middle)* SMTH simulation & *(right)* Difference (CTL – SMTH). Orange boundary encloses area where SSTs are 0.25 - 1°C warmer in CTL simulation. Red boundary encloses area where SSTs are > 1°C warmer in CTL simulation. *(Bottom)* Grey box encloses developed storm.

Table 3.3.1 indicates that a deeper (- 8.3 ± 9.15 m) developed storm was modelled in the CTL run. Lower rainfall intensity (- 0.24 ± 0.570 $mm.hr^{-1}$), higher surface wind speeds (+ 0.089 ± 1.2307 $m.s^{-1}$), greater storm energy (+ 81 ± 545 $m^2.s^{-2}$) and higher surface turbulent moisture fluxes (+ 0.057 ± 0.0120 $g.m^{-2}.s^{-1}$) were all found for the developed storm over the Agulhas Current. The standard deviations are larger than the mean difference for all but one variable.

WRF VARIABLE	AVERAGE DIFFERENCE
850mb geopotential height	**- 8.3 ± 9.15 m**
Surface rain rate	**- 0.24 ± 0.570 mm.hr^{-1}**
Surface wind speed	**+ 0.089 ± 1.2307 m.s^{-1}**
Eddy kinetic energy (EKE)	**+ 81 ± 545 m^2.s^{-2}**
Surface turbulent moisture flux	**+ 0.057 ± 0.0120 g.m^{-2}.s^{-1}**

Table 3.3.1: Storm A1: 19 – 21 July 2001. Average difference (CTL – SMTH) values for five WRF model variables. Values are for developed storm bounded by grey box. Standard deviations for average values are included.

Storm A2: 4 – 6 March 2003

This storm's cyclogenesis is initiated directly over the Current region within just a few hours. Figure 3.3.7 shows that on the 4th March there is no prevailing weather feature over the Agulhas Current at all *(Top left).* The next day however, a low pressure system starts to form directly over the Current core *(Top right).* This system intensifies over the next 24 hours and moves further offshore *(Bottom).*

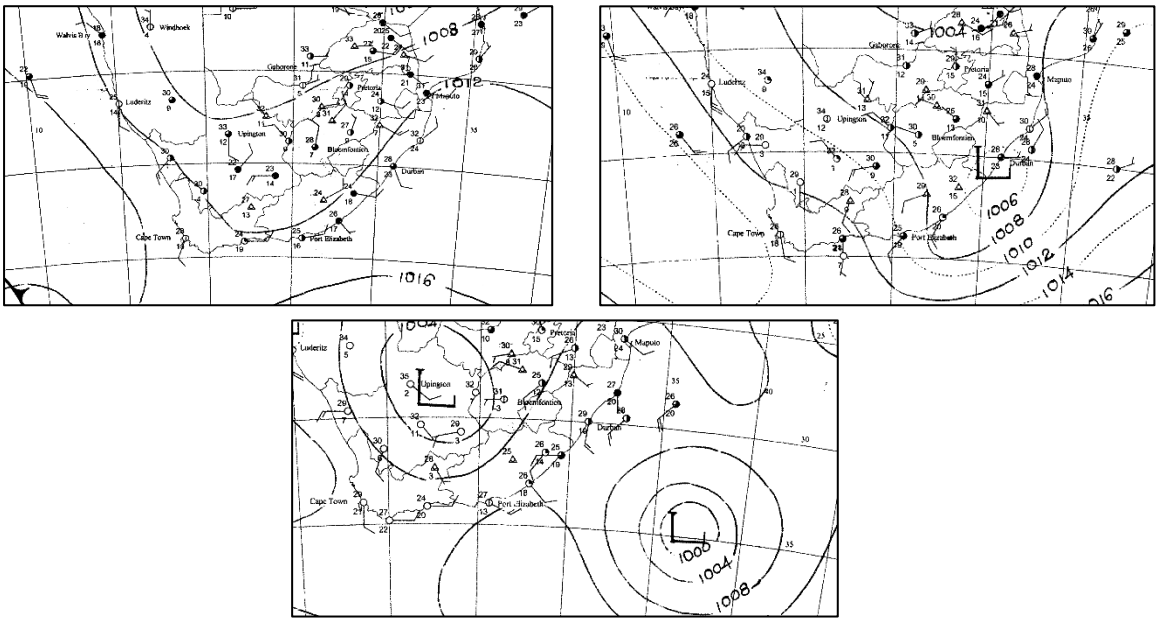

Figure 3.3.7: Storm A2. Surface synoptic conditions for *(Top left)* 4 March 2003 *(Top right)* 5 March 2003 & *(Bottom)* 6 March 2003. Charts were generated at 12h00 UTC.

Figure 3.3.8 shows the storm deepening in both simulations however less so in the SMTH run. A much deeper developed storm is modelled in the CTL run. However, the centre of the storm, as indicated by the centre closed geopotential height contour, is found further to the northeast in the SMTH run.

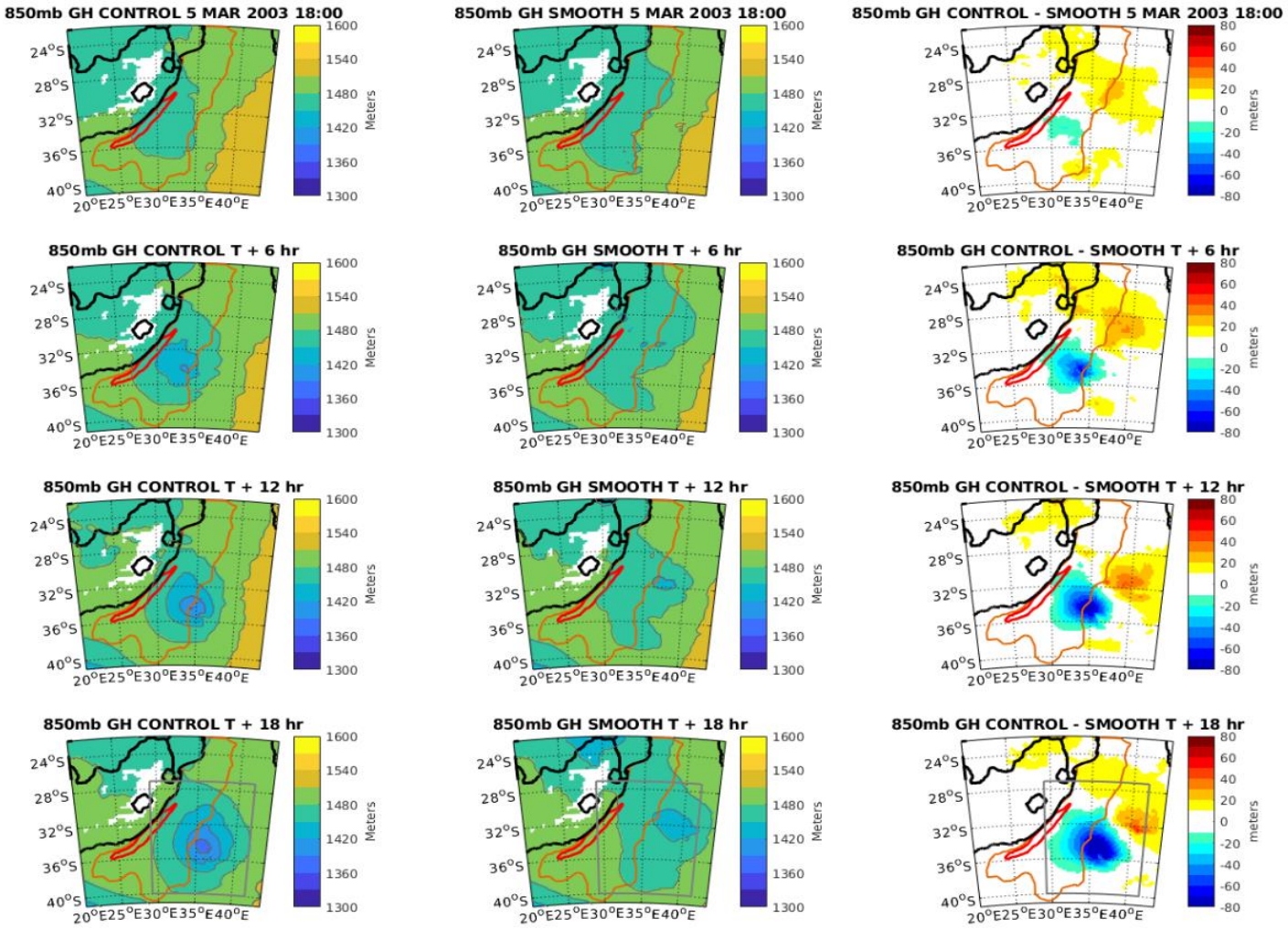

Figure 3.3.8: Storm A2. WRF model 850mb geopotential height (m) From top to bottom: 5 March 18:00; 6 March 00:00; 6 March 06:00 & 6 March 12:00. *(Left)* CTL simulation *(middle)* SMTH simulation & *(right)* Difference (CTL – SMTH). Orange boundary encloses area where SSTs are 0.25 - 1°C warmer in CTL simulation. Red boundary encloses area where SSTs are > 1°C warmer in CTL simulation. *(Bottom)* Grey box encloses developed storm.

High rain rates in both runs are found at the storm centre however these high rain rates in the SMTH run occur further to the northeast, co-located with the geopotential height centre at approximately 32°S, as shown in Figure 3.3.9. This figure also shows that when the storm

centre is located over the Current region in the CTL run, rain rates are sustained. However, in the SMTH run, even though the centre of the storm is modelled away from the Current region *(east of orange boundary)*, rainfall increases.

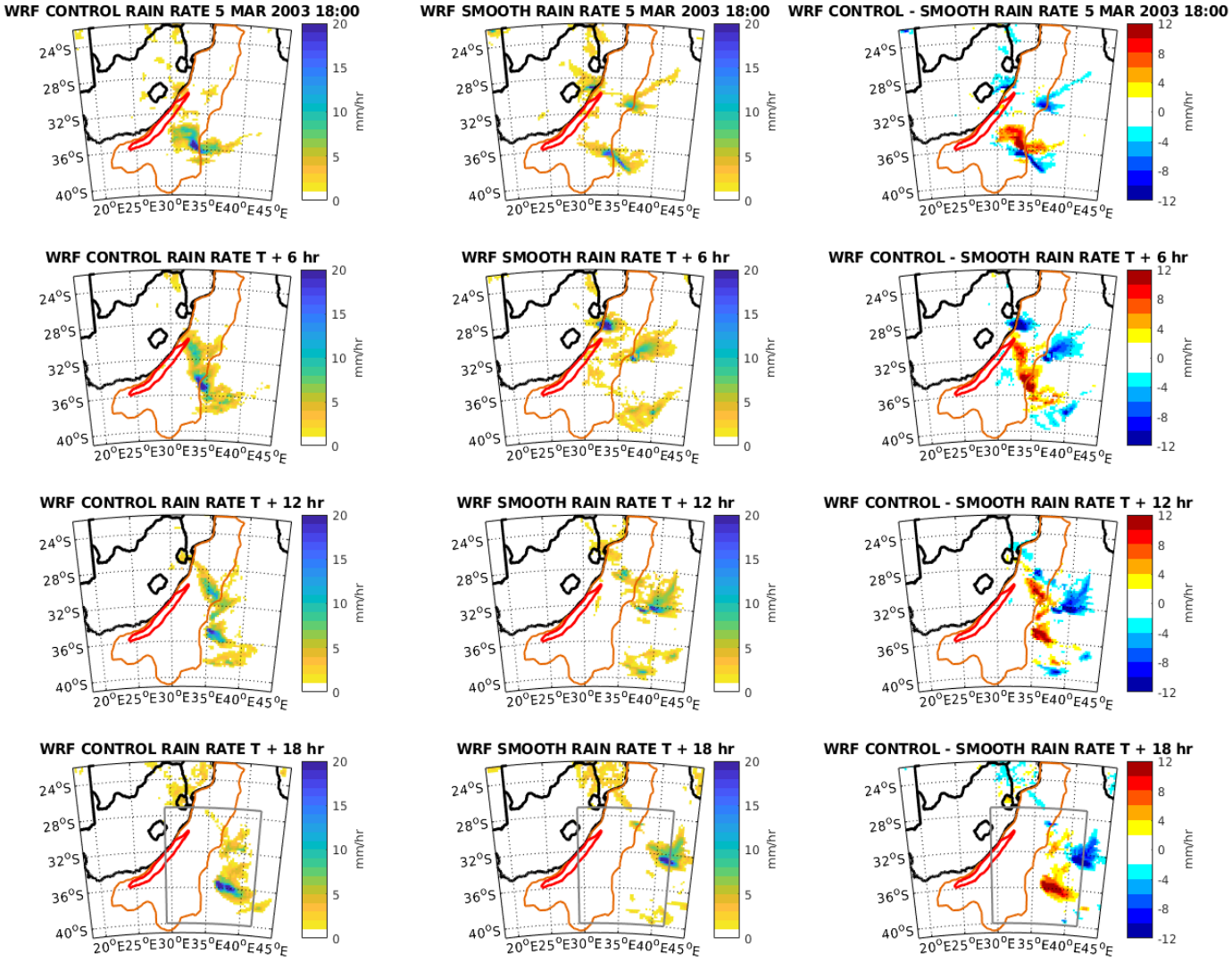

Figure 3.3.9: Storm A2. WRF model surface rain rate (mm.hr^{-1}). From top to bottom: 5 March 18:00; 6 March 00:00; 6 March 06:00 & 6 March 12:00. *(Left)* CTL simulation *(middle)* SMTH simulation & *(right)* Difference (CTL – SMTH). Orange boundary encloses area where SSTs are 0.25 - 1°C warmer in CTL simulation. Red boundary encloses area where SSTs are > 1°C warmer in CTL simulation. *(Bottom)* Grey box encloses developed storm.

Figure 3.3.10 shows a slight increase in surface wind speed in the CTL run whereas wind speeds are sustained in the SMTH run. A large difference in storm wind speed was observed at 6 March 2003 12:00.

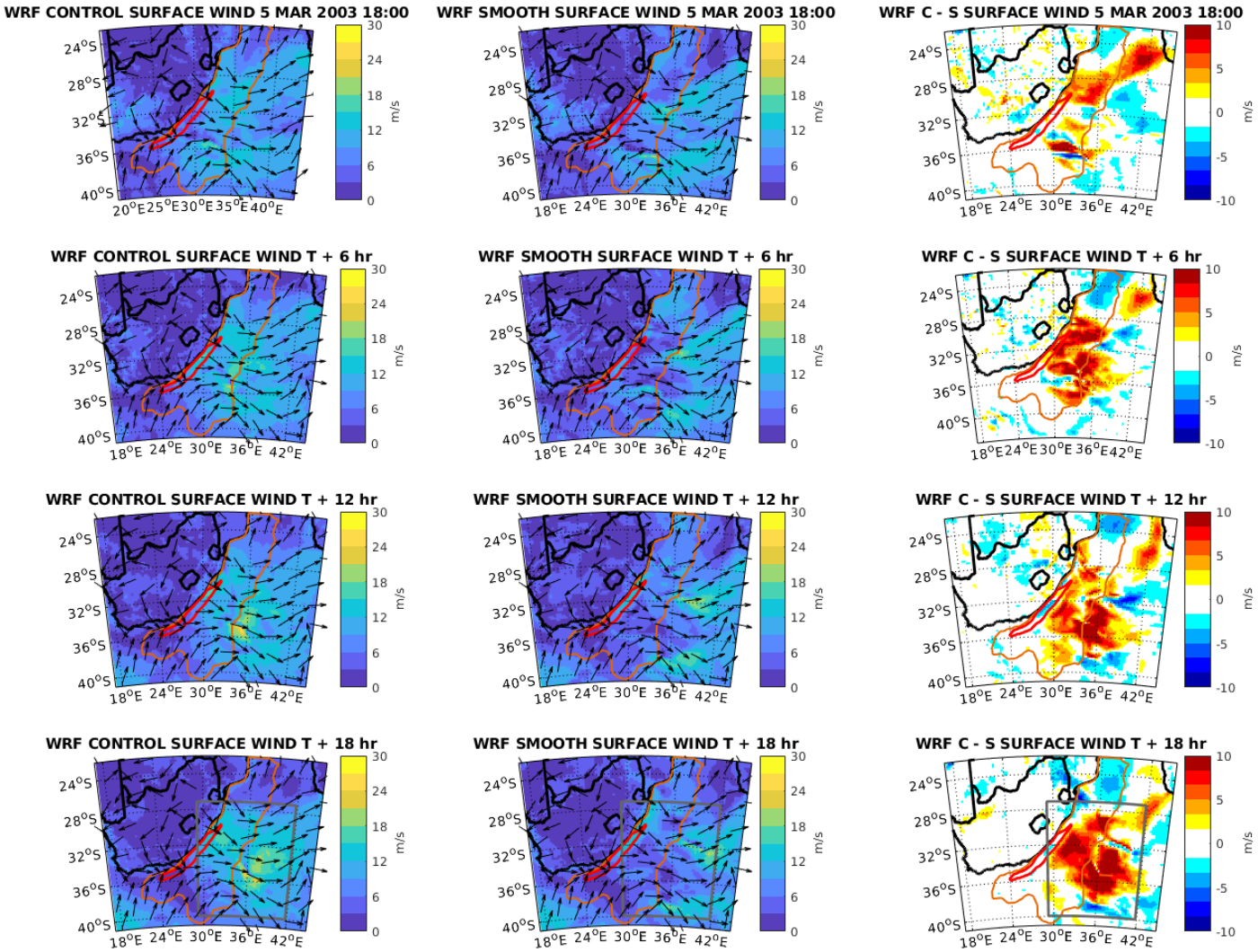

Figure 3.3.10: Storm A2. WRF model surface wind (m.s^{-1}). From top to bottom: 5 March 18:00; 6 March 00:00; 6 March 06:00 & 6 March 12:00. *(Left)* CTL simulation *(middle)* SMTH simulation & *(right)* Difference (CTL – SMTH). Black arrows indicate normalised surface wind vectors. Orange boundary encloses area where SSTs are 0.25 - 1°C warmer in CTL simulation. Red boundary encloses area where SSTs are > 1°C warmer in CTL simulation. *(Bottom)* Grey box encloses developed storm.

A large difference in storm energy is modelled between the two configurations as shown in Figure 3.3.11. In the CTL run along the boundary of the Agulhas region *(orange border),* storm EKE is found to increase as the system tracks away to the east. Minimal storm energy is found in the SMTH run and this lack of energy persists whilst the storm propagates over and eventually away from the Current region.

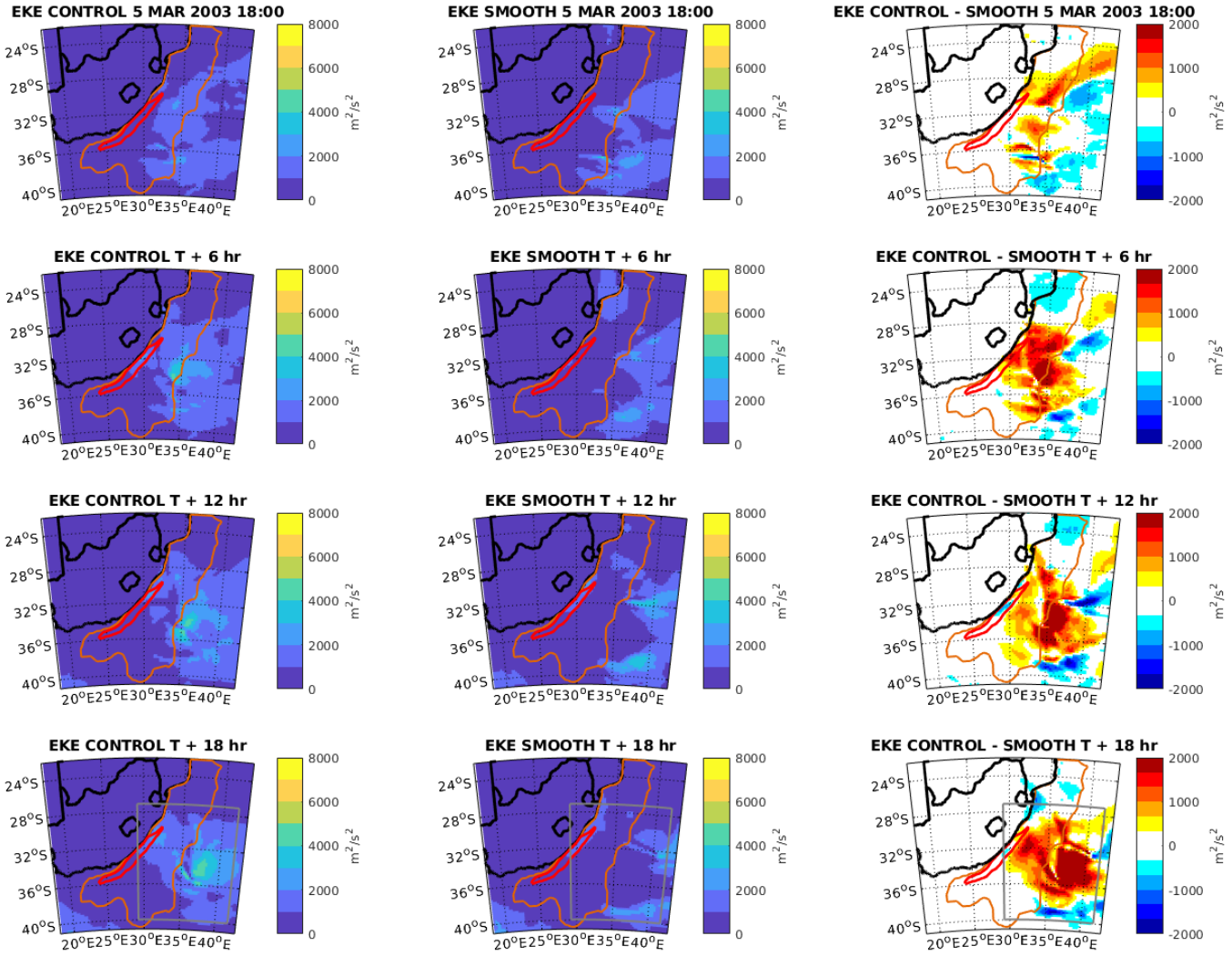

Figure 3.3.11: Storm A2. WRF model eddy kinetic energy up to the 850mb level ($m^2.s^{-2}$). From top to bottom: 5 March 18:00; 6 March 00:00; 6 March 06:00 & 6 March 12:00. *(Left)* CTL simulation *(middle)* SMTH simulation & *(right)* Difference (CTL – SMTH). Orange boundary encloses area where SSTs are 0.25 - 1°C warmer in CTL simulation. Red boundary encloses area where SSTs are > 1°C warmer in CTL simulation. *(Bottom)* Grey box encloses developed storm.

Figure 3.3.12 indicates sustained surface turbulent moisture fluxes in the vicinity of the storm in the CTL run are found however a slight rise is modelled at the storm's centre as the system evolves over the Current region. The same evolution pattern is modelled in the SMTH run, but increased fluxes are found away from the Agulhas region *(east of orange boundary)* in the SMTH run.

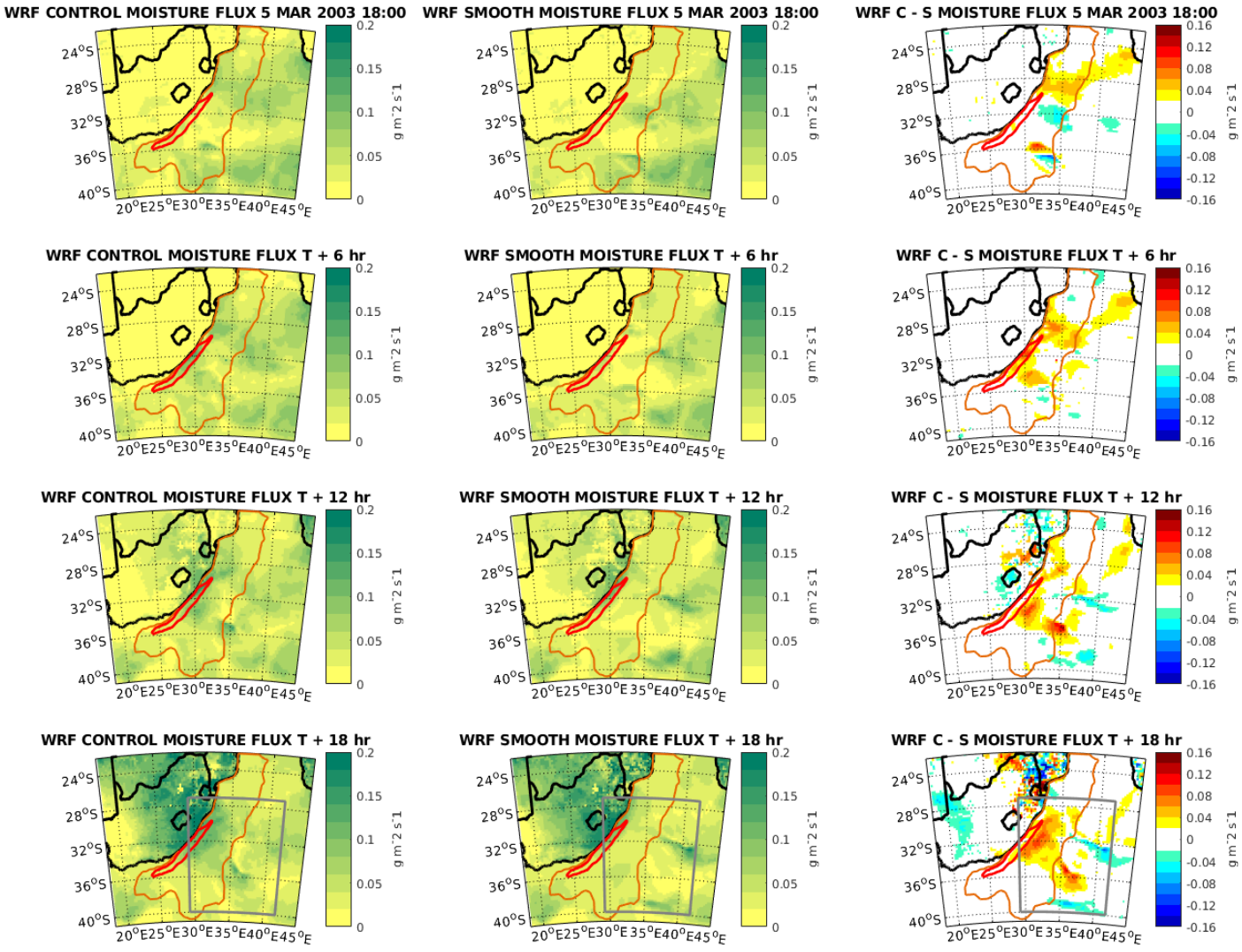

Figure 3.3.12: Storm A2. WRF model surface turbulent moisture flux ($g.m^{-2}.s^{-1}$). From top to bottom: 5 March 18:00; 6 March 00:00; 6 March 06:00 & 6 March 12:00. *(Left)* CTL simulation *(middle)* SMTH simulation & *(right)* Difference (CTL – SMTH). Orange boundary encloses area where SSTs are 0.25 - 1°C warmer in CTL simulation. Red boundary encloses area where SSTs are > 1°C warmer in CTL simulation. *(Bottom)* Grey box encloses developed storm.

Table 3.3.2 indicates that a deeper (- 8.2 ± 10.03 m) developed storm was modelled in the CTL run. Higher rainfall intensity (+ 0.35 ± 2.602 $mm.hr^{-1}$), higher surface wind speeds (+ 3.15 ± 1.342 $m.s^{-1}$), greater storm energy (+ 649 ± 326.3 $m^2.s^{-2}$) and higher surface turbulent moisture fluxes (+ 0.010 ± 0.0120 $g.m^{-2}.s^{-1}$) were all found for the developed storm over the Agulhas Current. The standard deviations are larger than the mean difference for all but two variables.

WRF VARIABLE	AVERAGE DIFFERENCE
850mb geopotential height	**- 8.2 ± 10.03 m**
Surface rain rate	**+ 0.35 ± 2.602 $mm.hr^{-1}$**
Surface wind speed	**+ 3.15 ± 1.342 $m.s^{-1}$**
Eddy kinetic energy (EKE)	**+ 649 ± 326.3 $m^2.s^{-2}$**
Surface turbulent moisture flux	**+ 0.010 ± 0.0120 $g.m^{-2}.s^{-1}$**

Table 3.3.2: Storm A2: 4 – 6 March 2003. Average difference (CTL – SMTH) values for five WRF model variables. Values are for developed storm bounded by grey box. Standard deviations for average values are included.

Storm A3: 5 – 7 June 2003

Figure 3.3.13 shows a small low pressure system developing over the Agulhas region. Once the cold front moves away from the coast on the 5th June *(Top left),* a weak low is initiated directly over the Current core over the next 24 hours *(Top right).* The system then intensifies dramatically as the centre isobar decreases from 1016 hPa to 1004 hPa over the following 24 hours *(Bottom).* During the storm's initial development, the storm centre remains close to the coastline however once it intensifies, it propagates eastward away from land.

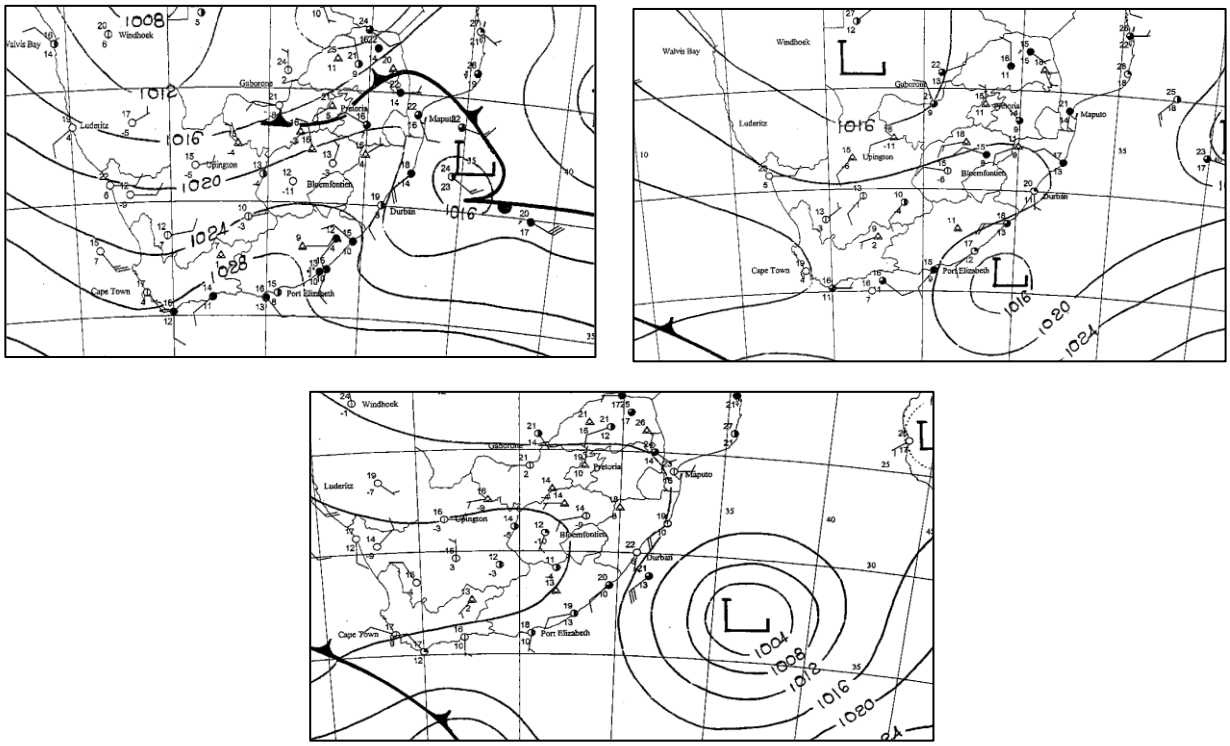

Figure 3.3.13: Storm A3. Surface synoptic conditions for *(Top left)* 5 June 2003 *(Top right)* 6 June 2003 & *(Bottom)* 7 June 2003. Charts are generated at 12h00 UTC.

Figure 3.3.14 shows an intense deepening of the storm in the CTL simulation over the northern region of the Agulhas core. A similar evolution occurs in the SMTH run however the intensification is less extreme. The storm is found to extend northeast in the CTL run however in the SMTH run, the storm is more centred over the Agulhas region.

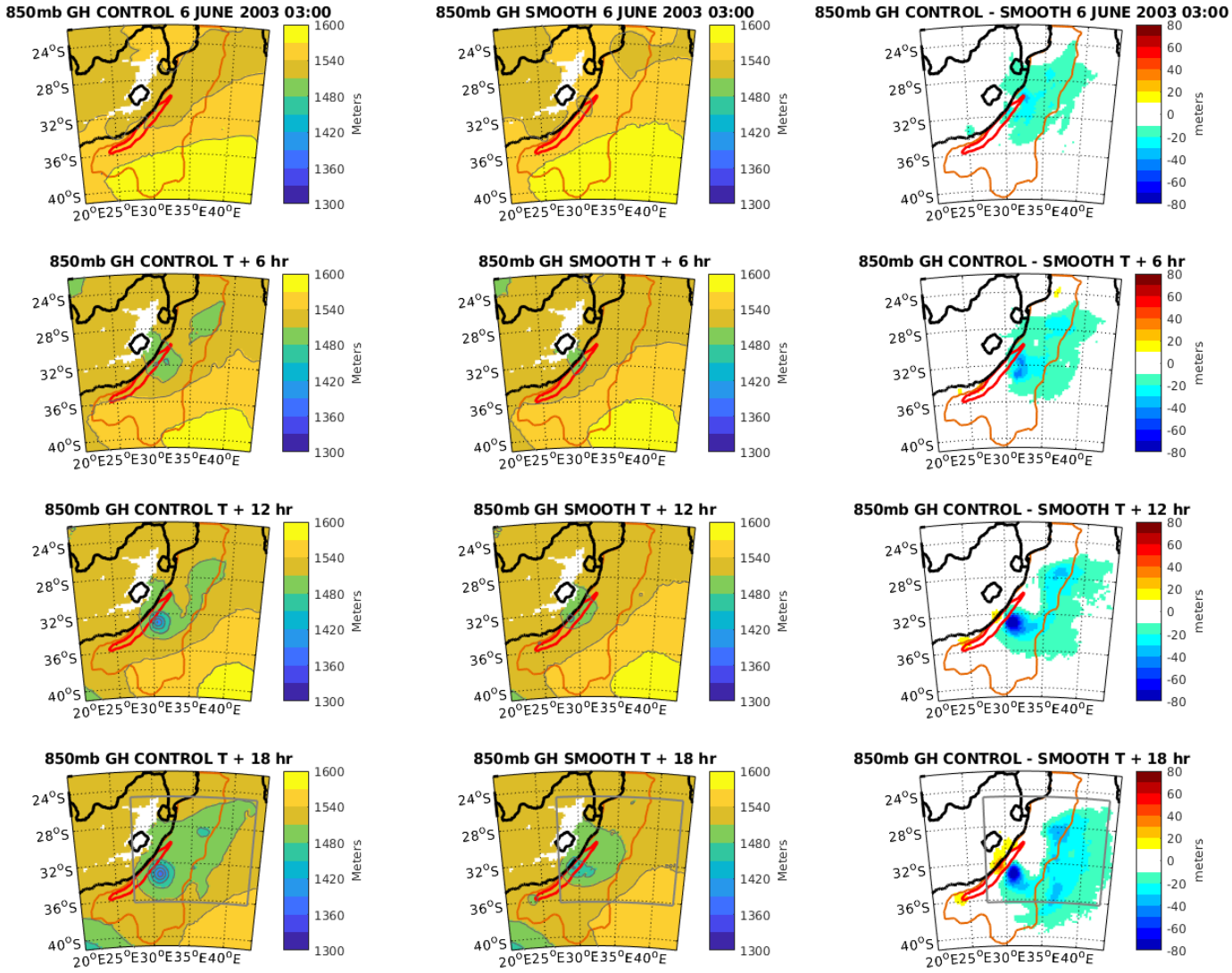

Figure 3.3.14: Storm A3. WRF model 850mb geopotential height (m). From top to bottom: 6 June 03:00, 6 June 09:00, 6 June 15:00 & 6 June 21:00. *(Left)* CTL simulation *(middle)* SMTH simulation & *(right)* Difference (CTL – SMTH). Orange boundary encloses area where SSTs are 0.25 - 1°C warmer in CTL simulation. Red boundary encloses area where SSTs are > 1°C warmer in CTL simulation. *(Bottom)* Grey box encloses developed storm.

Figure 3.3.15 shows model rainfall increasing whilst the storm tracks southeast over the Agulhas Current in both runs. However, as the system develops, higher rain rates are found in the CTL run but the region of high rainfall is modelled further east relative to the SMTH run.

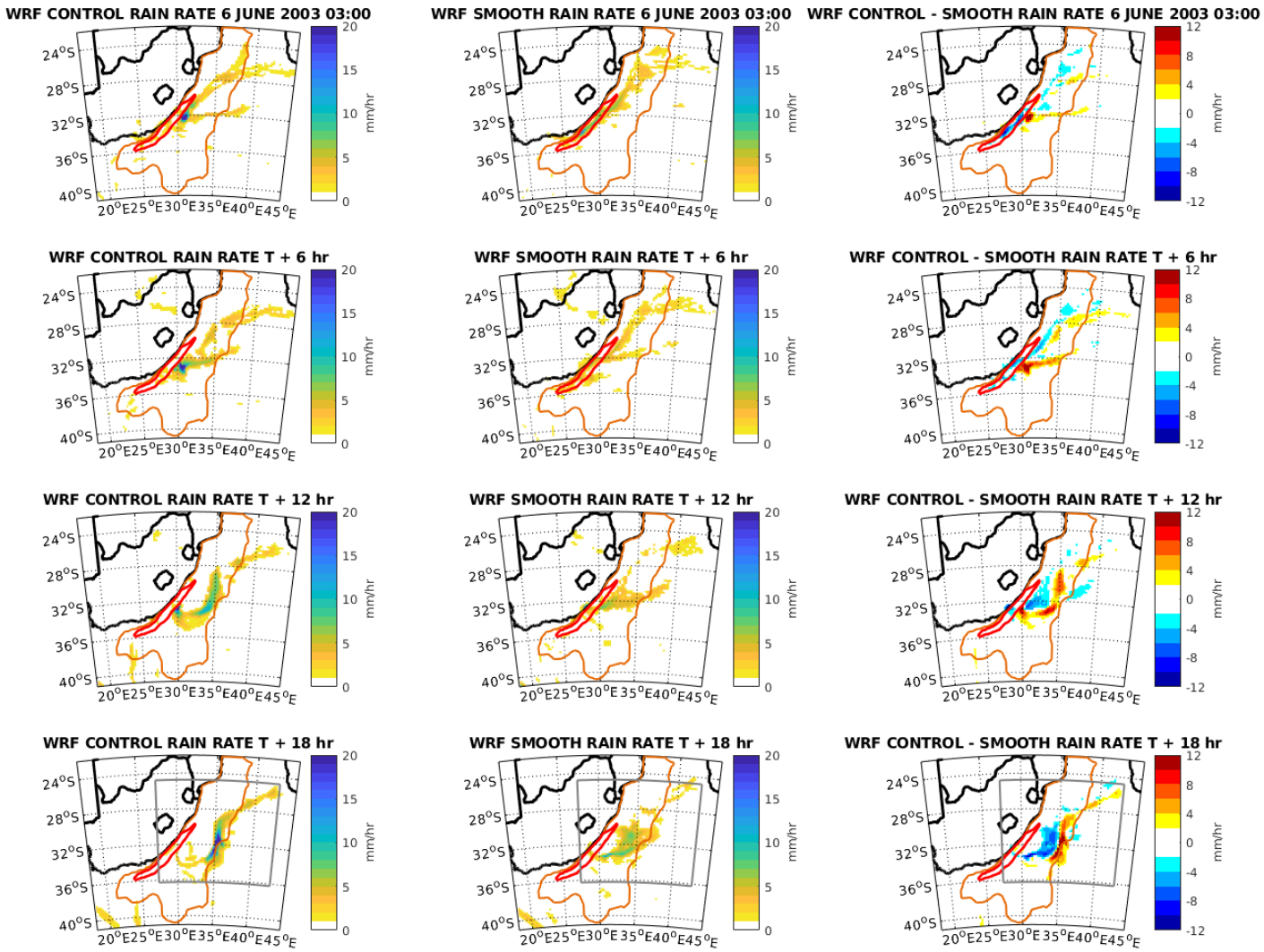

Figure 3.3.15: Storm A3. WRF model surface rain rate (mm.hr^{-1}). From top to bottom: 6 June 03:00, 6 June 09:00, 6 June 15:00 & 6 June 21:00. *(Left)* CTL simulation *(middle)* SMTH simulation & *(right)* Difference (CTL – SMTH). Orange boundary encloses area where SSTs are 0.25 - 1°C warmer in CTL simulation. Red boundary encloses area where SSTs are > 1°C warmer in CTL simulation. *(Bottom)* Grey box encloses developed storm.

Surface wind shown in Figure 3.3.16 indicates winds speeds increase gradually in the CTL run as the system propagates over the Current. Increased storm wind speeds also occur in the SMTH run, but the degree of intensification is less severe than the CTL run. The storm's vorticity can be observed in the CTL run once the storm has developed at 6 June 2003 21:00.

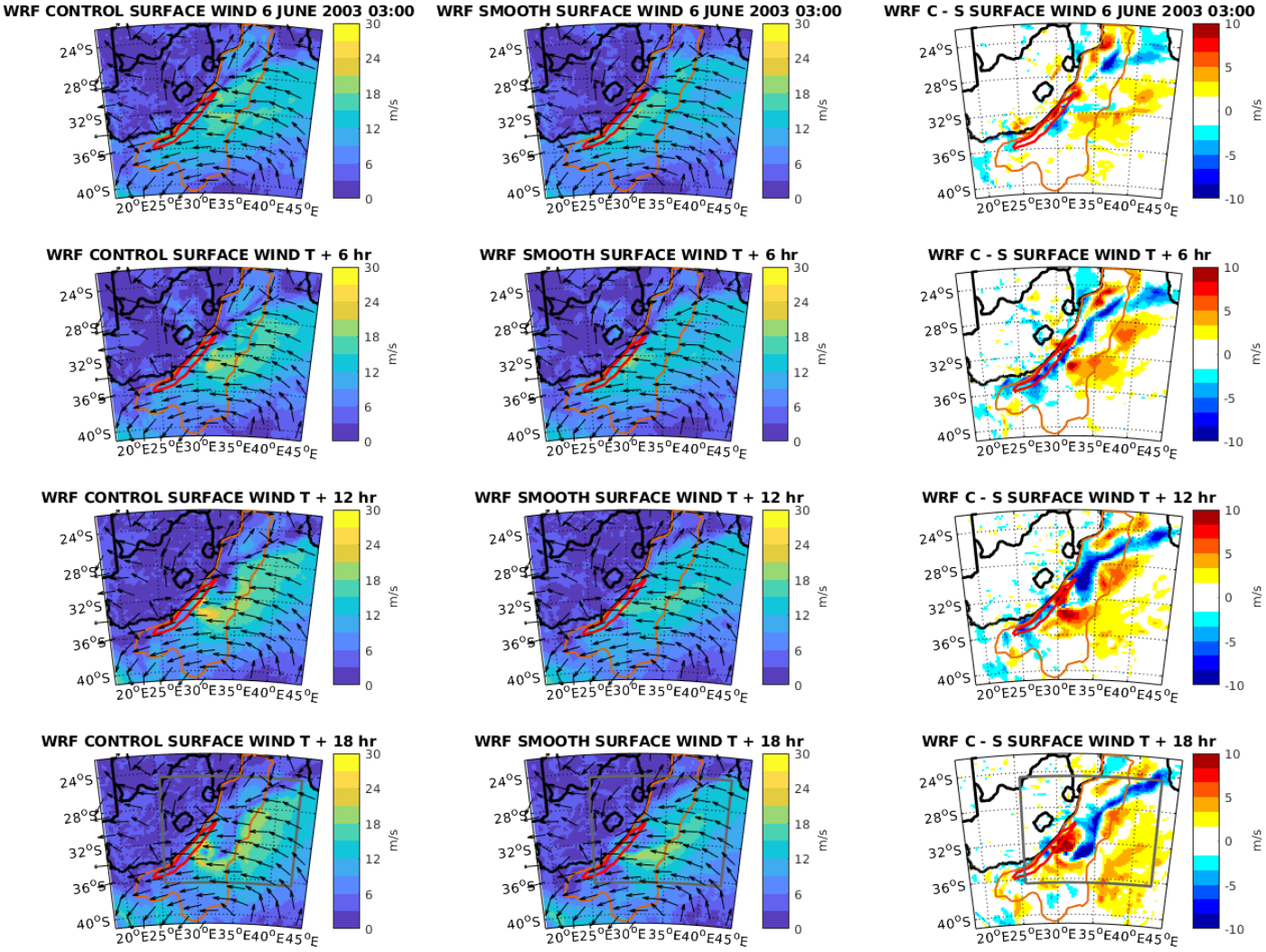

Figure 3.3.16: Storm A3. WRF model surface wind (m.s^{-1}). From top to bottom: 6 June 03:00, 6 June 09:00, 6 June 15:00 & 6 June 21:00. *(Left)* CTL simulation *(middle)* SMTH simulation & *(right)* Difference (CTL – SMTH). Black arrows indicate normalised surface wind vectors. Orange boundary encloses area where SSTs are 0.25 - 1°C warmer in CTL simulation. Red boundary encloses area where SSTs are > 1°C warmer in CTL simulation. *(Bottom)* Grey box encloses developed storm.

Figure 3.3.17 shows increasing storm energy in both runs as the storm tracks over the Current. There is greater intensification of the storm's EKE in the CTL run relative to the SMTH. The vorticity of the developed storm can be observed at 6 June 2003 21:00 in the CTL simulation.

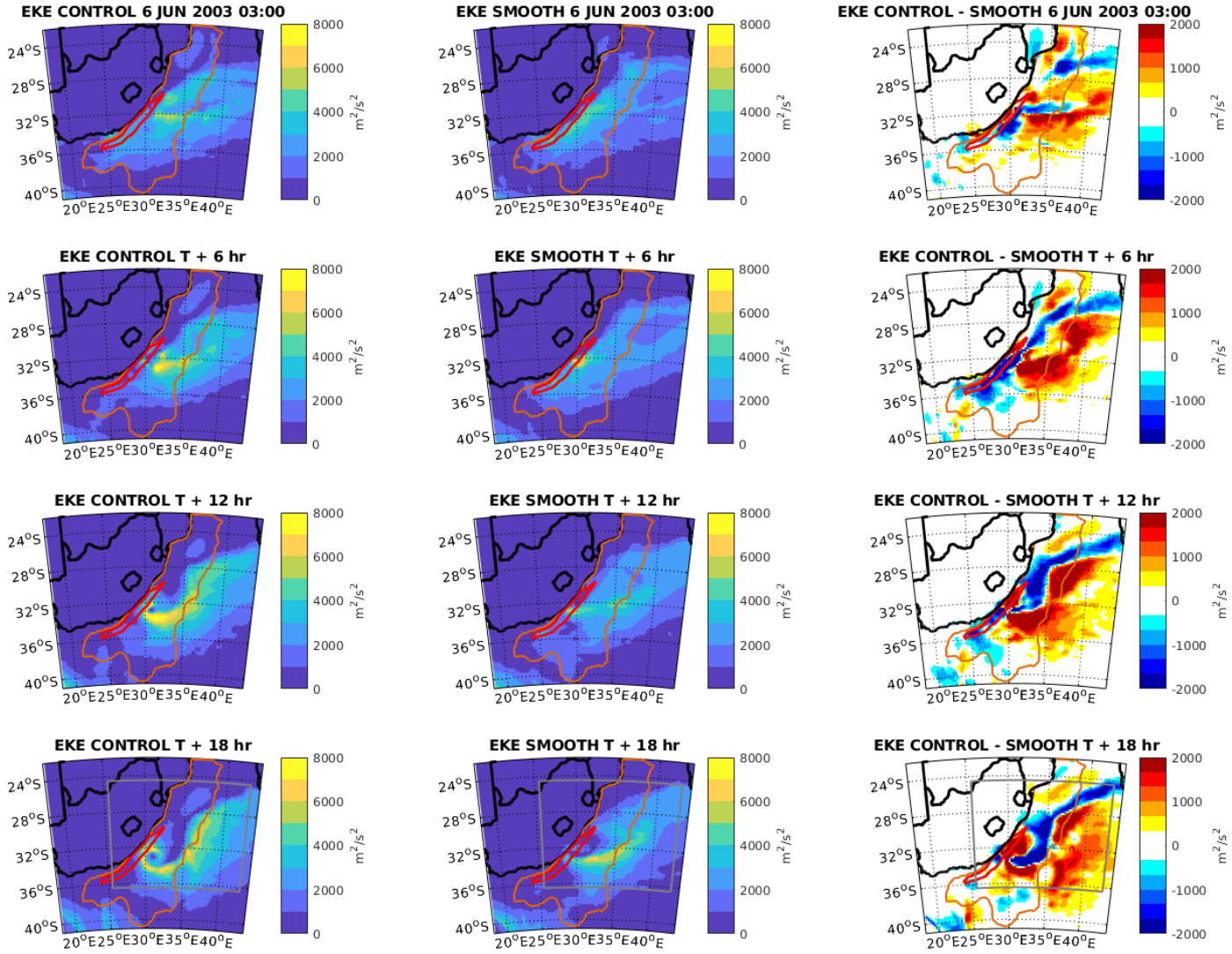

Figure 3.3.17: Storm A3. WRF model eddy kinetic energy up to 850mb level ($m^2.s^{-2}$). From top to bottom: 6 June 03:00, 6 June 09:00, 6 June 15:00 & 6 June 21:00. *(Left)* CTL simulation *(middle)* SMTH simulation & *(right)* Difference (CTL – SMTH). Orange boundary encloses area where SSTs are 0.25 - 1°C warmer in CTL simulation. Red boundary encloses area where SSTs are > 1°C warmer in CTL simulation. *(Bottom)* Grey box encloses developed storm.

Figure 3.3.18 indicates sustained high surface turbulent moisture fluxes over the storm's location in the CTL run, however fluxes decrease in the SMTH run. The vorticity of the developed storm can be observed at 6 June 2003 21:00 in the CTL run.

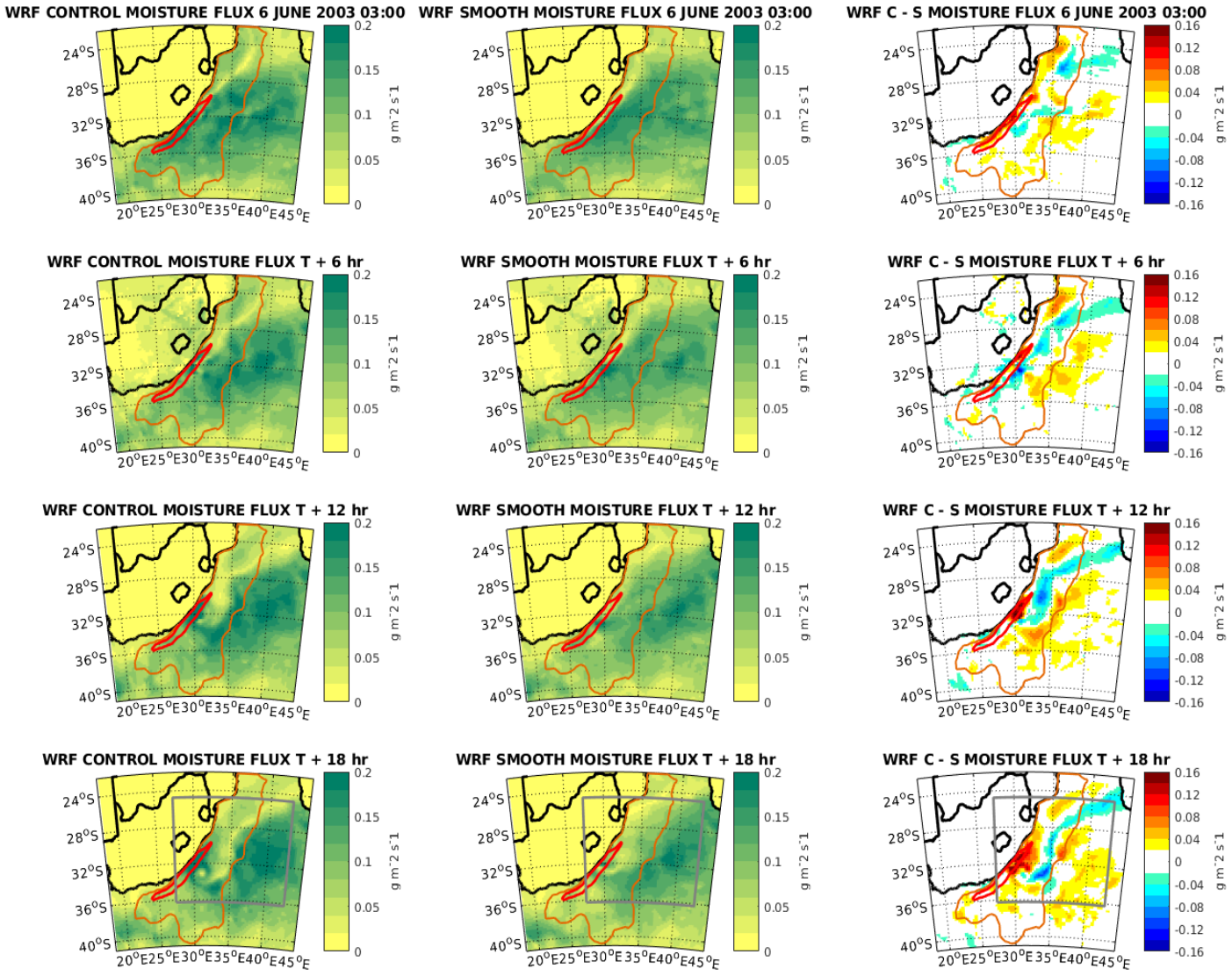

Figure 3.3.18: Storm A3. WRF model surface turbulent moisture flux ($g.m^{-2}.s^{-1}$). From top to bottom: 6 June 03:00, 6 June 09:00, 6 June 15:00 & 6 June 21:00. *(Left)* CTL simulation *(middle)* SMTH simulation & *(right)* Difference (CTL – SMTH). Orange boundary encloses area where SSTs are 0.25 - 1°C warmer in CTL simulation. Red boundary encloses area where SSTs are > 1°C warmer in CTL simulation. *(Bottom)* Grey box encloses developed storm.

Table 3.3.3 shows that a deeper (- 13.2 ± 5.03 m) developed storm was modelled in the CTL run. Higher rainfall intensity (+ 0.07 ± 1.461 mm.hr^{-}), higher surface wind speeds (+ 0.76 ± 0.992 m.s^{-1}), greater storm energy (+ 359 ± 540.4 m^2.s^{-2}) and higher surface turbulent moisture fluxes (+ 0.013 ± 0.0095 g.m^{-2}.s^{-1}) were all found for the developed storm over the Agulhas Current. The standard deviations are larger than the mean difference for all but two variables.

WRF VARIABLE	AVERAGE DIFFERENCE
850mb geopotential height	**- 13.2 ± 5.03 m**
Surface rain rate	**+ 0.07 ± 1.461 mm.hr^{-1}**
Surface wind speed	**+ 0.76 ± 0.992 m.s^{-1}**
Eddy kinetic energy (EKE)	**+ 359 ± 540.4 m^2.s^{-2}**
Surface turbulent moisture flux	**+ 0.013 ± 0.0095 g.m^{-2}.s^{-1}**

Table 3.3.3: Storm A3: 5 – 7 June 2003. Average difference (CTL – SMTH) values for five WRF model variables. Values are for developed storm bounded by grey box. Standard deviations for average values are included.

3.4 Category B storms

Mid-latitude cyclones frequently pass over South Africa, particularly in the winter months (May – September). These were the second type of weather features identified showing intensification evolution patterns. Up to 90% of rainfall in mid-latitude storm tracks are associated with fronts (Catto et. al 2012) and these cold fronts generally sweep over the South African landmass in the winter. These cold fronts as well as the cyclone centres were analysed comparatively. These systems are much larger than the other two types of storms identified and have a very predictable track path of approaching the current region from southwest and propagating away to the southeast.

Storm B1: 8 – 11 September 2002

Figure 3.4.1 shows a cold front approaching South Africa from the west on the 8th September 2002 with a shallow coastal low in front of it *(Top left).* Over the next two days the mid-latitude cyclone migrates eastward over the country with a cold front sweeping through the interior *(Top right, bottom left).* The centre of the storm is located close to the coastline whilst the cold front is over land but eventually moves offshore on the 11th *(Bottom right).* A slight deepening of the storm is observed once the centre of the cyclone moves eastward towards Port Elizabeth as the centre isobar decreases from 1008 hPa on the 8th September to 1004 hPa on the 9th September. However, over the next 24 hours the storm intensifies dramatically with the centre isobar decreasing from 1004 hPa to 992 hPa on the 11th September.

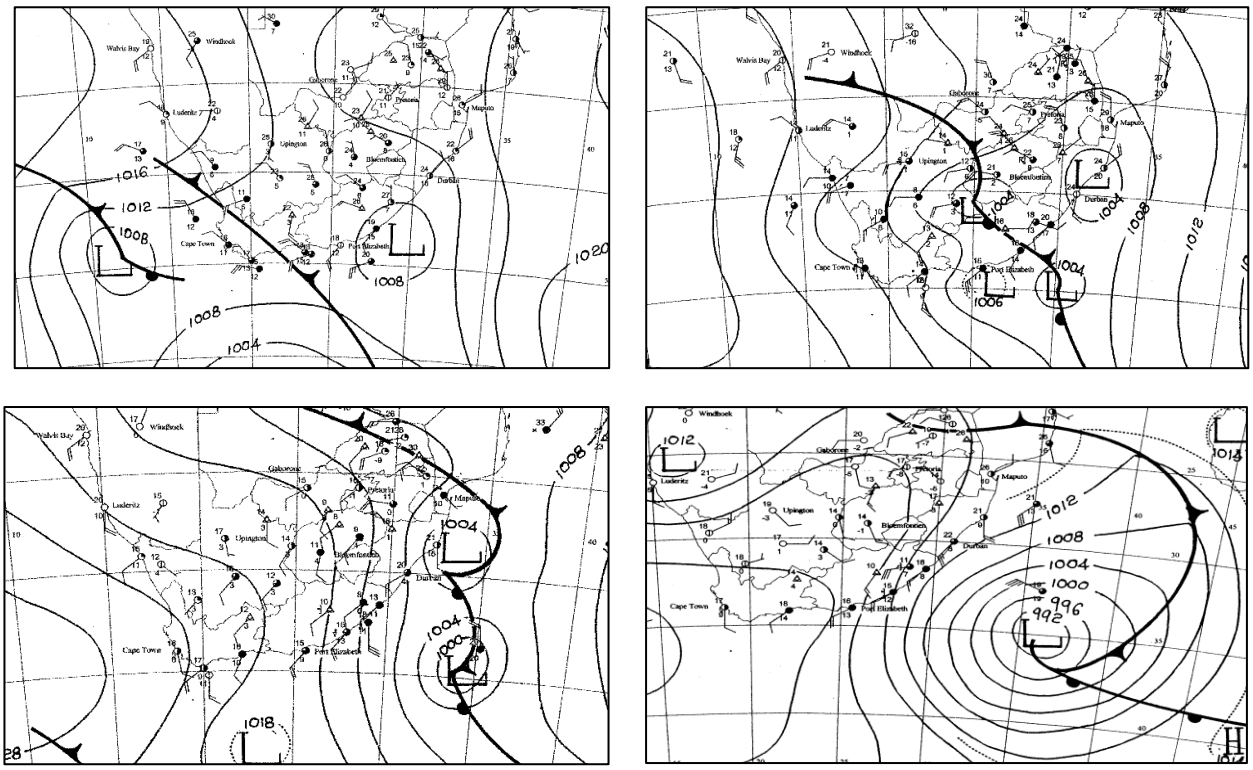

Figure 3.4.1: Storm B1. Surface synoptic conditions for *(Top left)* 8 September 2002 *(Top right)* 9 September 2002 *(Bottom Left)* 10 September 2002 & *(Bottom Right)* 11 September 2002. Charts were generated at 12h00 UTC.

On the 9th September the cyclone centre is modelled over the Agulhas core in both configurations as shown in Figure 3.4.2. Deepening of the system is found in both configurations as the system centre moves more offshore to the east. The degree of intensification between the two runs is virtually identical whilst the storm is centred over the Agulhas region.

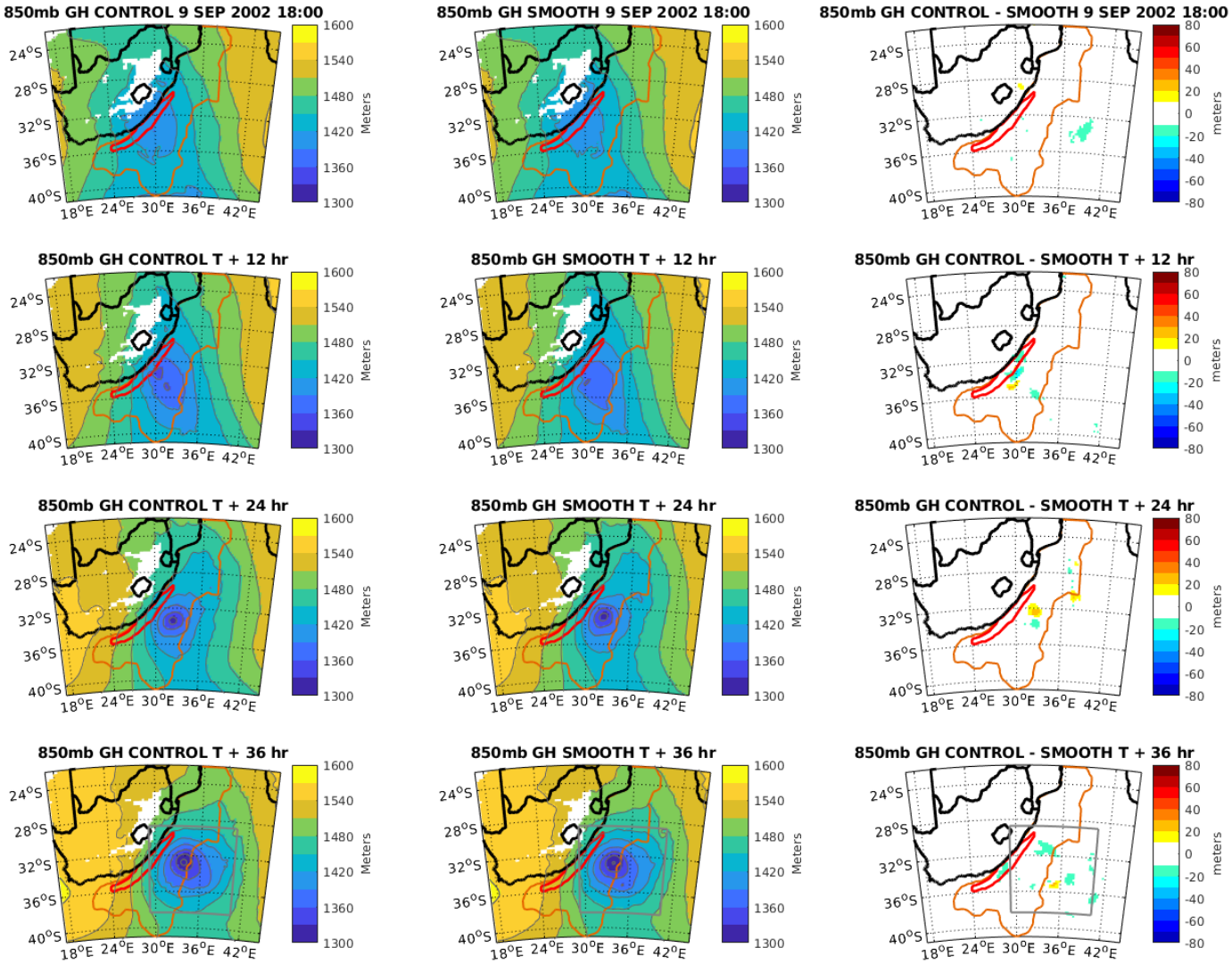

Figure 3.4.2: Storm B1. WRF model 850mb geopotential height (m). From top to bottom: 9 September 18:00; 10 September 06:00; 10 September 18:00 & 11 September 06:00. *(Left)* CTL simulation *(middle)* SMTH simulation & *(right)* Difference (CTL – SMTH). Orange boundary encloses area where SSTs are 0.25 - 1°C warmer in CTL simulation. Red boundary encloses area where SSTs are > 1°C warmer in CTL simulation. *(Bottom)* Grey box encloses developed storm.

Figure 3.4.3 shows contrasting rainfall patterns in both runs between the rainfall found at the centre of the storm and the rainfall produced along the cold front. Extending northeast from the storm centre, model rainfall along the cold front is found to increase in both runs as the front moves offshore and over the northern part of the Agulhas region. This rainfall then decreases once the cold front moves away from the Agulhas region. The opposite occurs for the rainfall found at the storm centre as rain rates decreases whilst the storm iss centred over the Current in both runs.

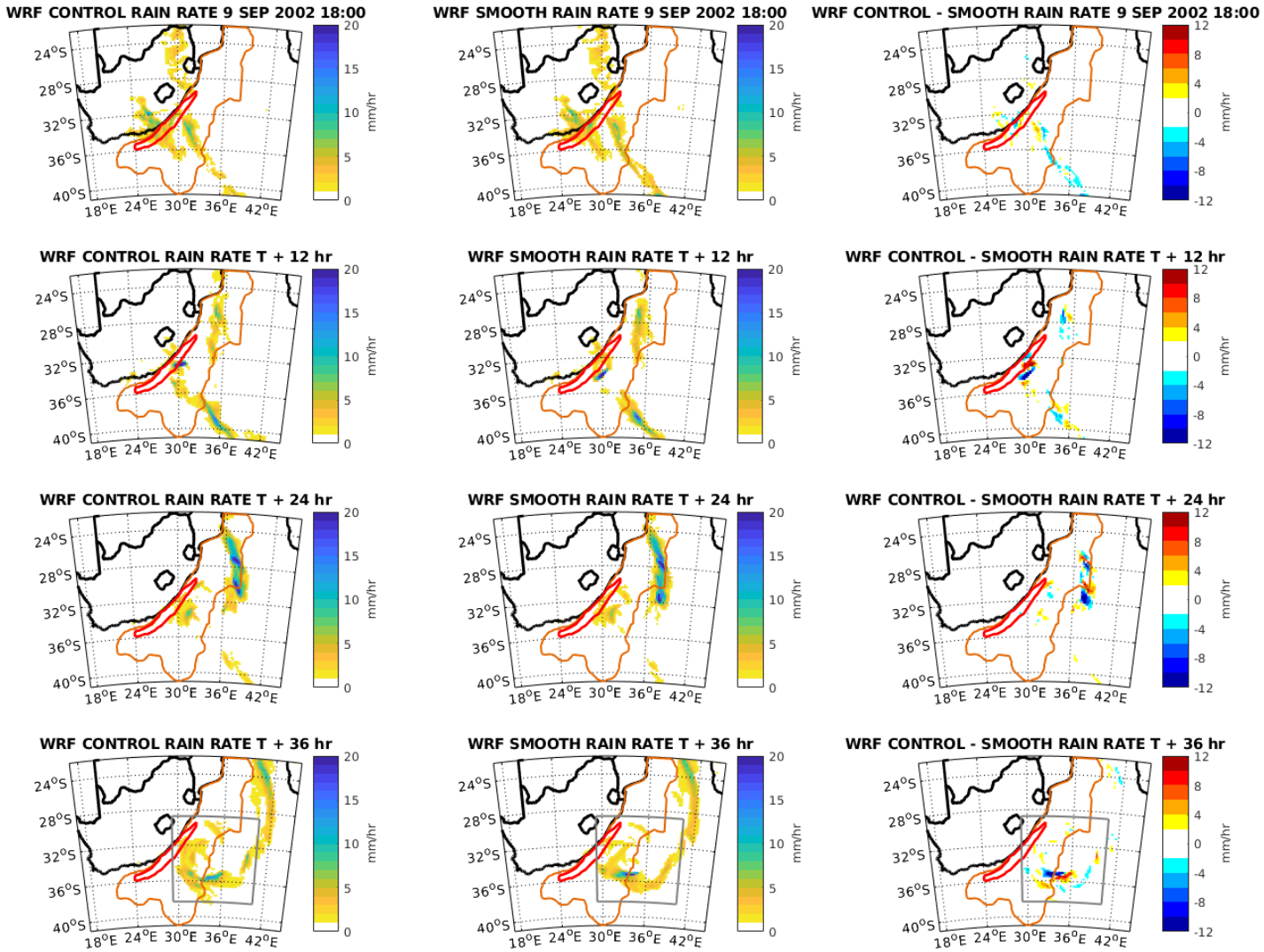

Figure 3.4.3: Storm B1. WRF model surface rain rate (mm.hr^{-1}). From top to bottom: 9 September 18:00; 10 September 06:00; 10 September 18:00 & 11 September 06:00. *(Left)* CTL simulation *(middle)* SMTH simulation & *(right)* Difference (CTL – SMTH). Orange boundary encloses area where SSTs are 0.25 - 1°C warmer in CTL simulation. Red boundary encloses area where SSTs are > 1°C warmer in CTL simulation. *(Bottom)* Grey box encloses developed storm.

Figure 3.4.4 indicates surface wind speeds increase in both runs as the system tracks over the Current region with high maximum wind speeds occurring close to the coastline. Similar intensification of wind speeds are found in both configurations.

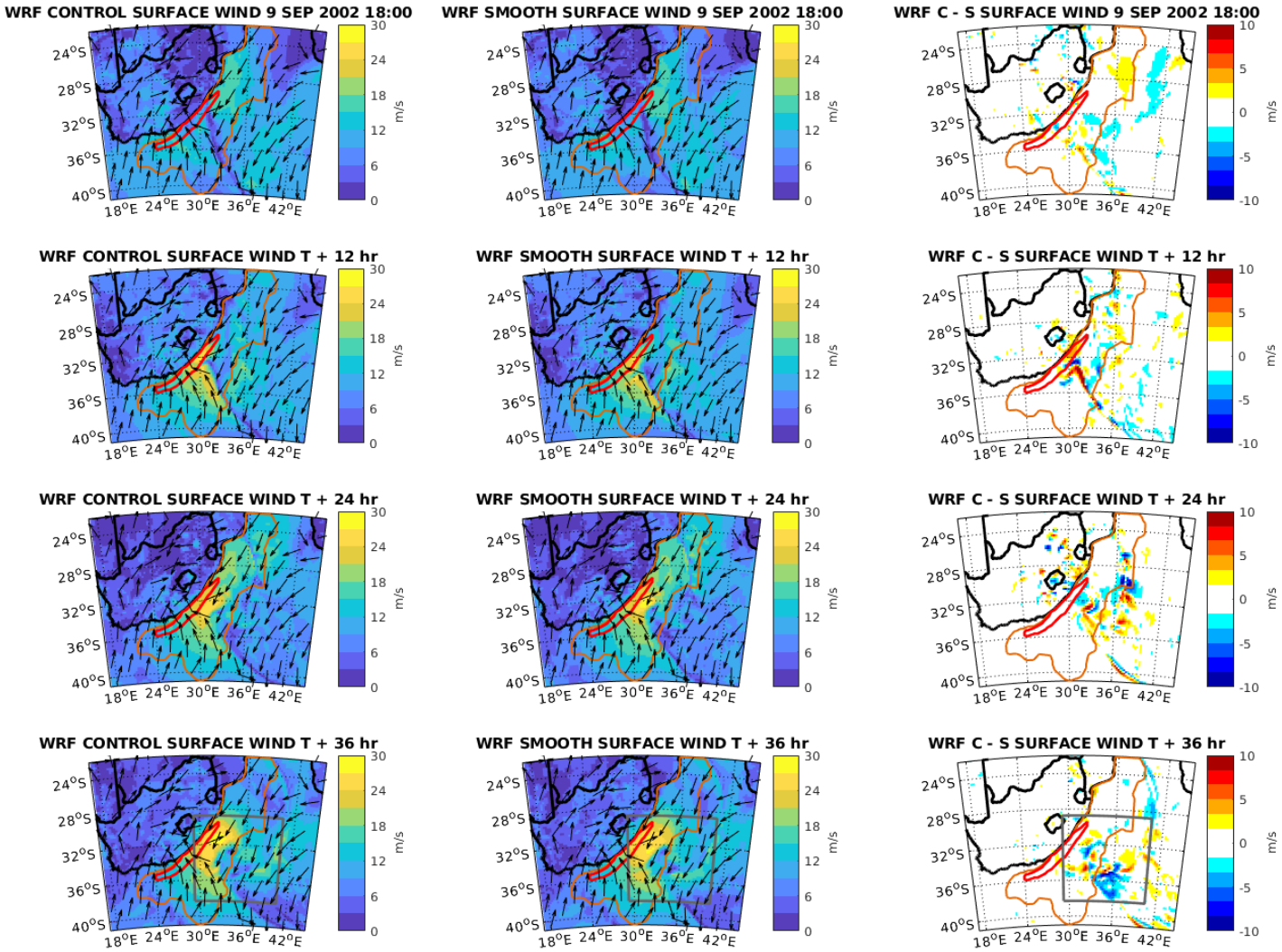

Figure 3.4.4: Storm B1. WRF model surface wind (m.s^{-1}). From top to bottom: 9 September 18:00; 10 September 06:00; 10 September 18:00 & 11 September 06:00. *(Left)* CTL simulation *(middle)* SMTH simulation & *(right)* Difference (CTL – SMTH). Black arrows indicate normalised surface wind vectors. Orange boundary encloses area where SSTs are 0.25 - 1°C warmer in CTL simulation. Red boundary encloses area where SSTs are > 1°C warmer in CTL simulation. *(Bottom)* Grey box

Figure 3.4.5 shows model storm energy increasing in both configurations with both runs showing a similar degree of intensification. However, the intensification occurs more directly over the northern region of the Agulhas core in both runs.

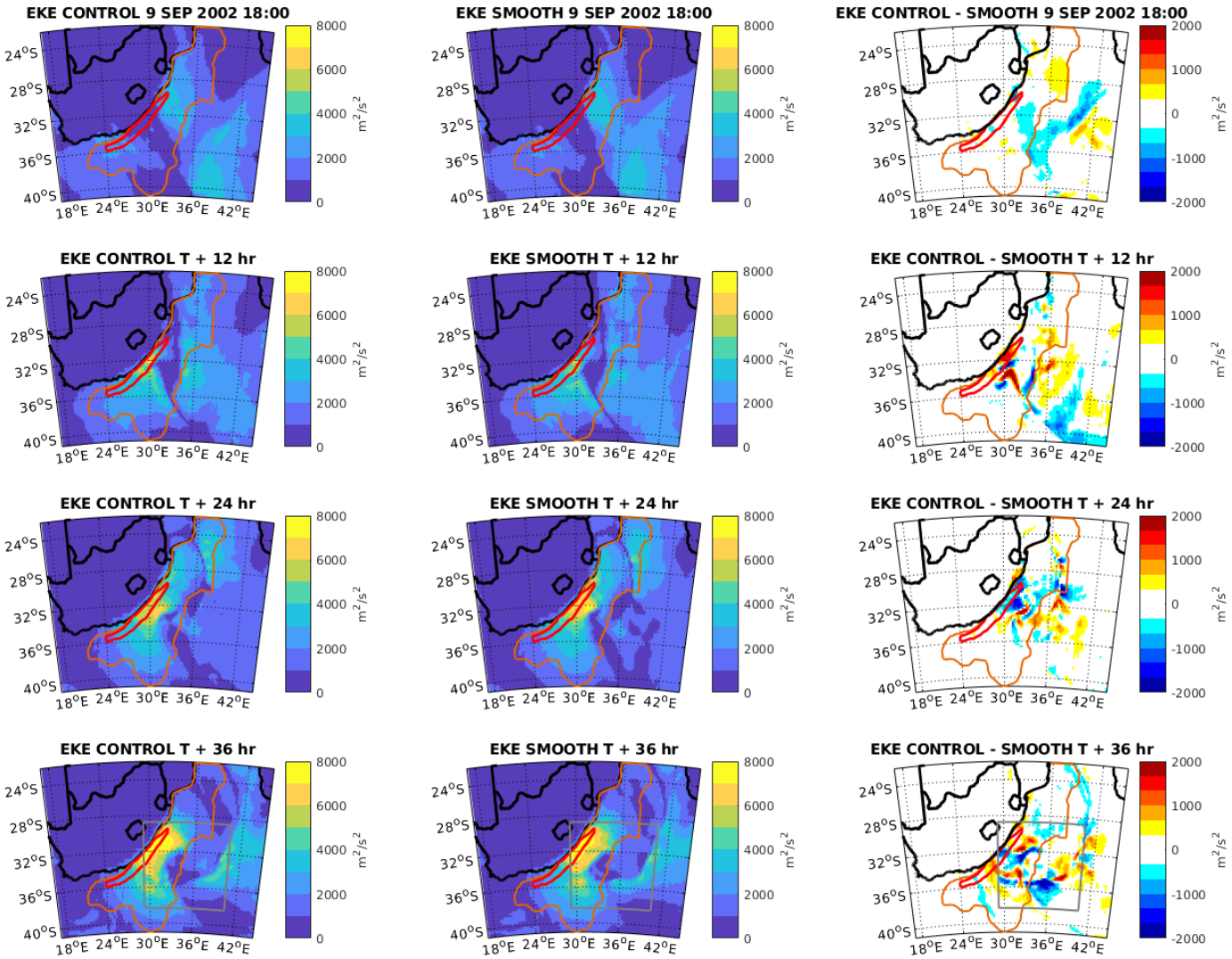

Figure 3.4.5: Storm B1. WRF model eddy kinetic energy up to 850mb level ($m^2.s^{-2}$). From top to bottom: 9 September 18:00; 10 September 06:00; 10 September 18:00 & 11 September 06:00. *(Left)* CTL simulation *(middle)* SMTH simulation & *(right)* Difference (CTL – SMTH). Orange boundary encloses area where SSTs are 0.25 - 1°C warmer in CTL simulation. Red boundary encloses area where SSTs are > 1°C warmer in CTL simulation. *(Bottom)* Grey box encloses developed storm.

Figure 3.4.6 shows increasing surface turbulent moisture fluxes over the Agulhas core and surrounding ocean waters however fluxes at the cyclone's centre remain low throughout the storm's propagation in both runs.

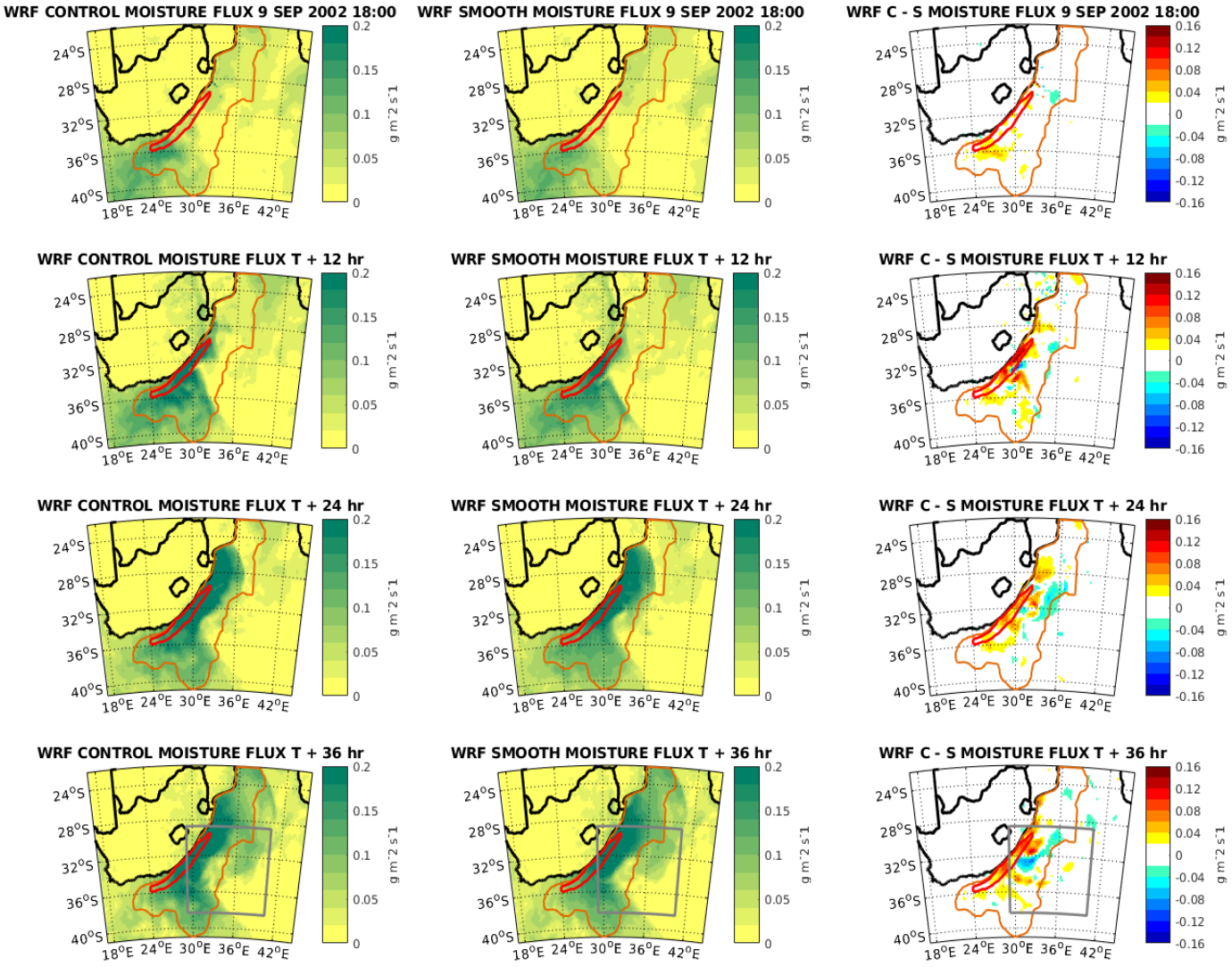

Figure 3.4.6: Storm B1. WRF model surface turbulent moisture flux ($g.m^{-2}.s^{-1}$). From top to bottom: 9 September 18:00; 10 September 06:00; 10 September 18:00 & 11 September 06:00. *(Left)* CTL simulation *(middle)* SMTH simulation & *(right)* Difference (CTL – SMTH). Orange boundary encloses area where SSTs are 0.25 - 1°C warmer in CTL simulation. Red boundary encloses area where SSTs are > 1°C warmer in CTL simulation. *(Bottom)* Grey box encloses developed storm.

Table 3.4.1 indicates that a deeper (- 2.8 ± 1.46 m) developed storm was modelled in the CTL run. Higher rainfall intensity (+ 0.08 ± 1.251 $mm.hr^{-1}$), lower surface wind speeds (- 0.07 ± 0.601 $m.s^{-1}$), lower storm energy (- 14 ± 218.1 $m^2.s^{-2}$) and higher surface turbulent moisture fluxes (+ 0.005 ± 0.0130 $g.m^{-2}.s^{-1}$) were all found for the developed storm over the Agulhas Current. The standard deviations are larger than the mean difference for all but one variable.

WRF VARIABLE	AVERAGE DIFFERENCE
850mb geopotential height	**- 2.8 ± 1.46 m**
Surface rain rate	**+ 0.08 ± 1.251 mm.hr^{-1}**
Surface wind speed	**- 0.07 ± 0.601 m.s^{-1}**
Eddy kinetic energy (EKE)	**- 14 ± 218.1 m^2.s^{-2}**
Surface turbulent moisture flux	**+ 0.005 ± 0.0130 g.m^{-2}.s^{-1}**

Table 3.4.1: Storm B1: 8 – 11 September 2002. Average difference (CTL – SMTH) values for five WRF model variables. Values are for developed storm bounded by grey box. Standard deviations for average values are included

Storm B2: 10 - 12 August 2003

A well-developed mid-latitude cyclone is located south of South Africa with a centre isobar pressure of 1000 hPa as shown in Figure 3.4.7. A cold front extends northeast but does not make landfall. The storm is observed to weaken as the centre surface pressure increases from 1000 hPa on the 10th August *(Top left)* to 1008 hPa on the 11th August *(Top right)* however the cold front is then observed to extend further inland. On next day the storm intensifies strongly as the storm centre isobar decreased from 1008 hPa to 992 hPa as the cyclone moves further east *(Bottom)*

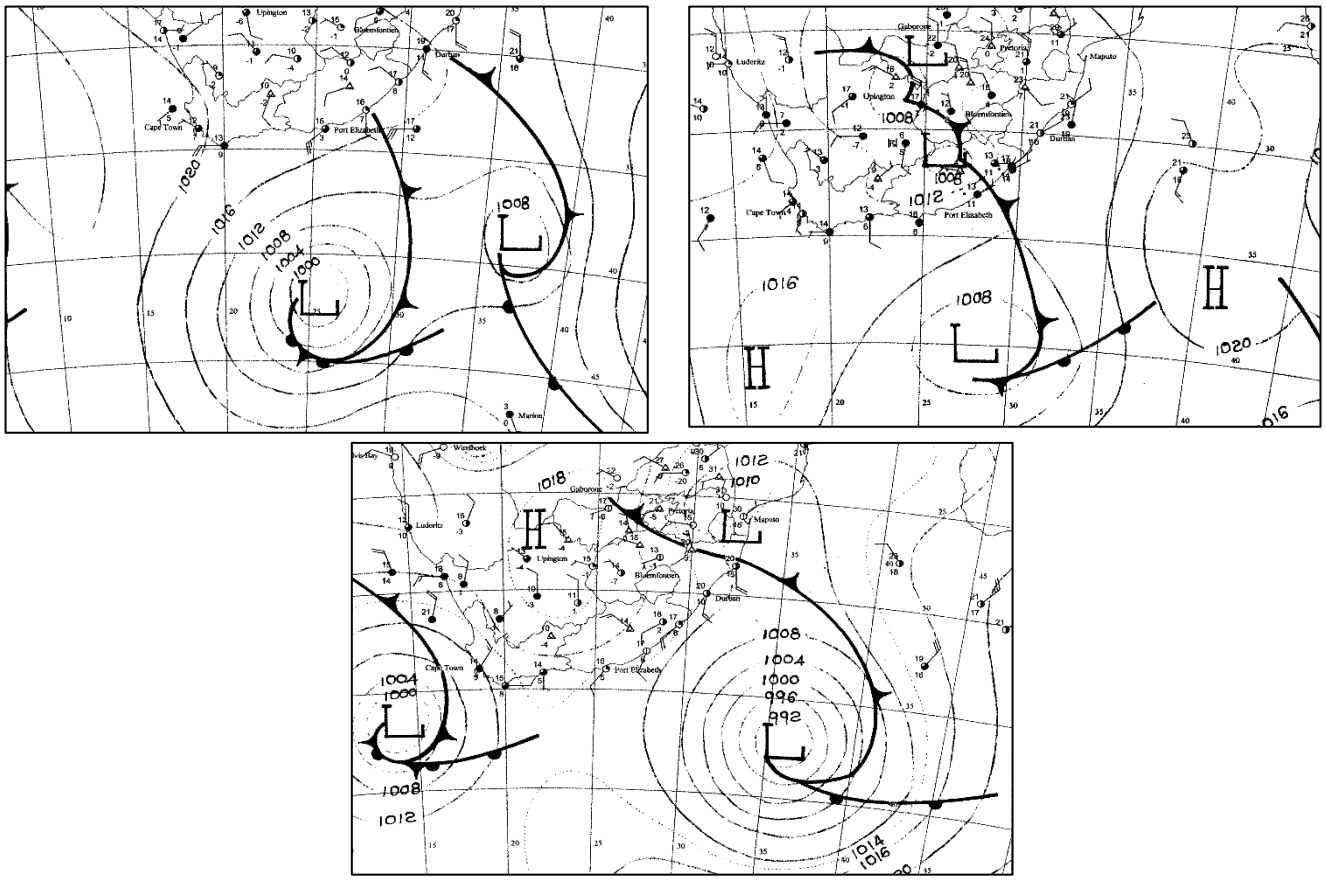

Figure 3.4.7: Storm B2. Surface synoptic conditions for *(Top left)* 10 August 2003 *(Top right)* 11 August 2003 & *(Bottom)* 12 August 2003. Charts were generated at 12h00 UTC.

Figure 3.4.8 indicates a deepening of the system centre as the cyclone tracks over the Agulhas core and then over the southern part of the Agulhas region in both simulations. The severity of intensification is nearly identical in both runs as shown in the difference plots *(right).*

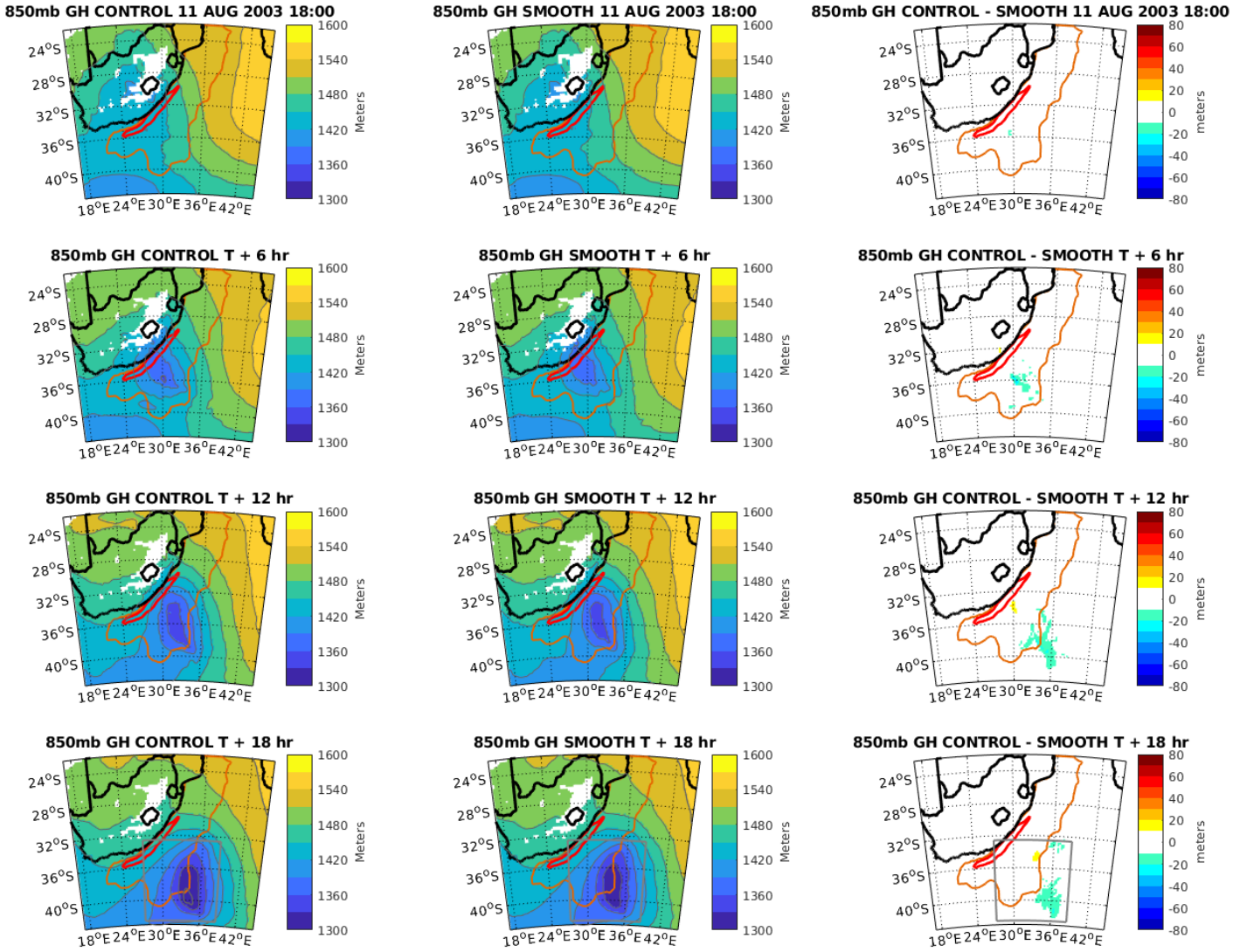

Figure 3.4.8: Storm B2. WRF model 850mb geopotential height (m). From top to bottom: 11 August 18:00; 12 August 00:00; 12 August 06:00 & 12 August 12:00. *(Left)* CTL simulation *(middle)* SMTH simulation & *(right)* Difference (CTL – SMTH). Orange boundary encloses area where SSTs are 0.25 - 1°C warmer in CTL simulation. Red boundary encloses area where SSTs are > 1°C warmer in CTL simulation. *(Bottom)* Grey box encloses developed storm.

Figure 3.4.9 indicates a slight increase in model rainfall when the cyclone is located over the Agulhas region in both runs. This rainfall then dissipates once the storm moves southeast away from the current region. Virtually no difference in evolution of the storm is found between the CTL and SMTH runs.

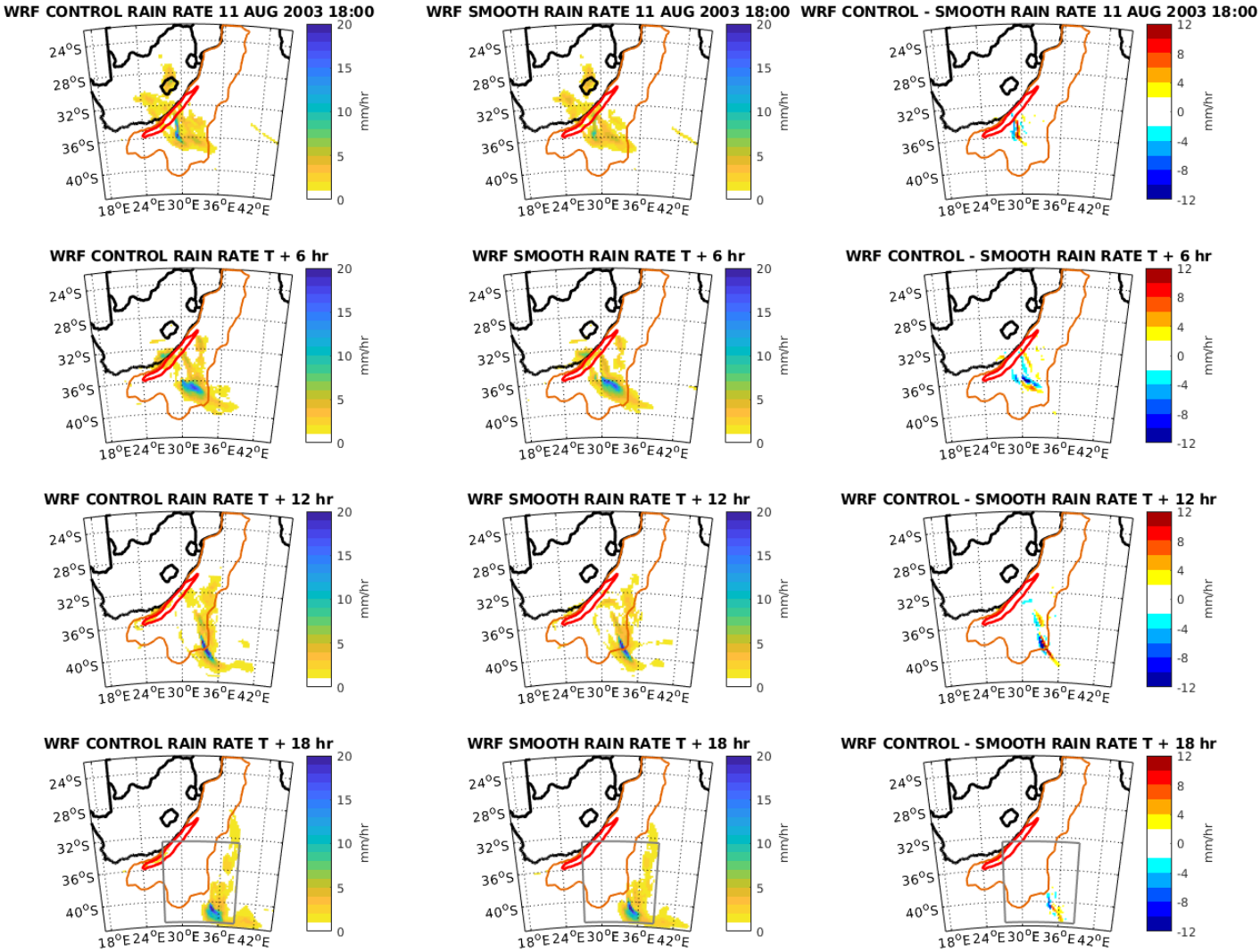

Figure 3.4.9: Storm B2. WRF model surface rain rate (mm.hr^{-1}). From top to bottom: 11 August 18:00; 12 August 00:00; 12 August 06:00 & 12 August 12:00. *(Left)* CTL simulation *(middle)* SMTH simulation & *(right)* Difference (CTL – SMTH). Orange boundary encloses area where SSTs are 0.25 - 1°C warmer in CTL simulation. Red boundary encloses area where SSTs are > 1°C warmer in CTL simulation. *(Bottom)* Grey box encloses developed storm.

Figure 3.4.10 shows a subtle increase in surface wind speeds throughout the system's propagation southeast over the Current region. A similar degree of intensification occurs in both configurations.

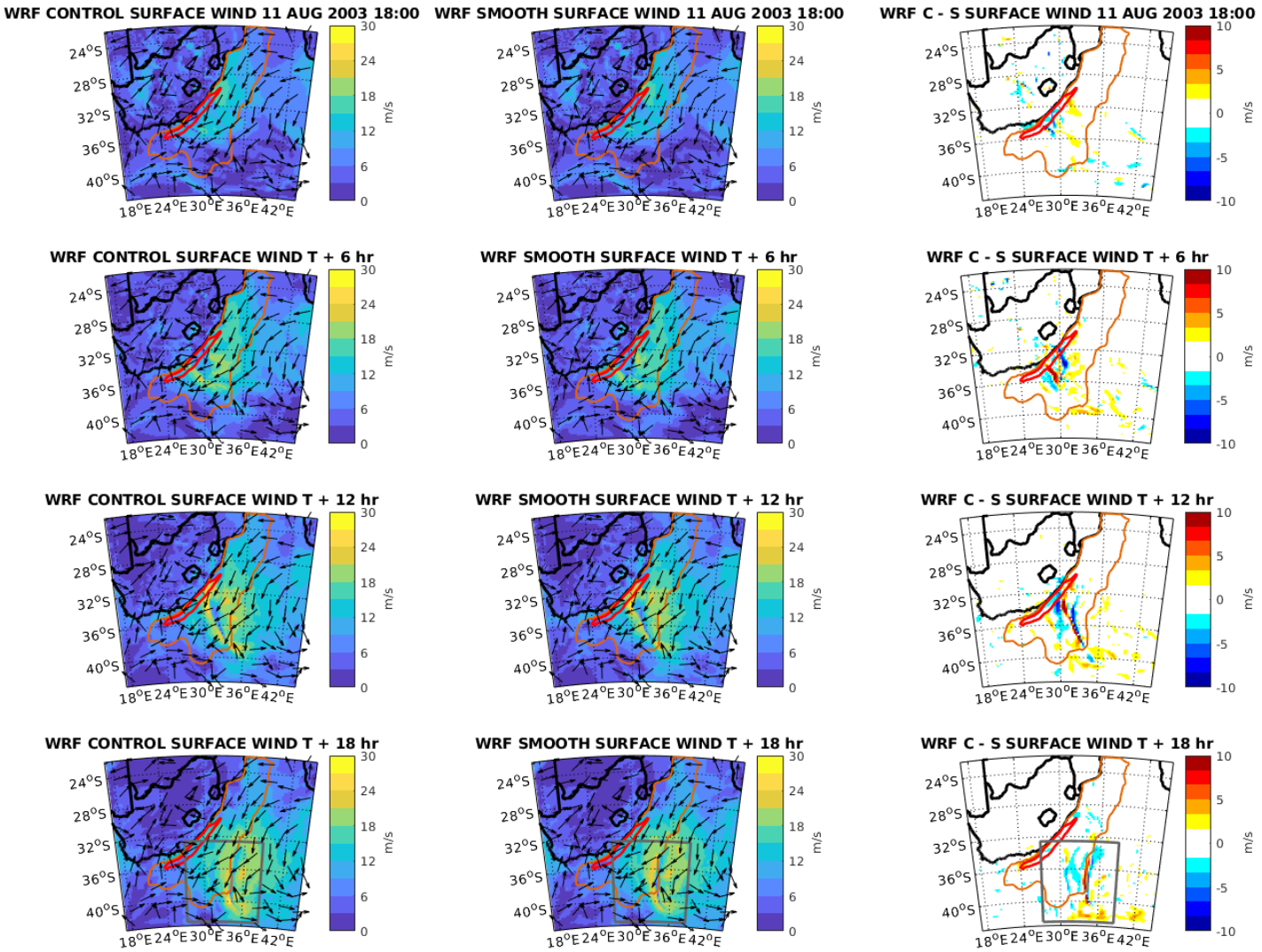

Figure 3.4.10: Storm B2. WRF model surface wind (m.s^{-1}). From top to bottom: 11 August 18:00; 12 August 00:00; 12 August 06:00 & 12 August 12:00. *(Left)* CTL simulation *(middle)* SMTH simulation & *(right)* Difference (CTL – SMTH). Orange boundary encloses area where SSTs are 0.25 - 1°C warmer in CTL simulation. Red boundary encloses area where SSTs are > 1°C warmer in CTL simulation. *(Bottom)* Grey box encloses developed storm.

Figure 3.4.11 shows a slight increase in storm EKE as the cyclone tracks southeast over the Current region. Little difference in storm evolution with regards to storm energy is modelled between the two configurations.

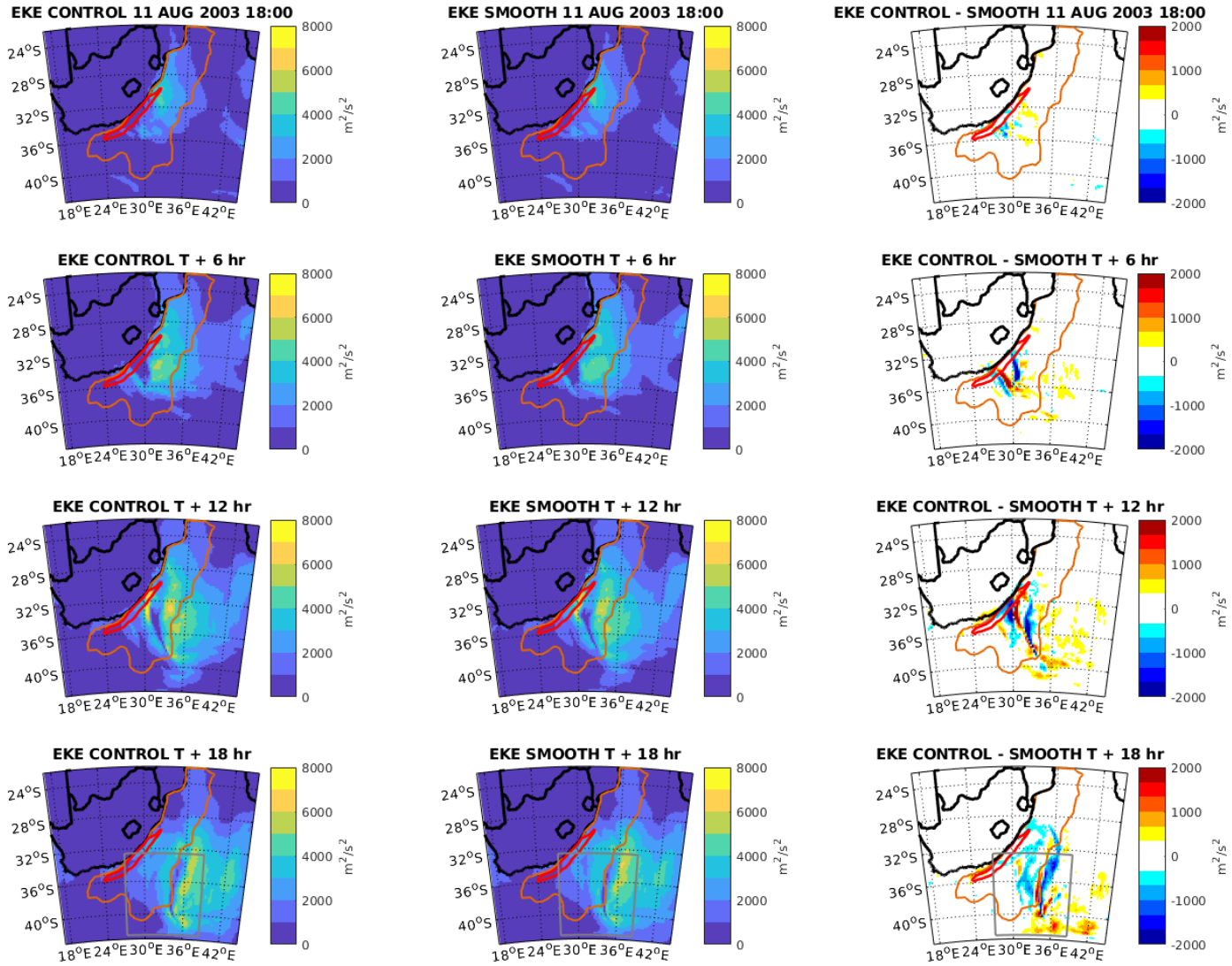

Figure 3.4.11: Storm B2. WRF model eddy kinetic energy up to 850mb level ($m^2.s^{-2}$). From top to bottom: 11 August 18:00; 12 August 00:00; 12 August 06:00 & 12 August 12:00. *(Left)* CTL simulation *(middle)* SMTH simulation & *(right)* Difference (CTL – SMTH). Orange boundary encloses area where SSTs are 0.25 - 1°C warmer in CTL simulation. Red boundary encloses area where SSTs are > 1°C warmer in CTL simulation. *(Bottom)* Grey box encloses developed storm.

Figure 3.4.12 shows surface turbulent moisture fluxes increasing gradually over the cyclone's location in both runs. High fluxes are found in both configurations for the developed cyclone.

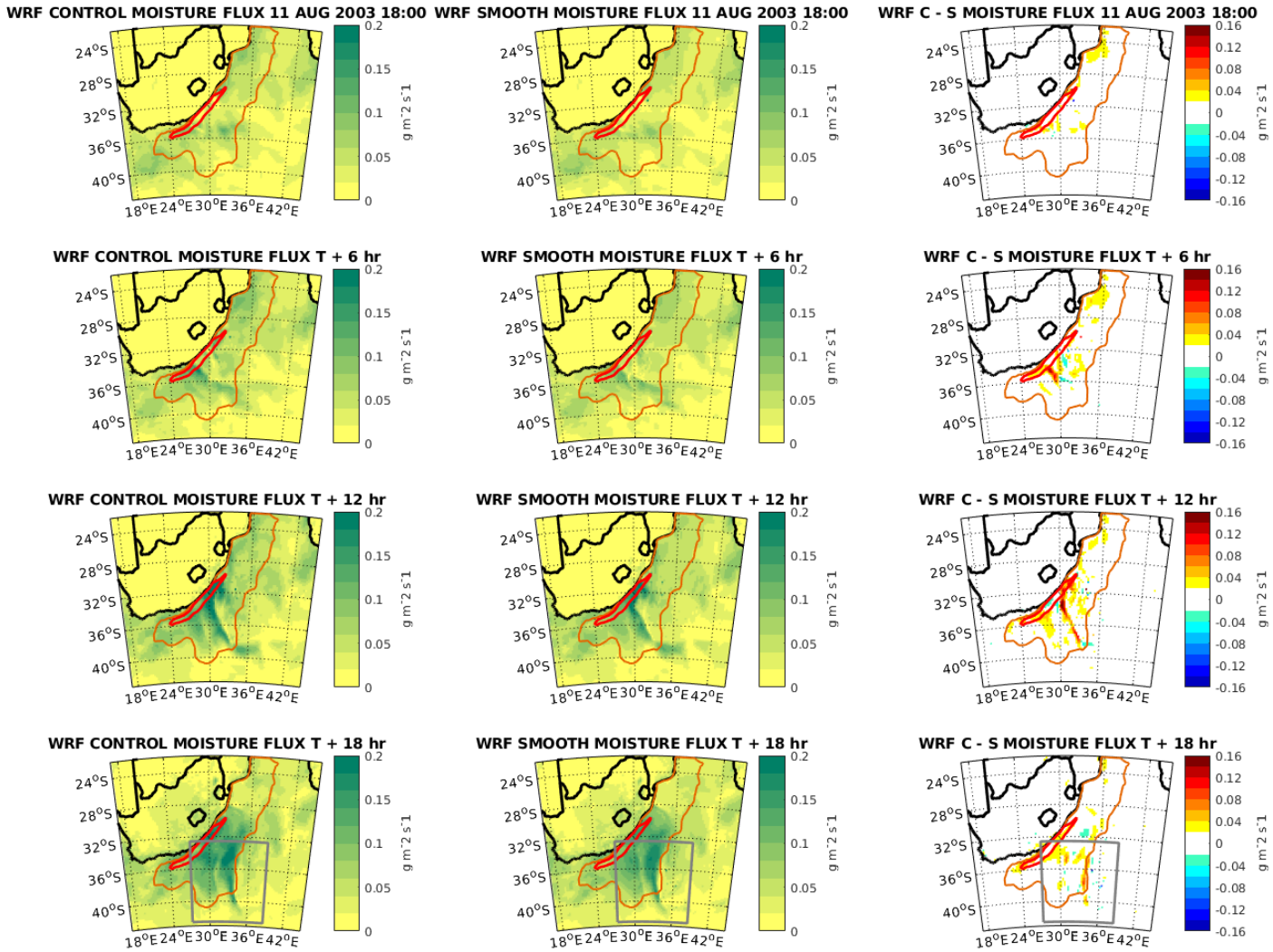

Figure 3.4.12: Storm B2. WRF model surface turbulent moisture flux ($g.m^{-2}.s^{-1}$). From top to bottom: 11 August 18:00; 12 August 00:00; 12 August 06:00 & 12 August 12:00. *(Left)* CTL simulation *(middle)* SMTH simulation & *(right)* Difference (CTL – SMTH). Orange boundary encloses area where SSTs are 0.25 - 1°C warmer in CTL simulation. Red boundary encloses area where SSTs are > 1°C warmer in CTL simulation. *(Bottom)* Grey box encloses developed storm.

Table 3.4.2 shows that a deeper (- 2.2 ± 0.71 m) developed storm was modelled in the CTL run. Lower rainfall intensity (- 0.01 ± 0.581 $mm.hr^{-1}$), higher surface wind speeds (+ 0.07 ± 0.921 $m.s^{-1}$), lower storm energy (- 19 ± 105.3 $m^2.s^{-2}$) and higher surface turbulent moisture fluxes (+ 0.004 ± 0.0051 $g.m^{-2}.s^{-1}$) were all found for the developed storm over the Agulhas Current. The standard deviations are larger than the mean difference for all but one variable.

WRF VARIABLE	AVERAGE DIFFERENCE
850mb geopotential height	**- 2.2 ± 0.71 m**
Surface rain rate	**- 0.01 ± 0.581 mm.hr^{-1}**
Surface wind speed	**+ 0.07 ± 0.921 m.s^{-1}**
Eddy kinetic energy (EKE)	**- 19 ± 105.3 m^2.s^{-2}**
Surface turbulent moisture flux	**+ 0.004 ± 0.0051 g.m^{-2}.s^{-1}**

Table 3.4.2: Storm B2: 10 – 12 August 2003. Average difference (CTL – SMTH) values for five WRF model variables. Values are for developed storm bounded by grey box. Standard deviations for average values are included

Storm B3: 28 – 30 May 2005

The synoptic evolution of the final category B storm is shown in Figure 3.6. On the 28th May, a cold front propagates towards the South African west coast with a storm centre of 1008 hPa *(Top left).* As the cold front sweeps through the interior the following day, the cyclone centre is observed to intensify slightly as the centre surface pressure decreases to 1004 hPa over the Agulhas core *(Top right).* Over the next 24 hours the system is sustained as the centre isobar remains at 1004 hPa as the cyclone tracks further offshore to the southeast *(Bottom).*

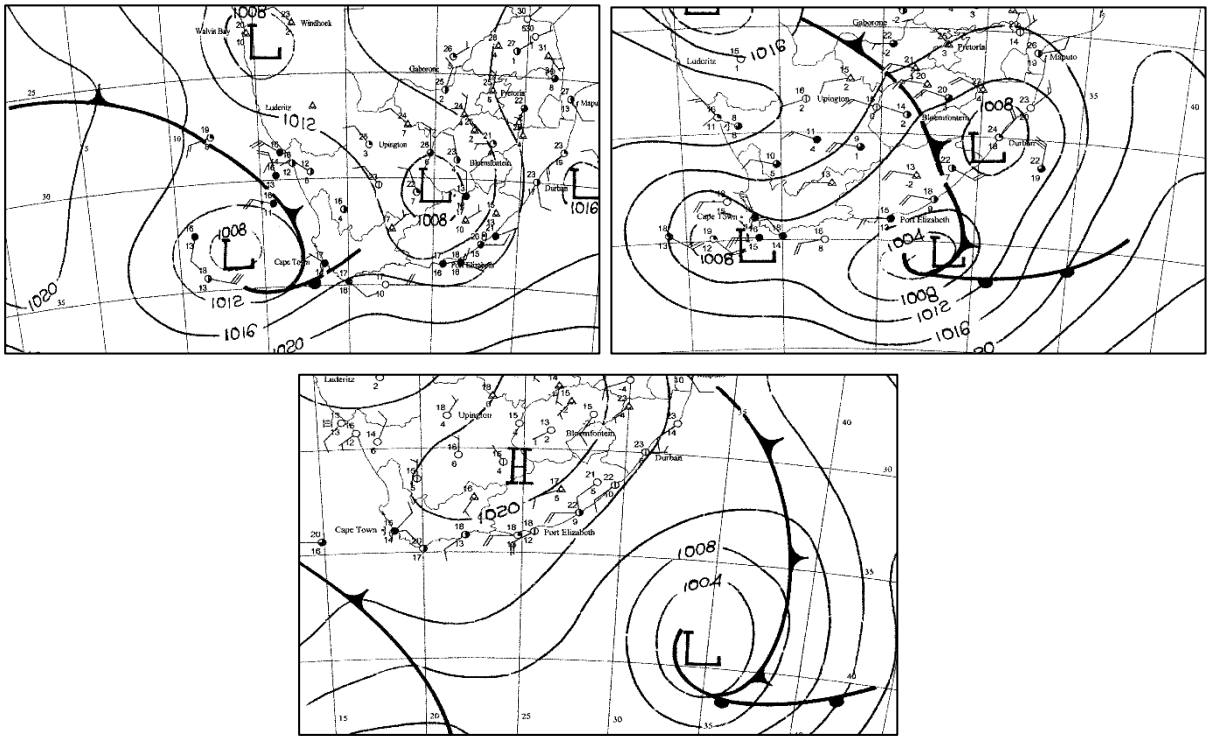

Figure 3.4.13: Storm B3. Surface synoptic conditions for *(Top left)* 28 May 2005 *(Top right)* 29 May 2005 & *(Bottom)* 30 May 2005. Charts were generated at 12h00 UTC.

The cyclone centre is found to track over the southern part of the Agulhas region in both configurations as shown in Figure 3.4.14. Whilst centred over the Current region, a slight deepening of the storm is modelled in both configurations.

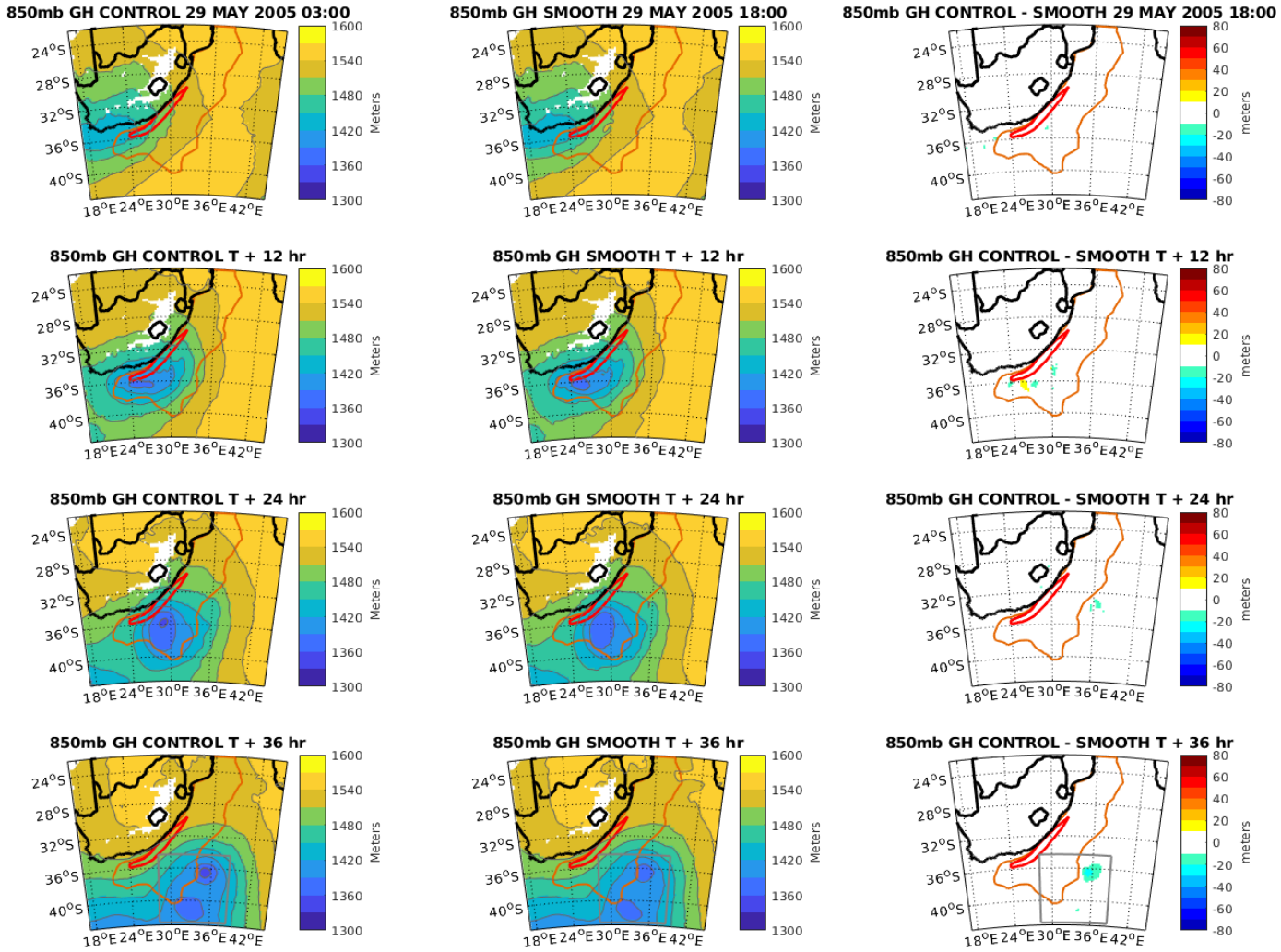

Figure 3.4.14: Storm B3. WRF model 850mb geopotential height (m). From top to bottom: 29 May 03:00; 29 May 15:00; 30 May 03:00 & 30 May 15:00. *(Left)* CTL simulation *(middle)* SMTH simulation & *(right)* Difference (CTL – SMTH). Orange boundary encloses area where SSTs are 0.25 - 1°C warmer in CTL simulation. Red boundary encloses area where SSTs are > 1°C warmer in CTL simulation. *(Bottom)* Grey box encloses developed storm.

Most of the model rainfall produced by the storm is located along the cold front as indicated in Figure 3.4.15. Rainfall is sustained in both runs when the cyclone centre is located over the southern region of the Agulhas Current. However, once the system moves further southeast, rain rates decrease along the cold front.

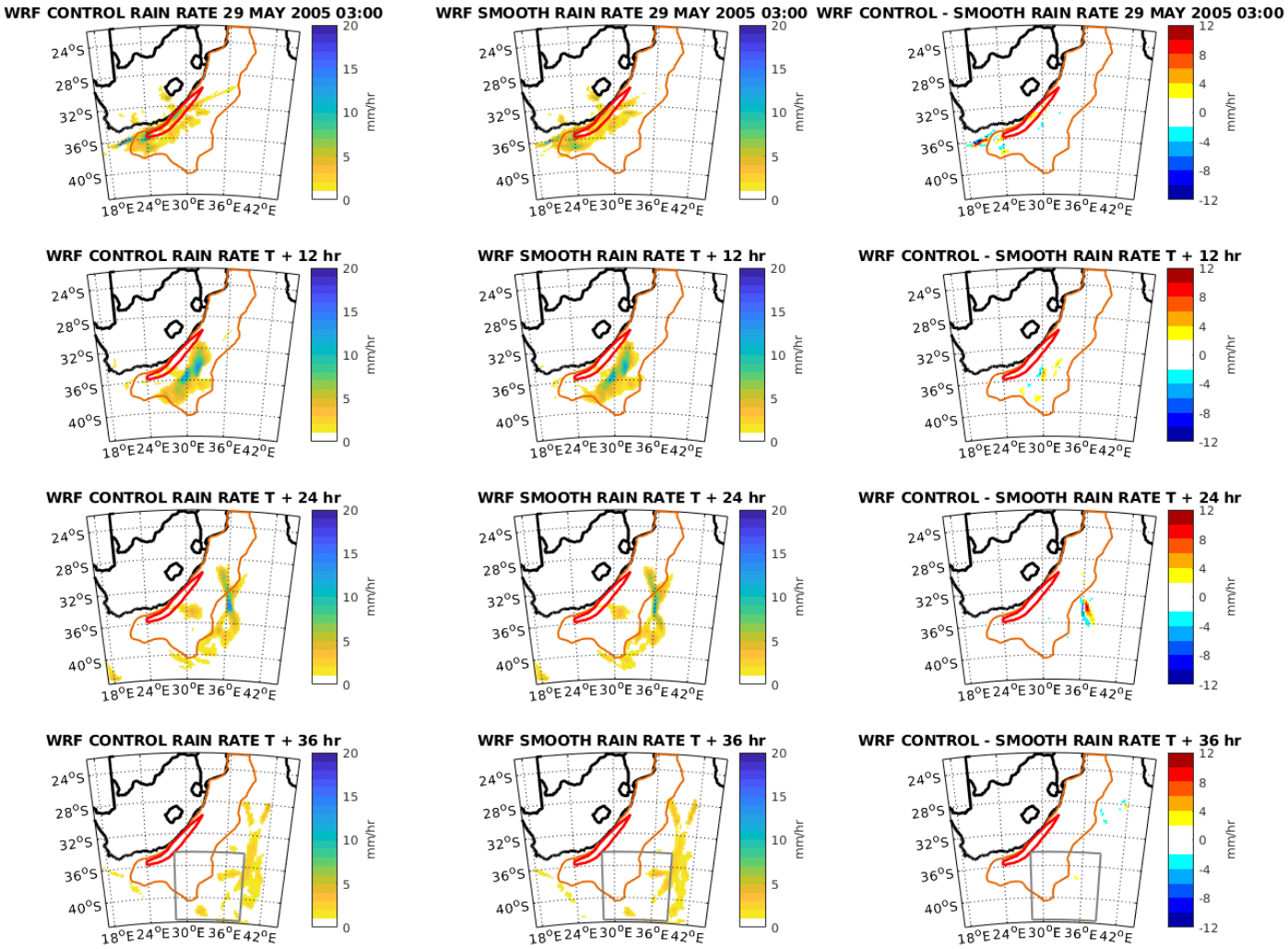

Figure 3.4.15: Storm B3. WRF model surface rain rate (mm.hr^{-1}). From top to bottom: 29 May 03:00; 29 May 15:00; 30 May 03:00 & 30 May 15:00. *(Left)* CTL simulation *(middle)* SMTH simulation & *(right)* Difference (CTL – SMTH). Orange boundary encloses area where SSTs are 0.25 - 1°C warmer in CTL simulation. Red boundary encloses area where SSTs are > 1°C warmer in CTL simulation. *(Bottom)* Grey box encloses developed storm.

Figure 3.4.16 shows the changes in surface wind for this cyclone. Increasing surface winds are found as the storm centre moves over the Agulhas region followed by a weakening of these winds as the cyclone moves further southeast away from the Current region. Similar evolution patterns are modelled in both runs.

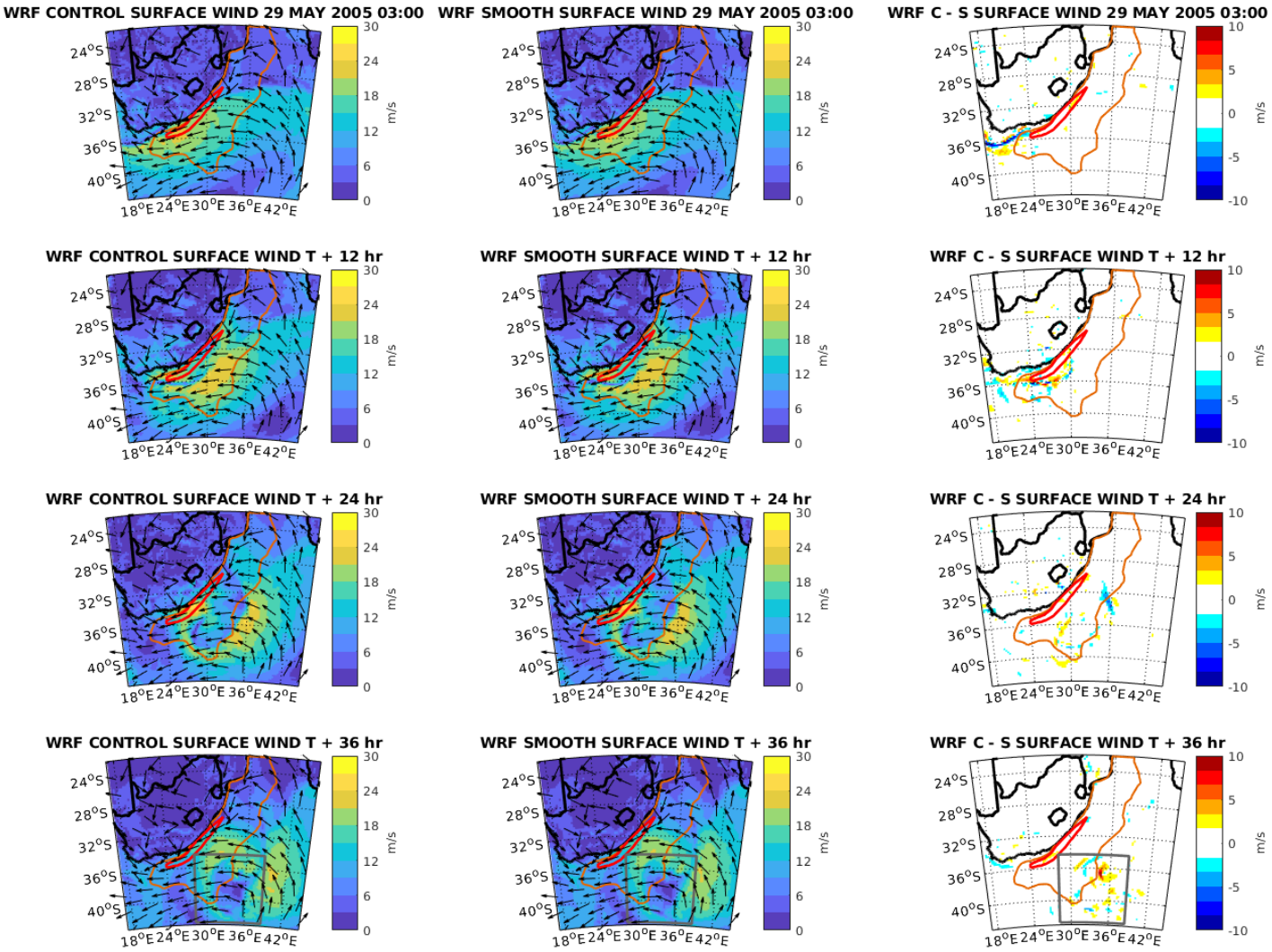

Figure 3.4.16: Storm B3. WRF model surface wind (m.s^{-1}). From top to bottom: 29 May 03:00; 29 May 15:00; 30 May 03:00 & 30 May 15:00. *(Left)* CTL simulation *(middle)* SMTH simulation & *(right)* Difference (CTL – SMTH). Orange boundary encloses area where SSTs are 0.25 - 1°C warmer in CTL simulation. Red boundary encloses area where SSTs are > 1°C warmer in CTL simulation. *(Bottom)* Grey box encloses developed storm.

Figure 3.4.17 shows when the storm is located over the southern part of the current region, storm EKE increases in both runs. Storm energy then decreases as the system moves away from the Current. Nearly identical developed cyclones are found in both runs.

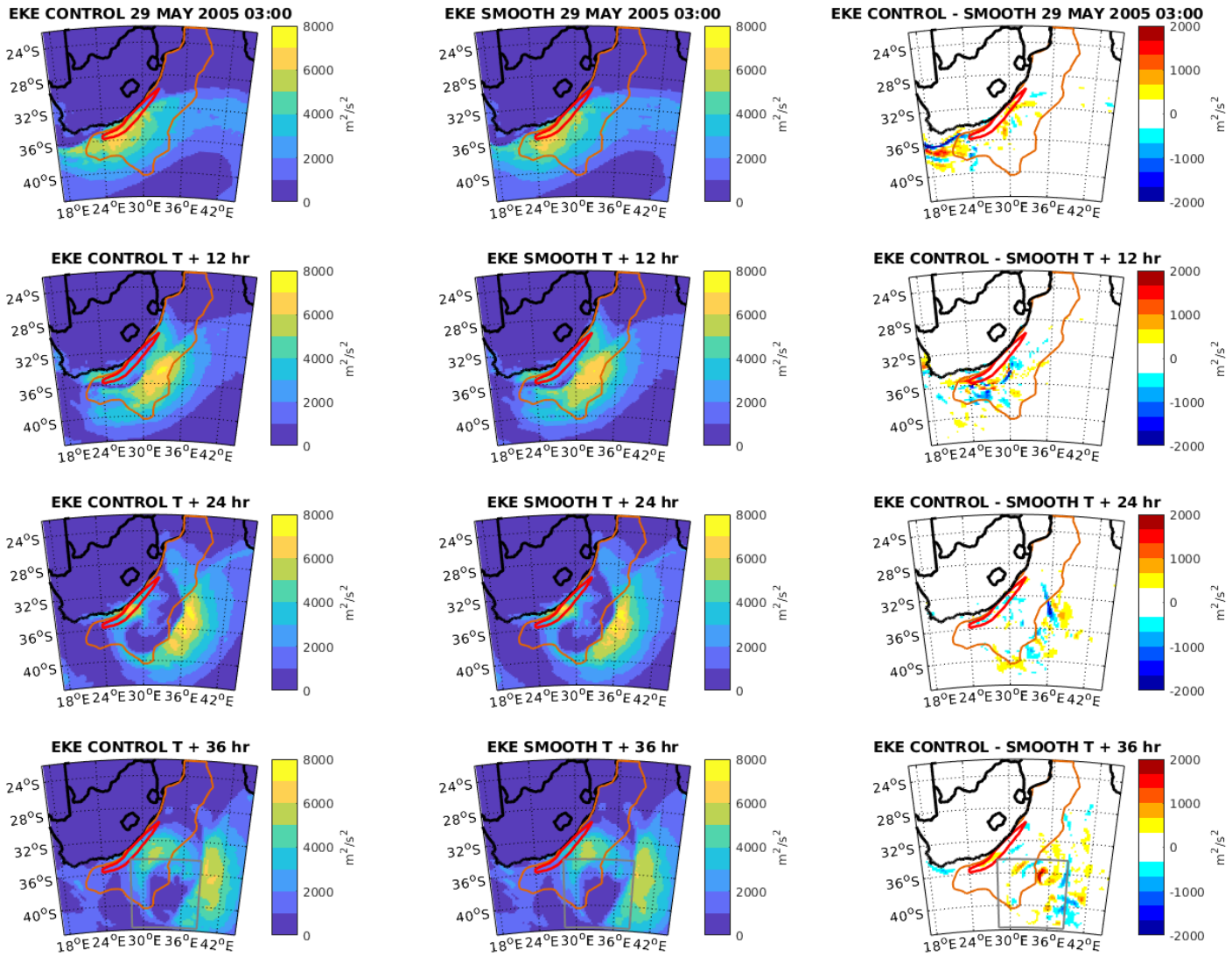

Figure 3.4.17: Storm B3. WRF model eddy kinetic energy up to 850mb level ($m^2.s^{-2}$). From top to bottom: 29 May 03:00; 29 May 15:00; 30 May 03:00 & 30 May 15:00. *(Left)* CTL simulation *(middle)* SMTH simulation & *(right)* Difference (CTL – SMTH). Orange boundary encloses area where SSTs are 0.25 - 1°C warmer in CTL simulation. Red boundary encloses area where SSTs are > 1°C warmer in CTL simulation. *(Bottom)* Grey box encloses developed storm.

Figure 3.4.18 shows high surface turbulent moisture fluxes when the cyclone starts to move over the Current at 12 August 2005 12:00 in both runs. These fluxes then decrease whilst the cyclone moves over the Current region and eventually further out to sea. Similar fluxes are found for the developed cyclone in both the CTL and SMTH configurations.

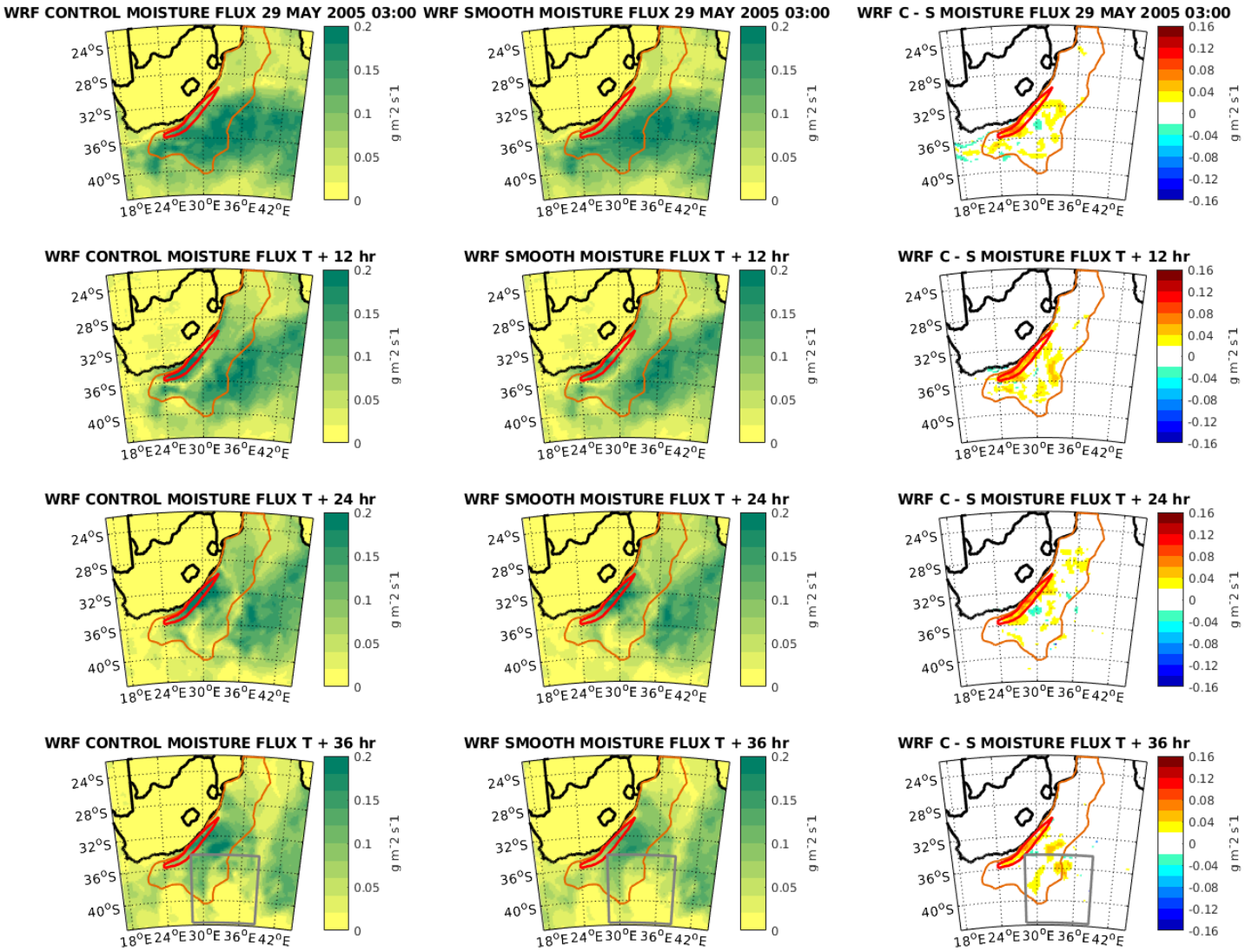

Figure 3.4.18: Storm B3. WRF model surface turbulent moisture flux ($g.m^{-2}.s^{-1}$). From top to bottom: 29 May 03:00; 29 May 15:00; 30 May 03:00 & 30 May 15:00. *(Left)* CTL simulation *(middle)* SMTH simulation & *(right)* Difference (CTL – SMTH). Orange boundary encloses area where SSTs are 0.25 - 1°C warmer in CTL simulation. Red boundary encloses area where SSTs are > 1°C warmer in CTL simulation. *(Bottom)* Grey box encloses developed storm.

Table 3.4.3 indicates that a deeper (- 3.5 ± 2.01 m) developed storm was modelled in the CTL run. Higher rainfall intensity (+ 0.02 ± 0.241 $mm.hr^{-1}$), higher surface wind speeds (+ 0.44 ± 0.552 $m.s^{-1}$), greater storm energy (+ 52 ± 139.4 $m^2.s^{-2}$) and higher surface turbulent moisture fluxes (+ 0.005 ± 0.0062 $g.m^{-2}.s^{-1}$) were all found for the developed storm over the Agulhas Current. The standard deviations are larger than the mean difference for all but one variable.

WRF VARIABLE	AVERAGE DIFFERENCE
850mb geopotential height	**- 3.5 ± 2.01 m**
Surface rain rate	**+ 0.02 ± 0.241 mm.hr^{-1}**
Surface wind speed	**+ 0.44 ± 0.552 m.s^{-1}**
Eddy kinetic energy (EKE)	**+ 52 ± 139.4 m^2.s^{-2}**
Surface turbulent moisture flux	**+ 0.005 ± 0.0062 g.m^{-2}.s^{-1}**

Table 3.4.3: Storm B3: 28 – 30 May 2005. Average difference (CTL – SMTH) values for five WRF model variables. Values are for developed storm bounded by grey box. Standard deviations for average values are included

3.5 Category C storms

The final type of storm identified in the WRF model output were pre-existing low pressure systems found over the South African landmass. These were interior low pressure systems that eventually moved offshore southeast over the Agulhas Current. These storms are similar to the category A storms but did not originate directly over the Current region but instead originated over land and then later propagated offshore over the Agulhas Current.

Storm C1: 16 – 18 October 2001

The first category C storm found in the model output occurred in October 2001 as shown in Figure 3.5.1. On 16th October, an interior low is centred over the southern part of South Africa with a centre surface pressure of 1008 hPa *(Top left).* The next day, this system moves offshore over the Current region and intensifies slightly as the centre isobar decreases to 1004 hPa (Top right). Over the next 24 hours the centre surface pressure is sustained at 1004 hPa as the storm tracks further offshore (Bottom).

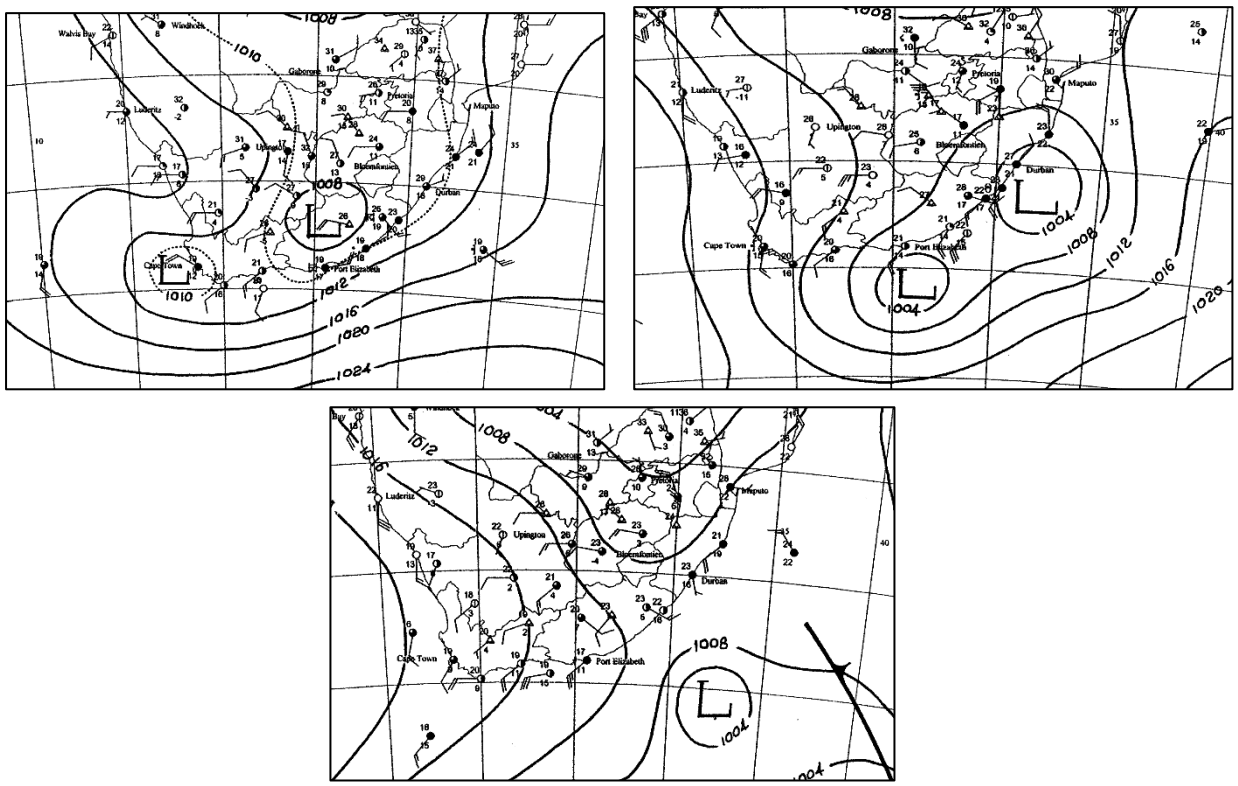

Figure 3.5.1: Storm C1. Surface synoptic conditions for *(Top left)* 16 October 2001 *(Top right)* 17 October 2001 & *(Bottom)* 18 October 2001. Charts were generated at 12h00 UTC.

Figure 3.5.2 shows a deepening of the system in both runs as the cell centre moves over the southern part of the Agulhas region. However, a more intense developed storm is found in the CTL run once the storm has developed over the Current region.

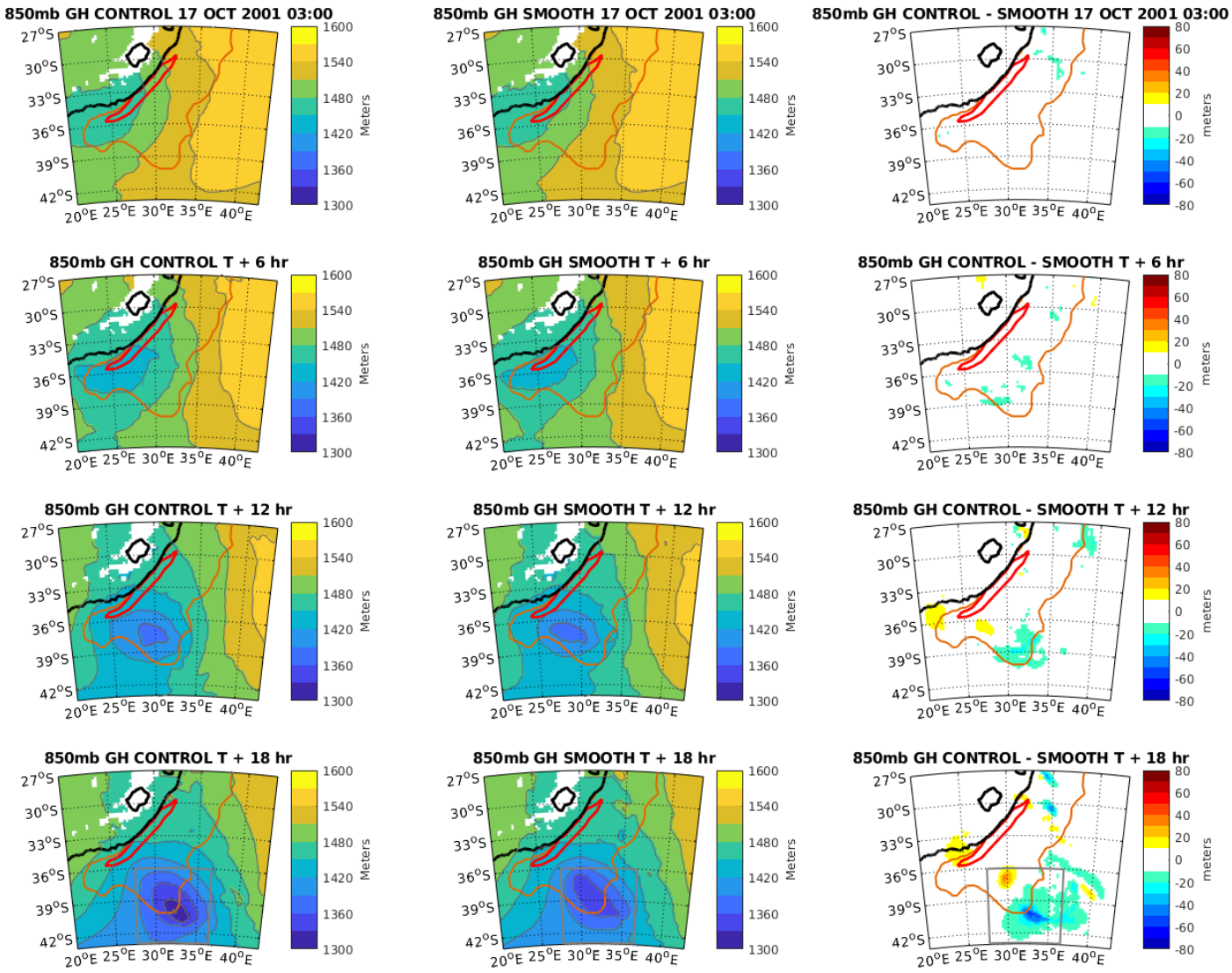

Figure 3.5.2: Storm C1. WRF model 850mb geopotential height (m). From top to bottom: 17 October 03:00; 17 October 09:00; 17 October 15:00 & 17 October 21:00. *(Left)* CTL simulation *(middle)* SMTH simulation & *(right)* Difference (CTL – SMTH). Orange boundary encloses area where SSTs are 0.25 - 1°C warmer in CTL simulation. Red boundary encloses area where SSTs are > 1°C warmer in CTL simulation. *(Bottom)* Grey box encloses developed storm.

Figure 3.5.3 indicates increasing rainfall in both configurations as slightly higher maximum rain rates are found in the CTL configuration once the storm has developed over the Current region.

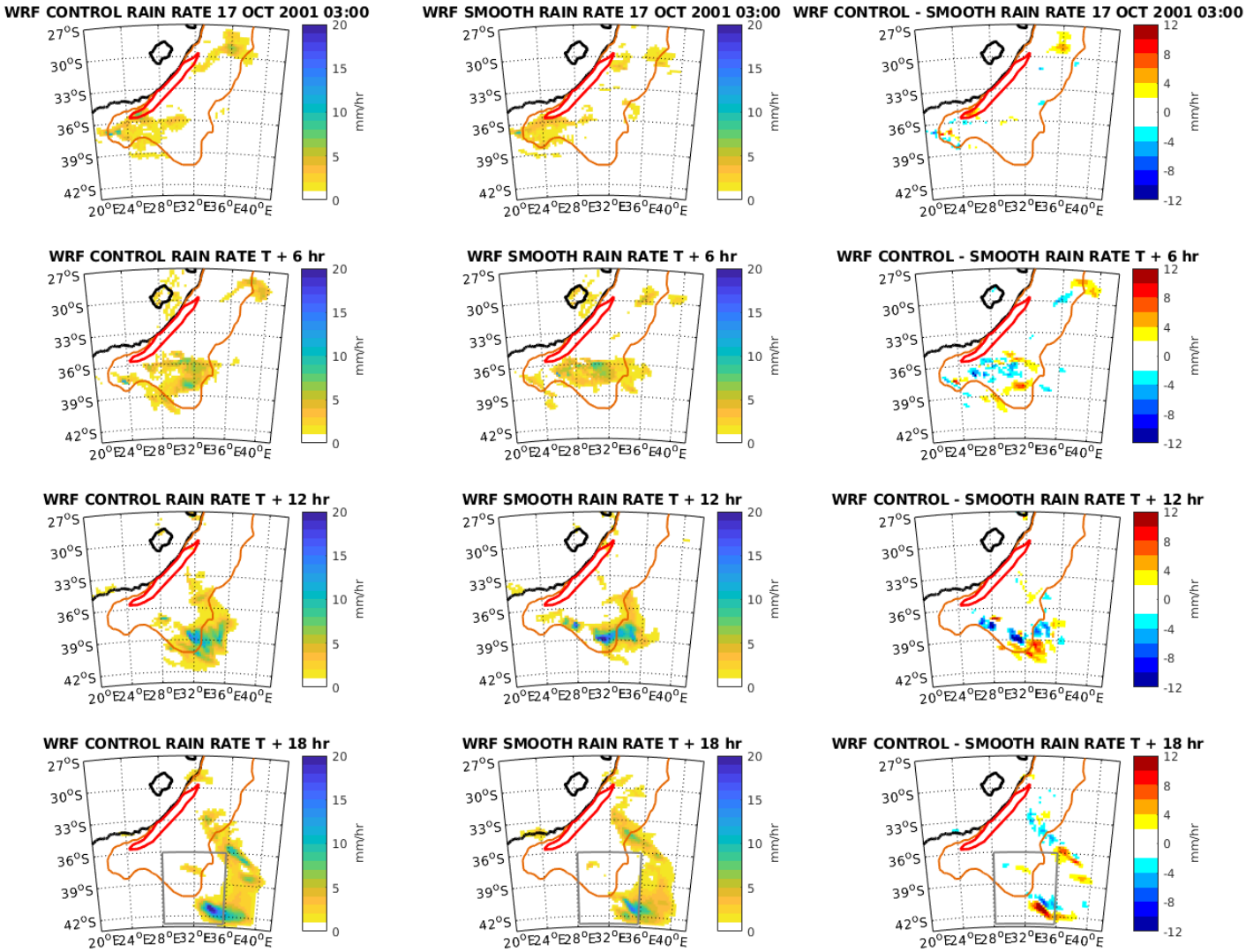

Figure 3.5.3: Storm C1. WRF model surface rain rate (mm.hr^{-1}). From top to bottom: 17 October 03:00; 17 October 09:00; 17 October 15:00 & 17 October 21:00. *(Left)* CTL simulation *(middle)* SMTH simulation & *(right)* Difference (CTL – SMTH). Orange boundary encloses area where SSTs are 0.25 - 1°C warmer in CTL simulation. Red boundary encloses area where SSTs are > 1°C warmer in CTL simulation. *(Bottom)* Grey box encloses developed storm.

From 17 October 2001 03:00 to 17 October 2001 09:00, surface wind speeds are sustained in both runs as displayed in Figure 3.5.4. However, there is a slight increase in wind speed as the

cell centre moves away from the Current region as higher maximum wind speeds are found in the CTL run.

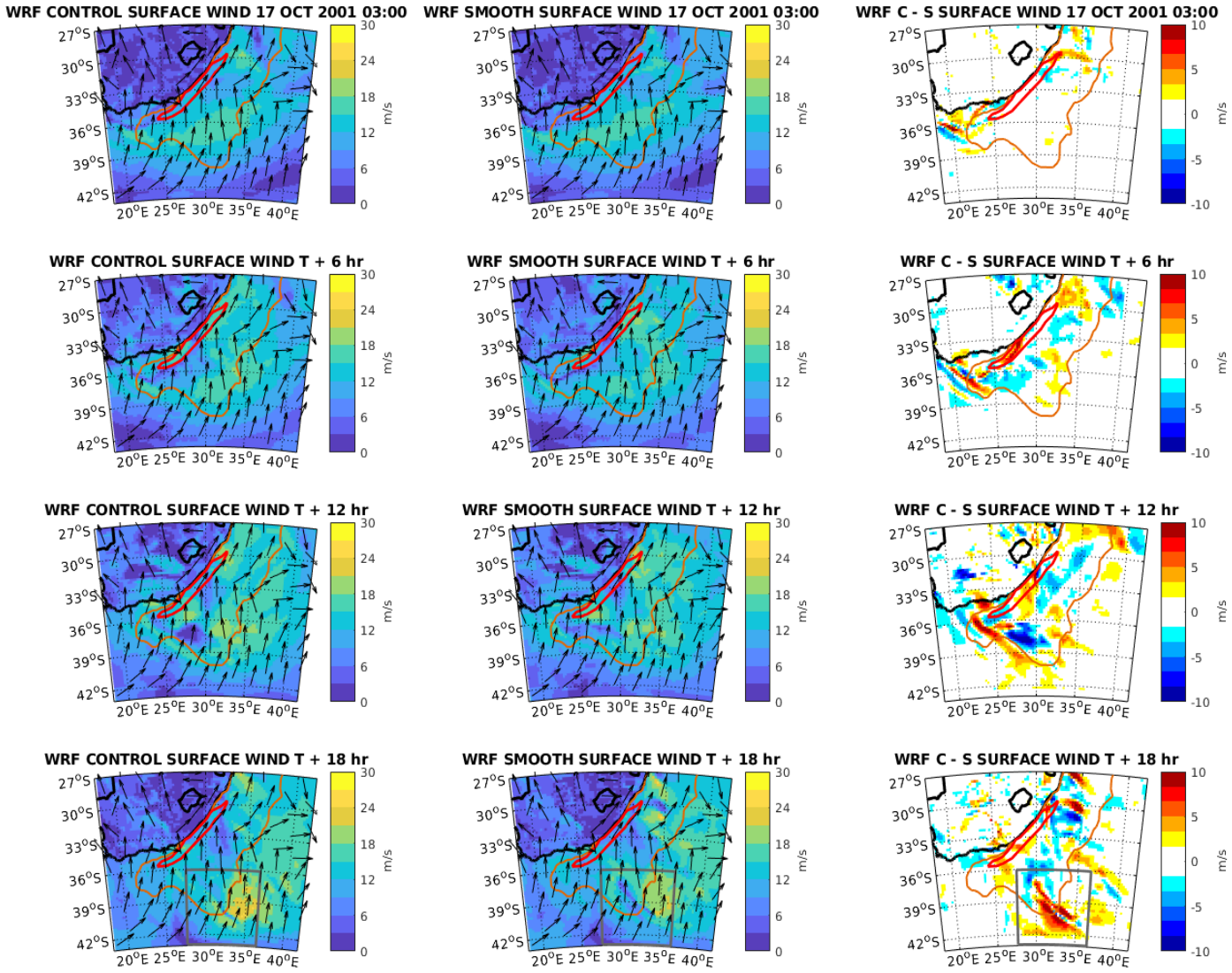

Figure 3.5.4: Storm C1. WRF model surface wind (m.s^{-1}). From top to bottom: 17 October 03:00; 17 October 09:00; 17 October 15:00 & 17 October 21:00. *(Left)* CTL simulation *(middle)* SMTH simulation & *(right)* Difference (CTL – SMTH). Black arrows indicate normalised surface wind vectors. Orange boundary encloses area where SSTs are 0.25 - 1°C warmer in CTL simulation. Red boundary encloses area where SSTs are > 1°C warmer in CTL simulation. *(Bottom)* Grey box encloses developed storm.

As the storm develops over from the Agulhas region, the storm becomes more energetic in both runs as indicated in Figure 3.5.5. Intensification of the storm occurs along the boundary of the Agulhas Current *(orange border)* in both runs. A more energetic developed storm is modelled in the CTL configuration.

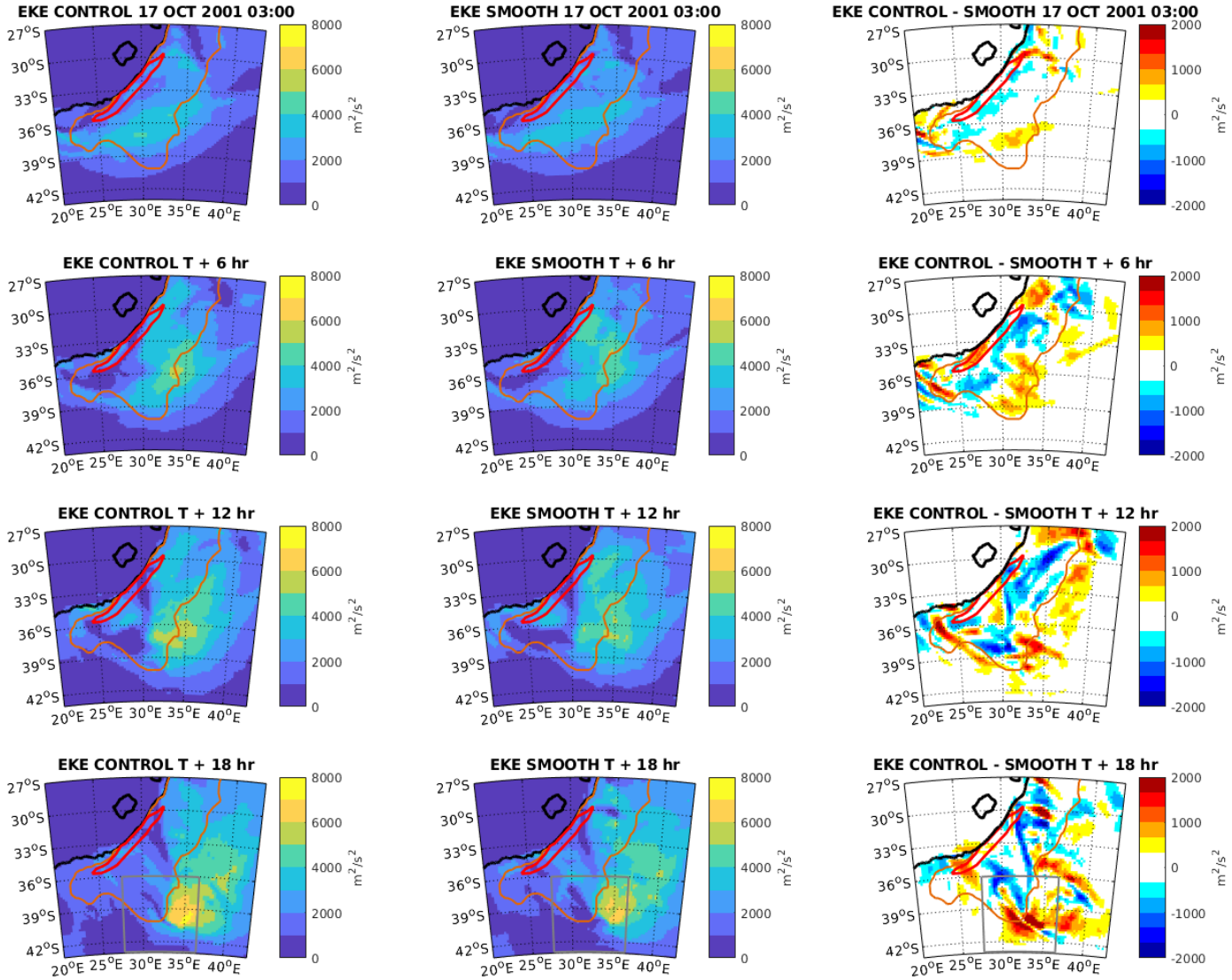

Figure 3.5.5: Storm C1. WRF model eddy kinetic energy up to 850mb level ($m^2.s^{-2}$). From top to bottom: 17 October 03:00; 17 October 09:00; 17 October 15:00 & 17 October 21:00. *(Left)* CTL simulation *(middle)* SMTH simulation & *(right)* Difference (CTL – SMTH). Orange boundary encloses area where SSTs are 0.25 - 1°C warmer in CTL simulation. Red boundary encloses area where SSTs are > 1°C warmer in CTL simulation. *(Bottom)* Grey box encloses developed storm.

Low surface turbulent moisture fluxes along the storm track are found in both runs as shown in Figure 3.5.6. These low fluxes are sustained throughout the storm's evolution over the Current region in both configurations.

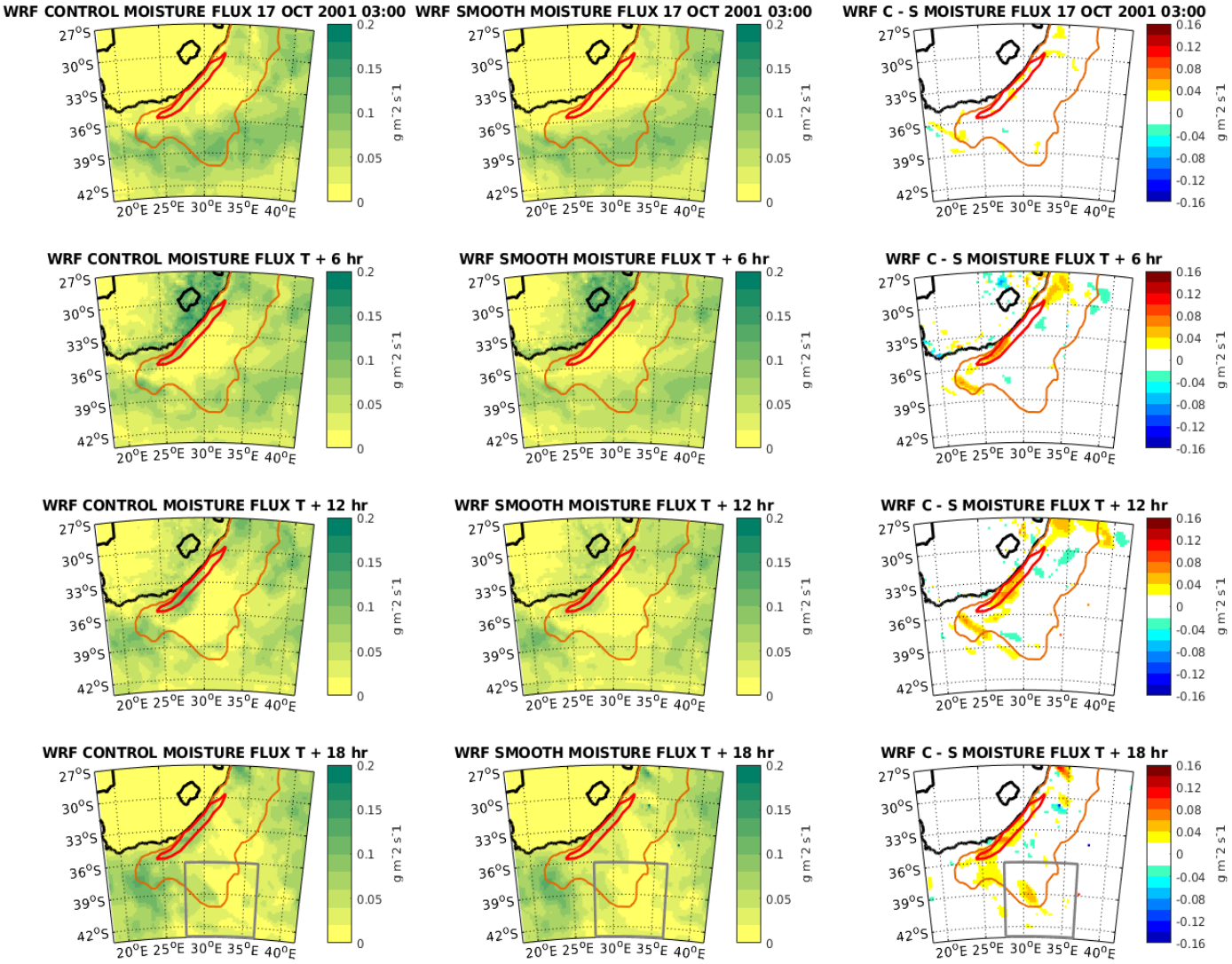

Figure 3.5.6: Storm C1. WRF model surface turbulent moisture flux ($g.m^{-2}.s^{-1}$). From top to bottom: 17 October 03:00; 17 October 09:00; 17 October 15:00 & 17 October 21:00. *(Left)* CTL simulation *(middle)* SMTH simulation & *(right)* Difference (CTL – SMTH). Orange boundary encloses area where SSTs are 0.25 - 1°C warmer in CTL simulation. Red boundary encloses area where SSTs are > 1°C warmer in CTL simulation. *(Bottom)* Grey box encloses developed storm.

Table 3.5.1 indicates that a deeper (- 9.0 ± 4.05 m) developed storm was modelled in the CTL run. Higher rainfall intensity (+ 0.37 ± 1.721 $mm.hr^{-1}$), higher surface wind speeds (+ 1.32 ±

1.203 $m.s^{-1}$), greater storm energy (+ 266 ± 337.3 $m^2.s^{-2}$) and higher surface turbulent moisture fluxes (+ 0.007 ± 0.0041 $g.m^{-2}.s^{-1}$) were all found for the developed storm over the Agulhas Current. The standard deviations are larger than the mean difference for surface rain and storm EKE variables only.

WRF VARIABLE	AVERAGE DIFFERENCE
850mb geopotential height	**- 9.0 ± 4.05 m**
Surface rain rate	**+ 0.37 ± 1.721 $mm.hr^{-1}$**
Surface wind speed	**+ 1.32 ± 1.203 $m.s^{-1}$**
Eddy kinetic energy (EKE)	**+ 266 ± 337.3 $m^2.s^{-2}$**
Surface turbulent moisture flux	**+ 0.007 ± 0.0041 $g.m^{-2}.s^{-1}$**

Table 3.5.1: Storm C1: 16 – 18 October 2001. Average difference (CTL – SMTH) values for five WRF model variables. Values are developed storm bounded by grey box. Standard deviations for average values are included

Storm C2: 13 – 15 January 2005

Two category C storms, both occurring in January 2005, show storm intensification over the Current region. The first occurred from 13th to 15th January shown in Figure 3.5.7. On the 13th January, an interior low persisting over the southwest region of South Africa *(Top left)* moves offshore just off the coast near Port Elizabeth the following day *(Top right).* Over the next 24 hours, the storm tracks over the Agulhas region and intensifies as the centre isobar decreases from 1008 hPa to 1000 hPa *(Bottom).*

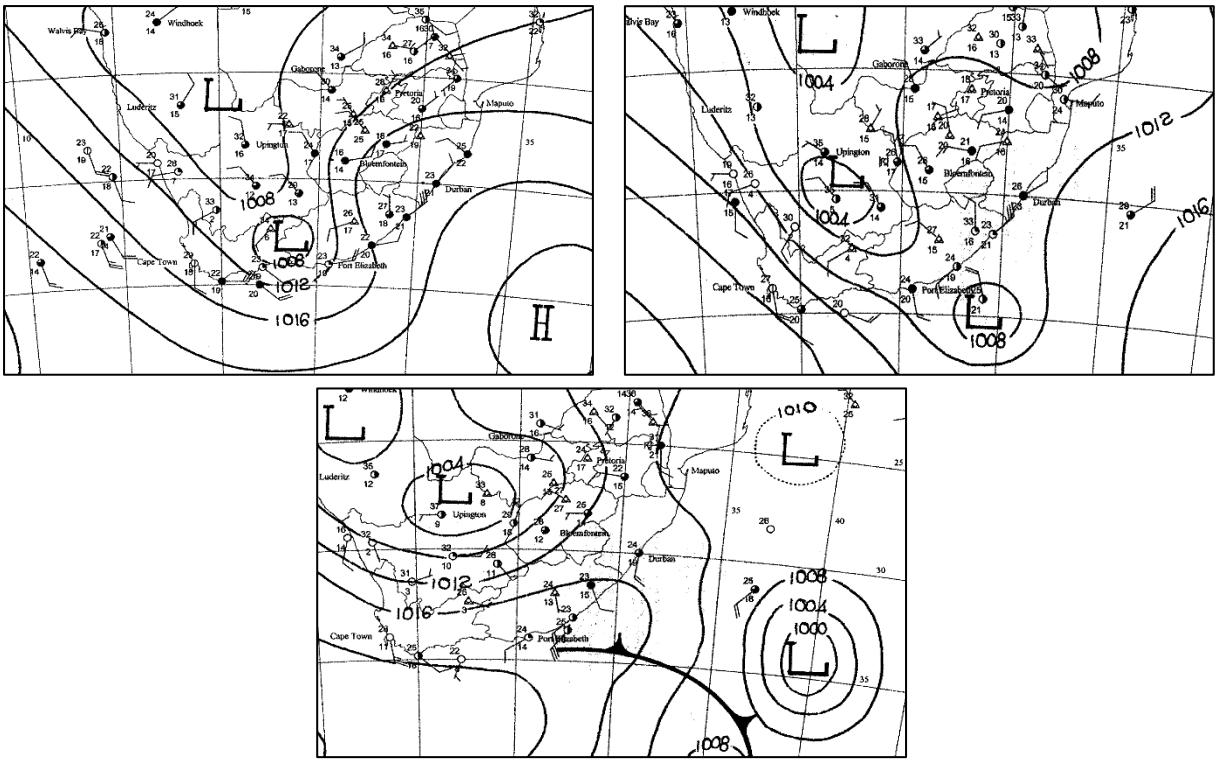

Figure 3.5.7: Storm C2. Surface synoptic conditions for *(Top left)* 13 January 2005 *(Top right)* 14 January 2005 & *(Bottom)* 15 January 2005. Charts were generated at 12h00 UTC.

Figure 3.5.8 shows the storm centre tracking over the northern part of the Agulhas core and then the outer Agulhas region in both runs. In both configurations, intensification of the storm occurs as the system moves offshore with a slightly deeper developed storm being modelled in the CTL run.

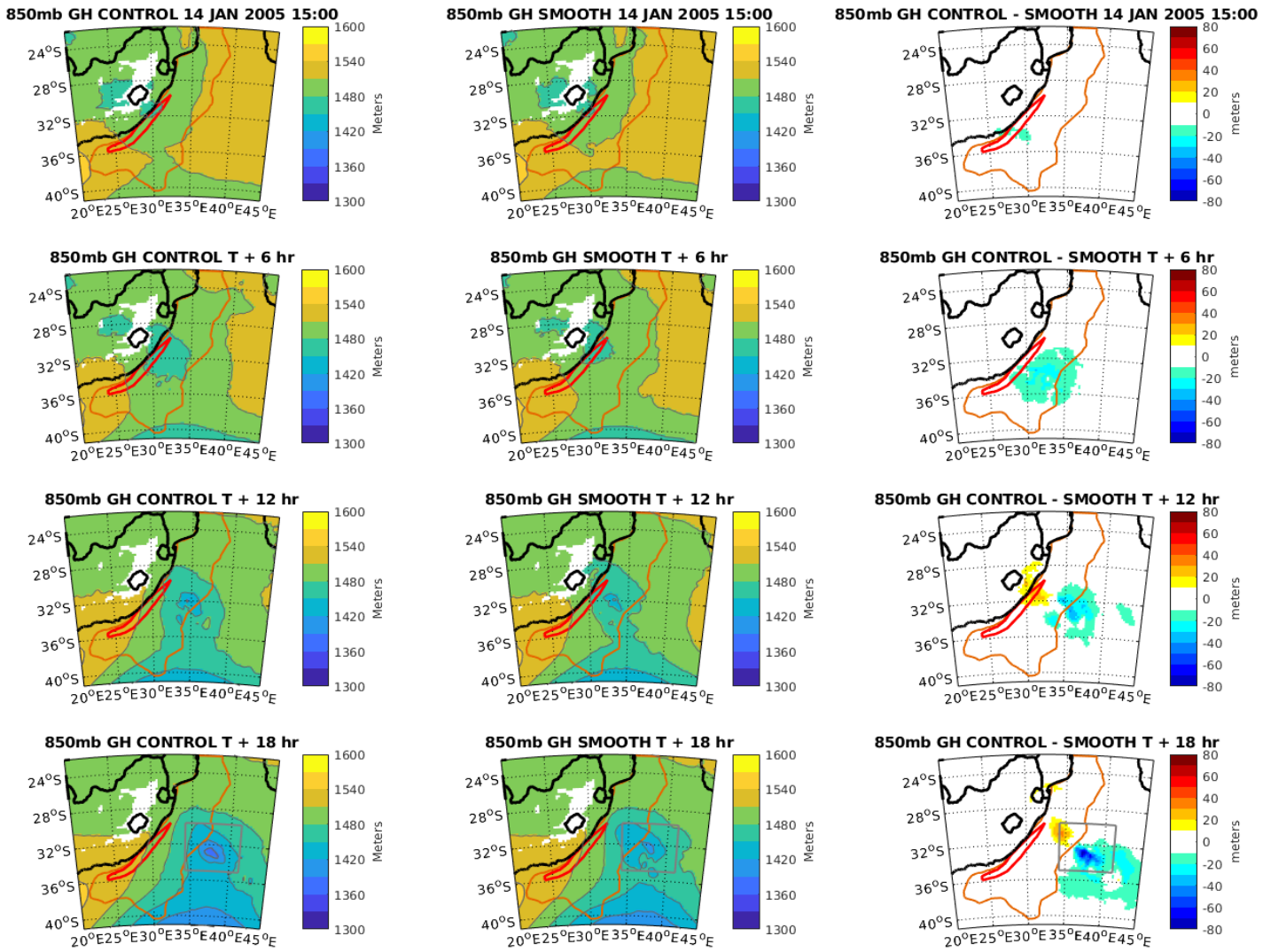

Figure 3.5.8: Storm C2. WRF model 850mb geopotential height (m). From top to bottom: 14 January 15:00; 14 January 21:00; 15 January 03:00 & 15 January 09:00. *(Left)* CTL simulation *(middle)* SMTH simulation & *(right)* Difference (CTL – SMTH). Orange boundary encloses area where SSTs are 0.25 - 1°C warmer in CTL simulation. Red boundary encloses area where SSTs are > 1°C warmer in CTL simulation. *(Bottom)* Grey box encloses developed storm.

Whilst the storm tracks over the Agulhas region, Figure 3.5.9 indicates increasing model rainfall in both simulations. However, once the system moves away from the Current region, rainfall decreases slightly in both runs

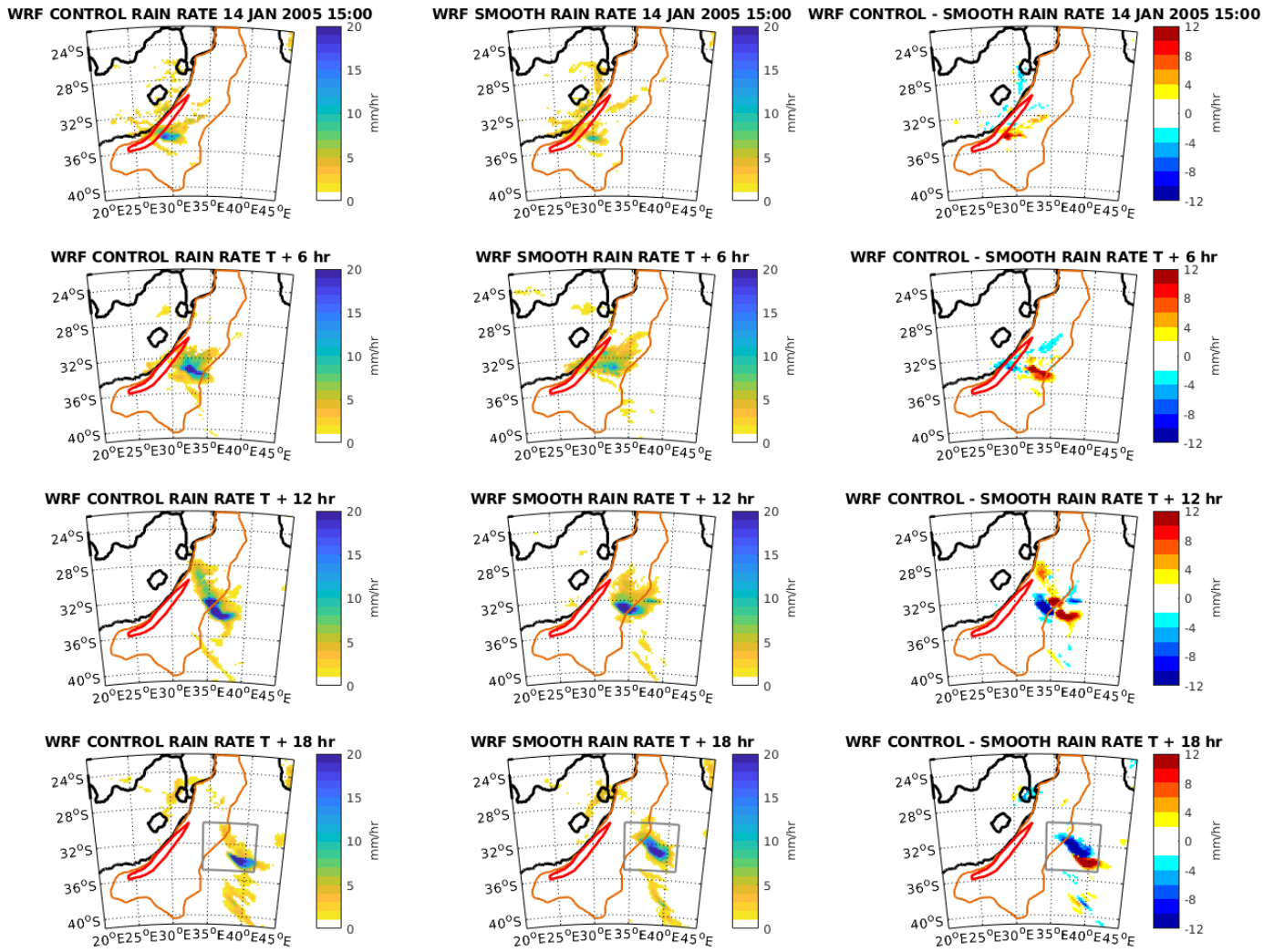

Figure 3.5.9: Storm C2. WRF model surface rain rate (mm.hr^{-1}). From top to bottom: 14 January 15:00; 14 January 21:00; 15 January 03:00 & 15 January 09:00. *(Left)* CTL simulation *(middle)* SMTH simulation & *(right)* Difference (CTL – SMTH). Orange boundary encloses area where SSTs are 0.25 - 1°C warmer in CTL simulation. Red boundary encloses area where SSTs are > 1°C warmer in CTL simulation. *(Bottom)* Grey box encloses developed storm.

A slight increase in surface wind speed is found in both runs throughout the storm's evolution over the Agulhas region as displayed in Figure 3.5.10. Similar degrees of intensification of these wind speeds are found in both runs.

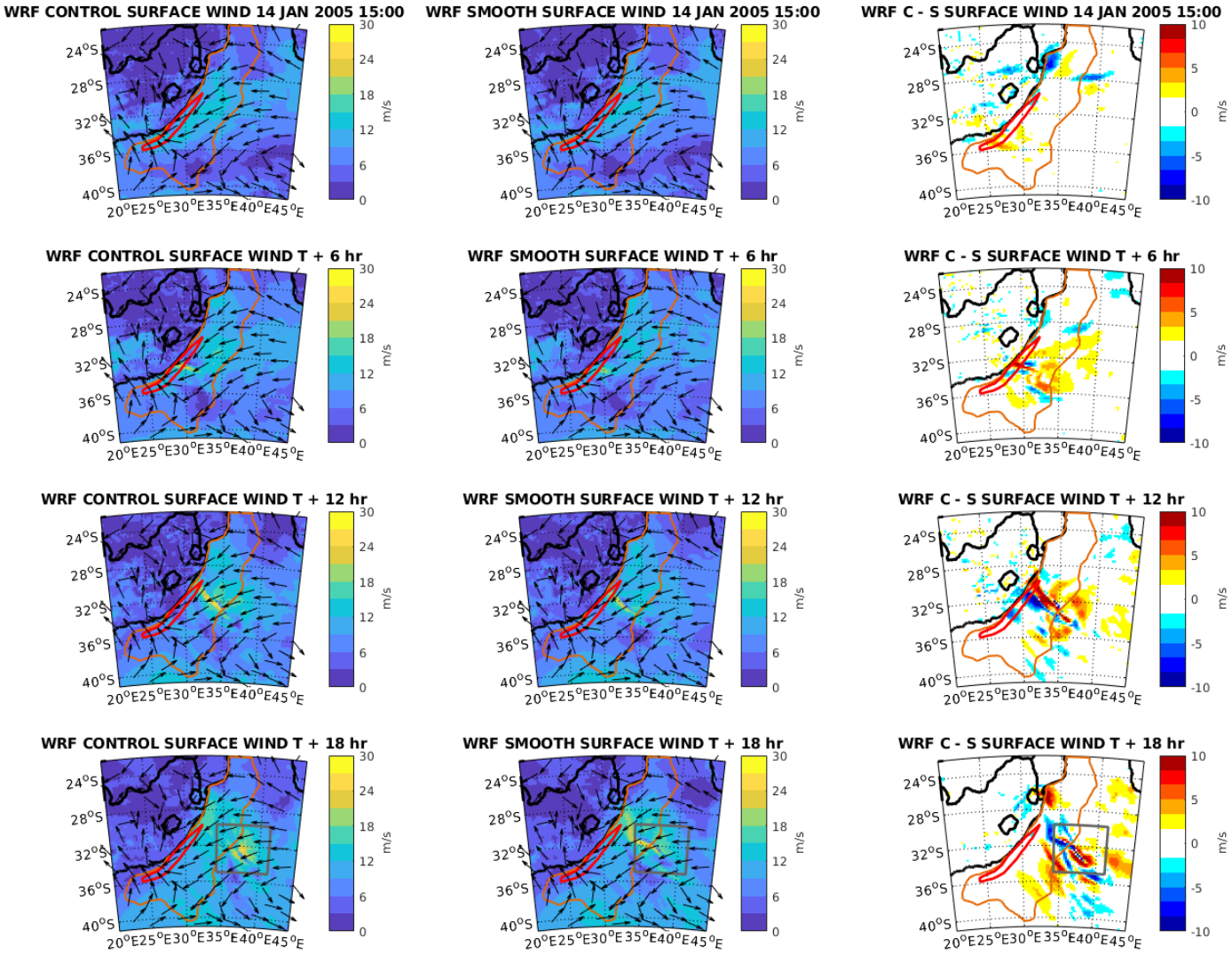

Figure 3.5.10: Storm C2. WRF model surface wind ($m.s^{-1}$). From top to bottom: 14 January 15:00; 14 January 21:00; 15 January 03:00 & 15 January 09:00. *(Left)* CTL simulation *(middle)* SMTH simulation & *(right)* Difference (CTL – SMTH). Black arrows indicate normalised surface wind vectors. Orange boundary encloses area where SSTs are 0.25 - 1°C warmer in CTL simulation. Red boundary encloses area where SSTs are > 1°C warmer in CTL simulation. *(Bottom)* Grey box encloses developed storm.

Figure 3.5.11 shows the change in storm EKE in both simulations. Storm energy is found to increase in both configurations however, in the CTL run, a more energetic developed storm is found once the system has developed over the Current.

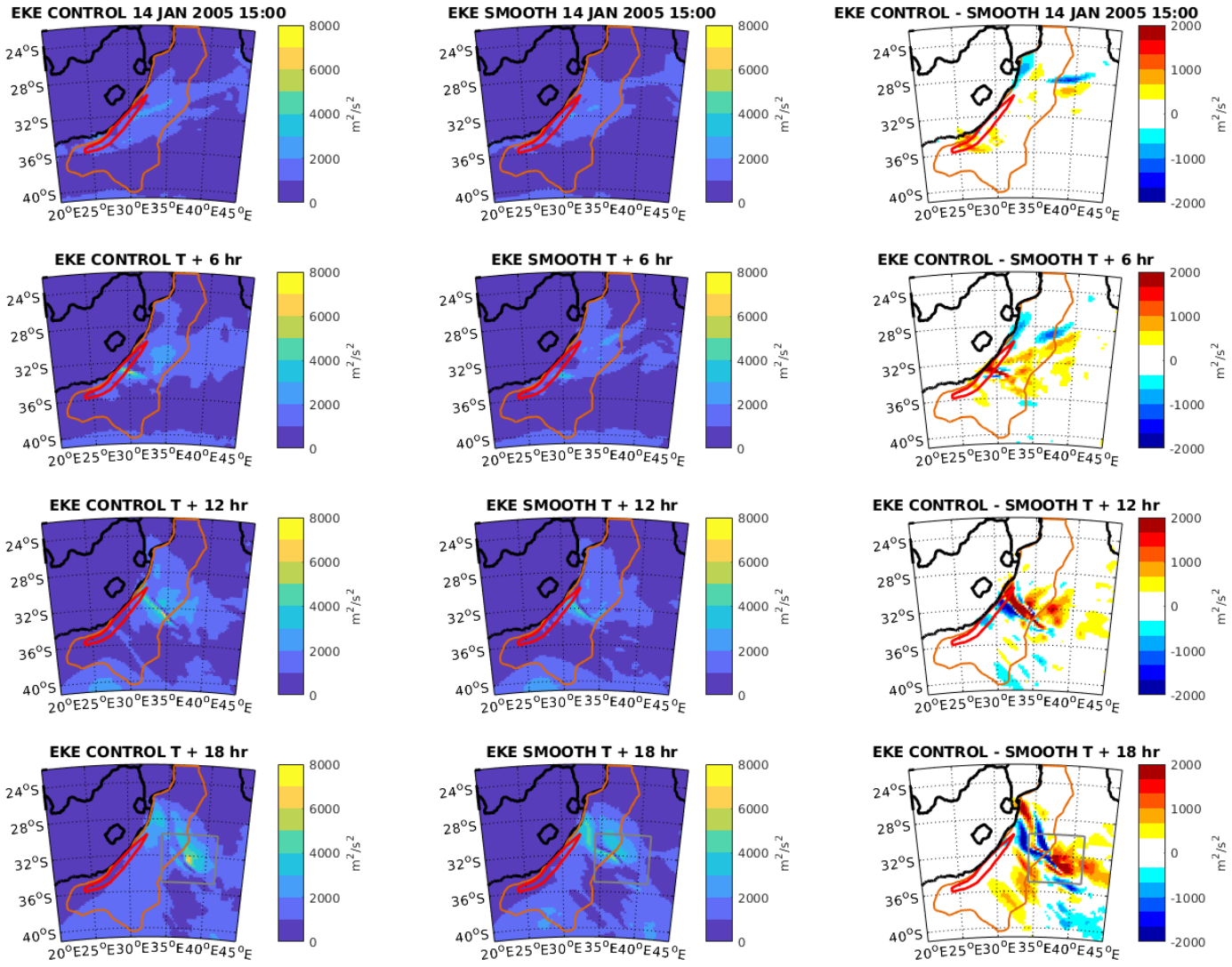

Figure 3.5.11: Storm C2. WRF model eddy kinetic energy up to 850mb level ($m^2.s^{-2}$). From top to bottom: 14 January 15:00; 14 January 21:00; 15 January 03:00 & 15 January 09:00. *(Left)* CTL simulation *(middle)* SMTH simulation & *(right)* Difference (CTL – SMTH). Orange boundary encloses area where SSTs are 0.25 - 1°C warmer in CTL simulation. Red boundary encloses area where SSTs are > 1°C warmer in CTL simulation. *(Bottom)* Grey box encloses developed storm.

Figure 3.5.12 shows high model surface turbulent moisture fluxes along the storm track, except at 14 January 2005 15:00. When the storm is centred over the Agulhas Current from 14 January 2005 21:00 to 15 January 2005 03:00, slightly higher moisture fluxes are found in the CTL run.

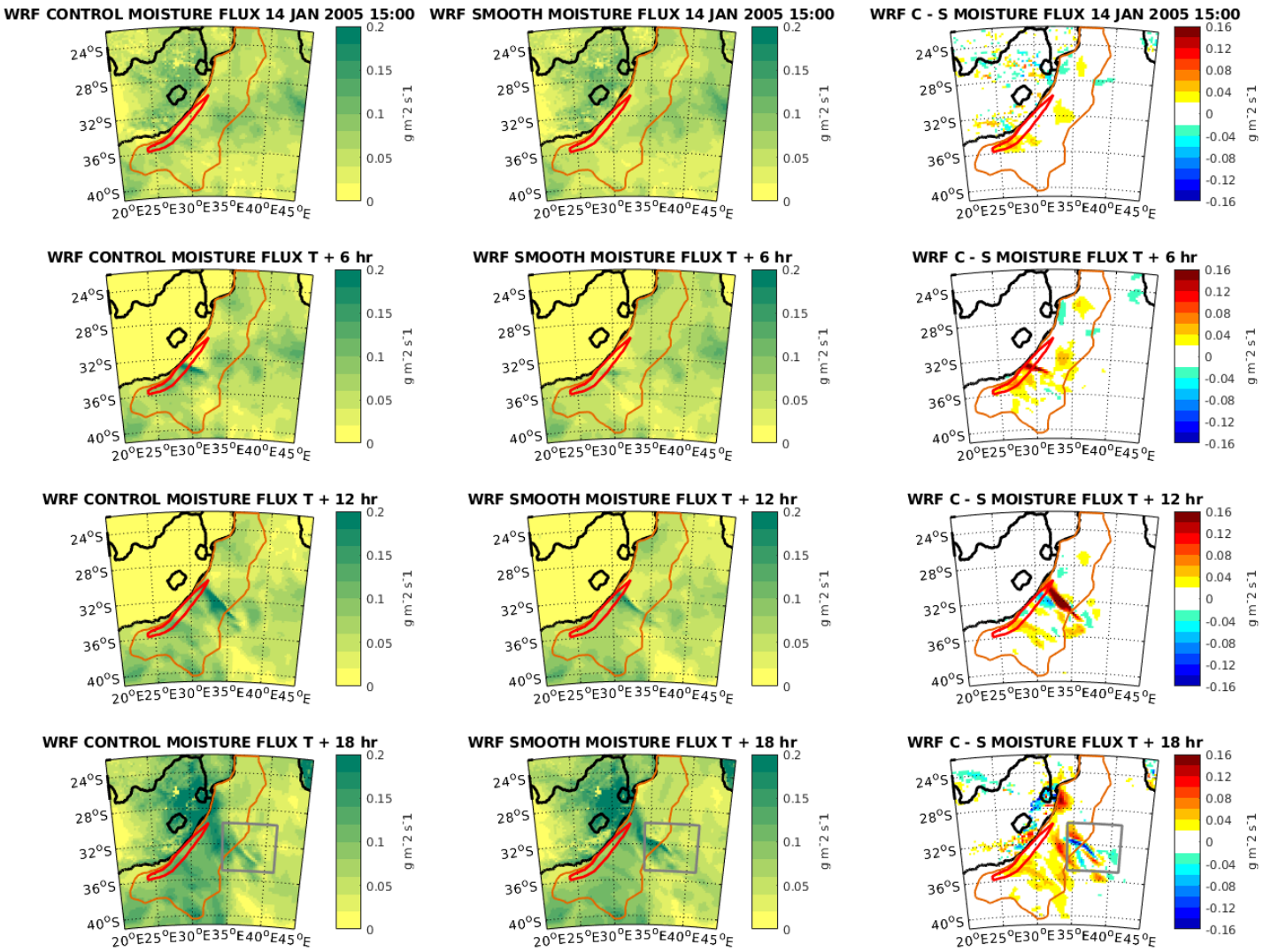

Figure 3.5.12: Storm C2. WRF model surface turbulent moisture flux ($g.m^{-2}.s^{-1}$). From top to bottom: 14 January 15:00; 14 January 21:00; 15 January 03:00 & 15 January 09:00. *(Left)* CTL simulation *(middle)* SMTH simulation & *(right)* Difference (CTL – SMTH). Orange boundary encloses area where SSTs are 0.25 - 1°C warmer in CTL simulation. Red boundary encloses area where SSTs are > 1°C warmer in CTL simulation. *(Bottom)* Grey box encloses developed storm.

Table 3.5.2 shows that a deeper *(*- 11.0 ± 4.97 m) developed storm was modelled in the CTL run. Lower rainfall intensity (- 0.82 ± 4.781 $mm.hr^{-1}$), higher surface wind speeds (+ 1.01 ± 1.623 $m.s^{-1}$), greater storm energy (+ 328 ± 388.4 $m^2.s^{-2}$) and lower surface turbulent moisture fluxes (- 0.002 ± 0.0183 $g.m^{-2}.s^{-1}$) were all found for the developed storm over the Agulhas Current. Standard deviations are larger than the mean difference for all but two variables.

WRF VARIABLE	AVERAGE DIFFERENCE
850mb geopotential height	**- 11.0 ± 4.97 m**
Surface rain rate	**- 0.82 ± 4.781 mm.hr^{-1}**
Surface wind speed	**+ 1.01 ± 1.623 m.s^{-1}**
Eddy kinetic energy (EKE)	**+ 328 ± 388.4 m^2.s^{-2}**
Surface turbulent moisture flux	**- 0.002 ± 0.0183 g.m^{-2}.s^{-1}**

Table 3.5.2: Storm C2: 13 – 15 January 2005. Average difference (CTL – SMTH) values for five WRF model variables. Values are for developed storm bounded by grey box. Standard deviations for average values are included

Storm C3: 20 – 22 January 2005

Another category C storm was identified from the 20th to 22nd January 2005 as shown in Figure 3.5.13. An interior low persisting over the western part of Southern Africa on the 20th *(Top left)* moves southeast to be centred directly over the Agulhas core the following day *(Top right).* During this time, the storm weakens as the centre isobar increases from 1000 hPa to 1004 hPa. The next day *(Bottom),* as the cell moves further southeast offshore, the storm centre pressure is sustained at 1004 hPa.

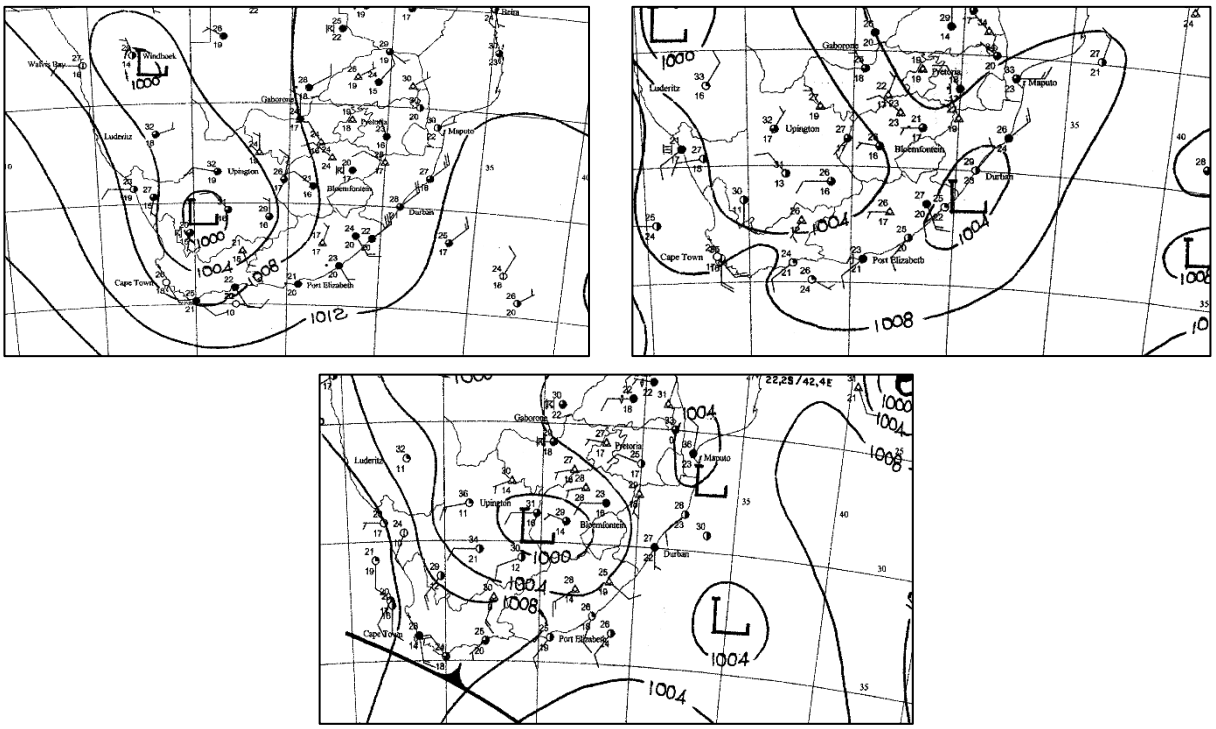

Figure 3.5.13: Storm C3. Surface synoptic conditions for *(Top left)* 20 January 2005 *(Top right)* 21 January 2005 & *(Bottom)* 22 January 2005. Charts are generated at 12h00 UTC.

Figure 3.5.14 shows a deepening of the interior low as the storm tracks offshore in both runs. The centre of the storm moves directly southeast over the Agulhas core and then over the outer Agulhas region in both configurations. The degree of intensification in the CTL run was greater than the SMTH run as indicated by the developed storm at 22 January 2005 00:00.

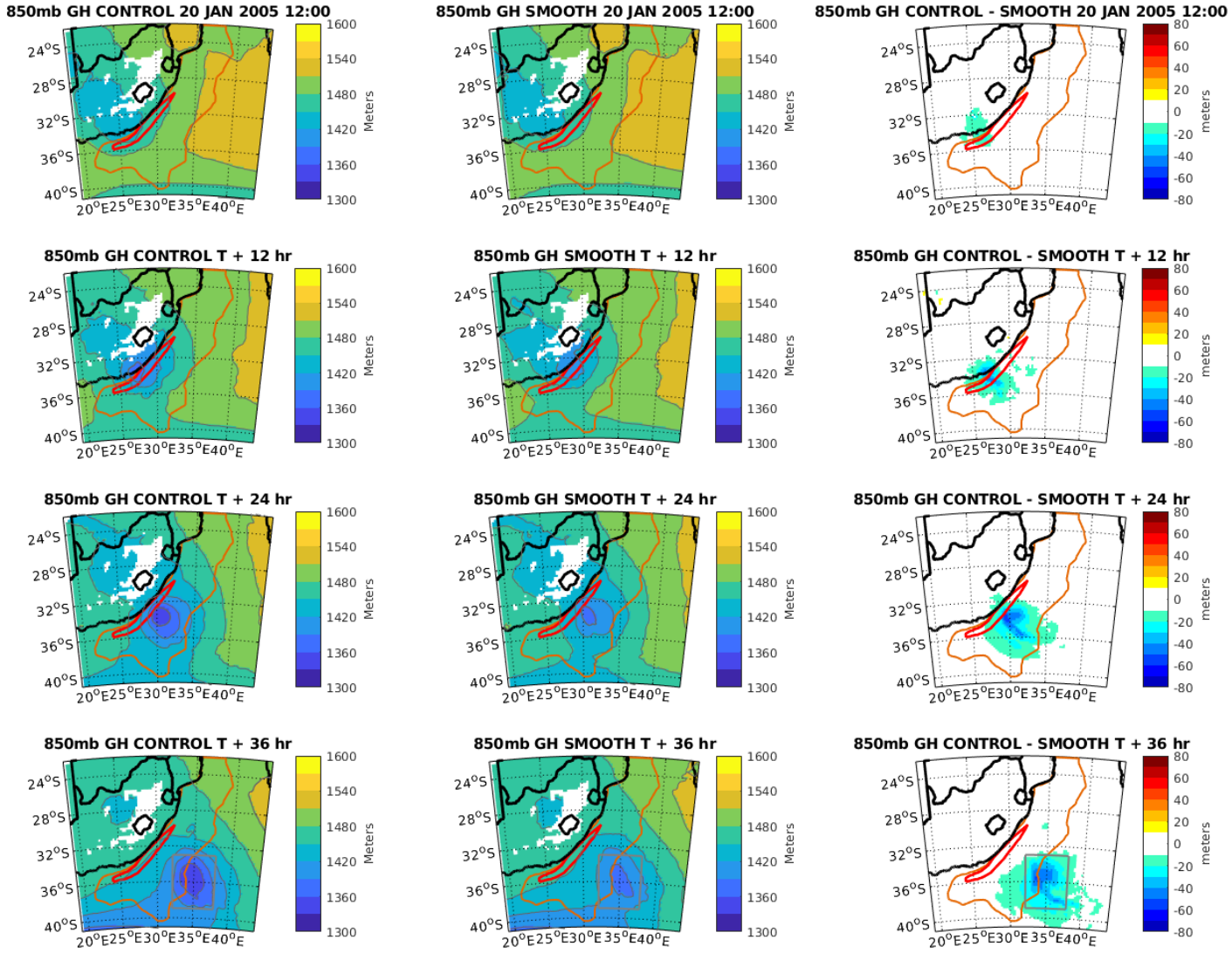

Figure 3.5.14: Storm C3. WRF model 850mb geopotential height (m). From top to bottom: 20 January 12:00; 21 January 00:00; 21 January 12:00 & 22 January 00:00. *(Left)* CTL simulation *(middle)* SMTH simulation & *(right)* Difference (CTL – SMTH). Orange boundary encloses area where SSTs are 0.25 - 1°C warmer in CTL simulation. Red boundary encloses area where SSTs are > 1°C warmer in CTL simulation. *(Bottom)* Grey box encloses developed storm.

Model rainfall patterns between the two configurations are displayed in Figure 3.5.15. Rain rates increase when the storm is centred over the Current region in both runs and then are sustained as the system moves away from the Current region *(east of orange boundary).*

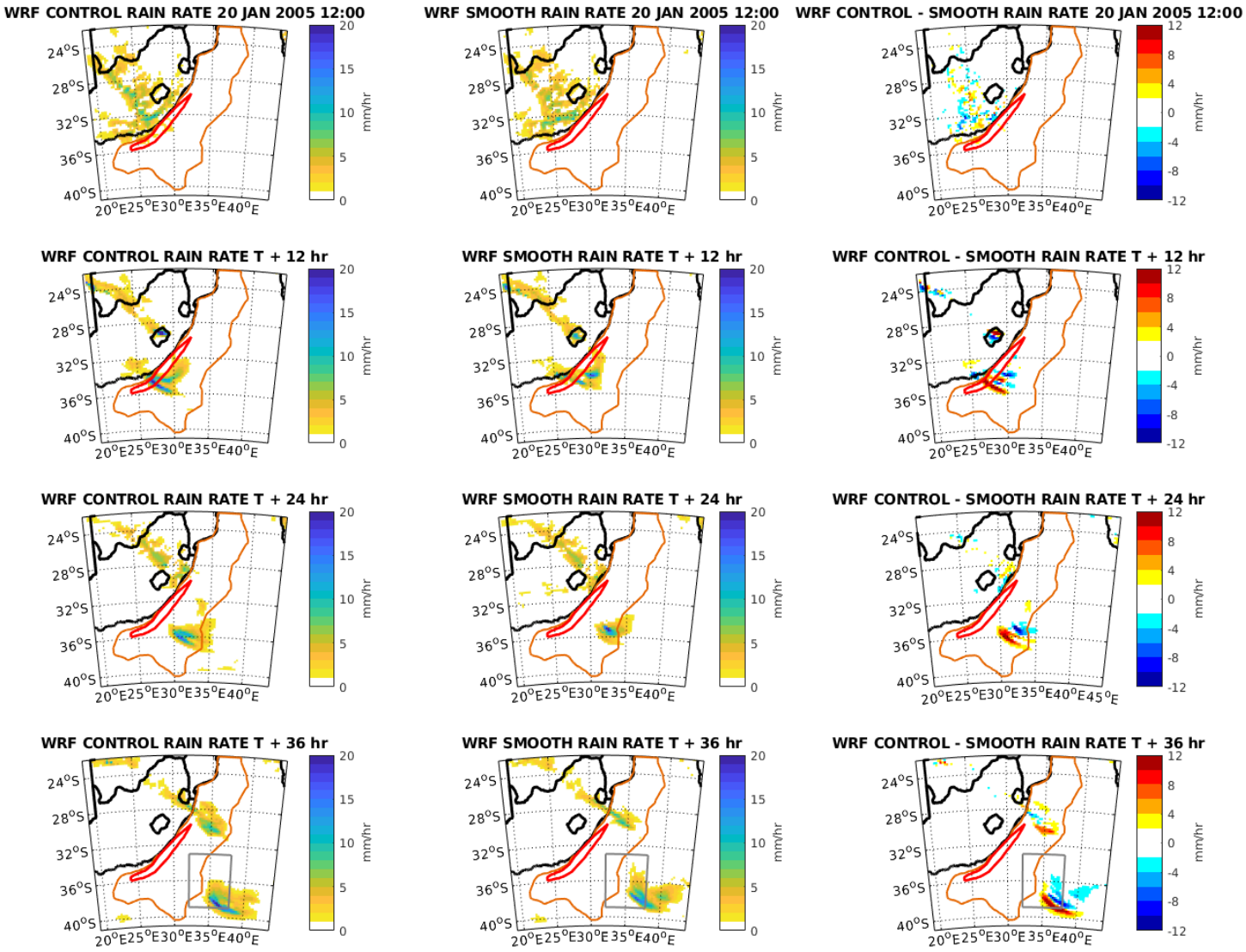

Figure 3.5.15: Storm C3. WRF model surface rain rate (mm.hr^{-1}) From top to bottom: 20 January 12:00; 21 January 00:00; 21 January 12:00 & 22 January 00:00. *(Left)* CTL simulation *(middle)* SMTH simulation & *(right)* Difference (CTL – SMTH). Orange boundary encloses area where SSTs are 0.25 - 1°C warmer in CTL simulation. Red boundary encloses area where SSTs are > 1°C warmer in CTL simulation. *(Bottom)* Grey box encloses developed storm.

Figure 3.5.16 indicates that whilst the storm propagates over the Agulhas region, surface wind speeds increase in both simulations but more so in the CTL run. Wind speeds then decrease in both runs as the cell passes away from the Current region

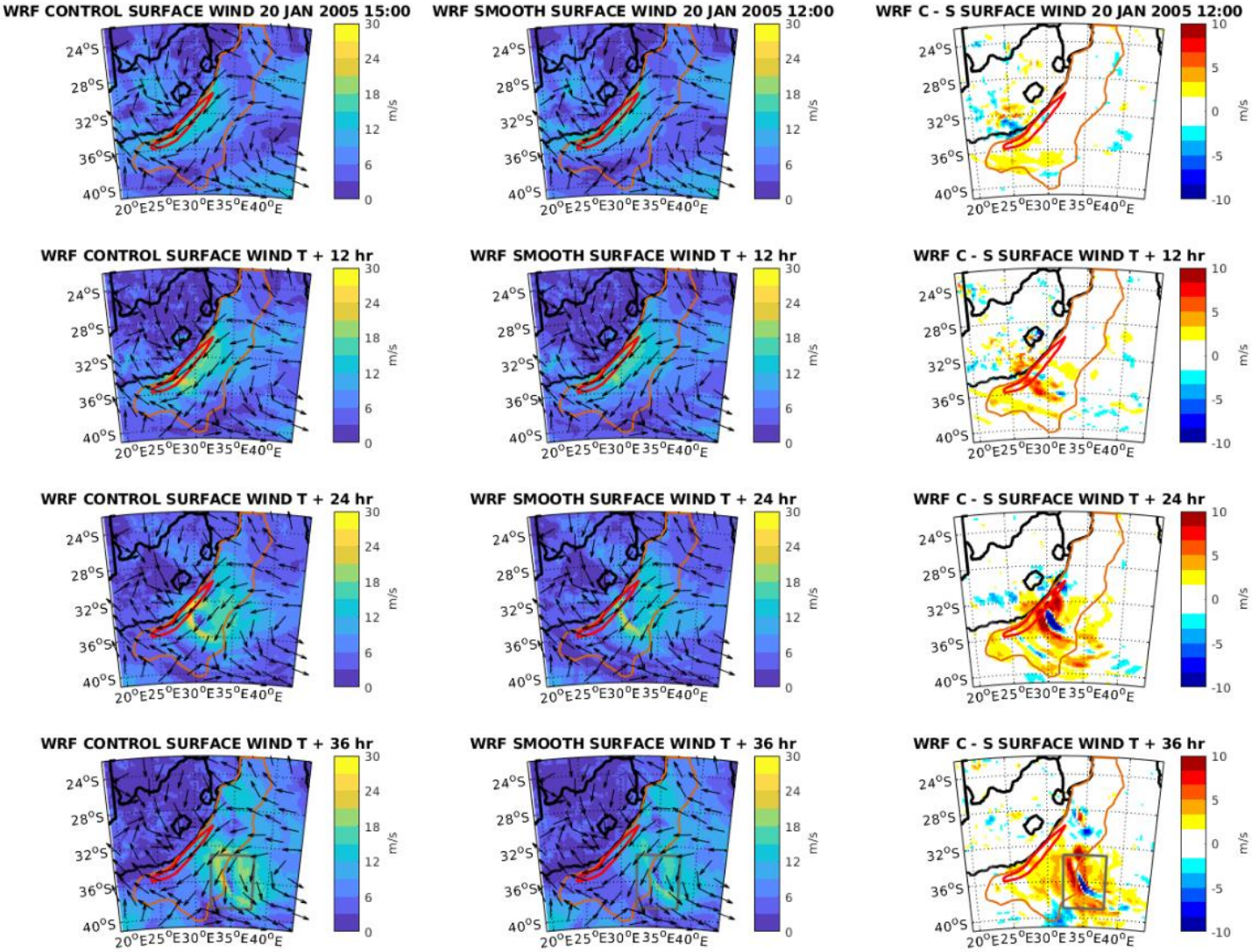

Figure 3.5.16: Storm C3. WRF model surface wind (m.s^{-1}). From top to bottom: 20 January 12:00; 21 January 00:00; 21 January 12:00 & 22 January 00:00. *(Left)* CTL simulation *(middle)* SMTH simulation & *(right)* Difference (CTL – SMTH). Black arrows indicate normalised surface wind vectors. Orange boundary encloses area where SSTs are 0.25 - 1°C warmer in CTL simulation. Red boundary encloses area where SSTs are > 1°C warmer in CTL simulation. *(Bottom)* Grey box

Figure 3.5.17 indicates model storm EKE increases slightly in the CTL run. The energy of the storm in the CTL run then decreases slightly once it is located away from the Current region. The SMTH run shows no increase in storm energy throughout its evolution over the Current.

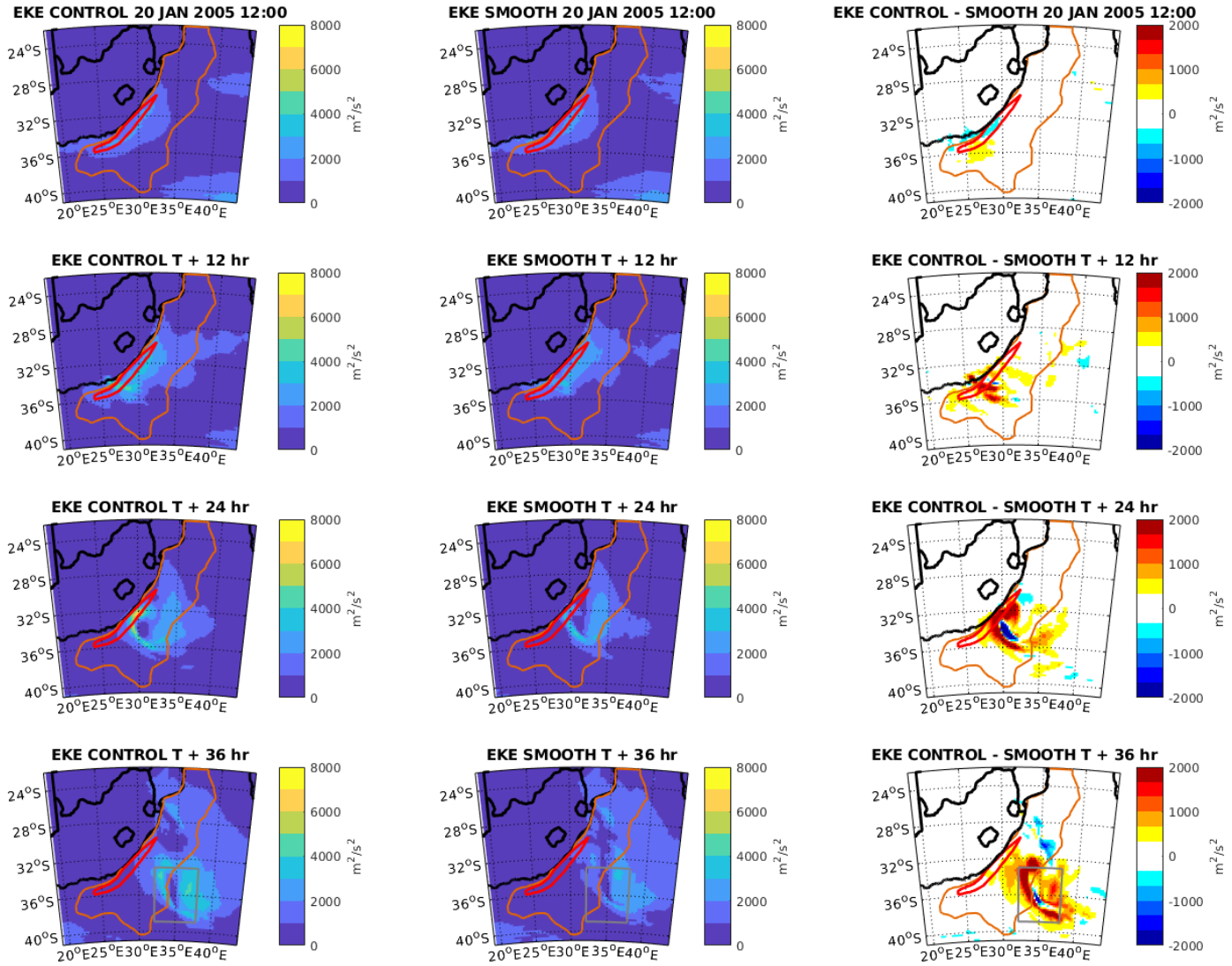

Figure 3.5.17: Storm C3. WRF model eddy kinetic energy up to 850mb level ($m^2.s^{-2}$). From top to bottom: 20 January 12:00; 21 January 00:00; 21 January 12:00 & 22 January 00:00. *(Left)* CTL simulation *(middle)* SMTH simulation & *(right)* Difference (CTL – SMTH). Orange boundary encloses area where SSTs are 0.25 - 1°C warmer in CTL simulation. Red boundary encloses area where SSTs are > 1°C warmer in CTL simulation. *(Bottom)* Grey box encloses developed storm.

Sustained high surface turbulent moisture fluxes are found in the CTL simulation whilst the storm is located over the Current as displayed in Figure 3.5.18. In the SMTH run, lower fluxes are found at the storm's location. Fluxes then decrease slightly in both runs when the storm moves away from the Current region.

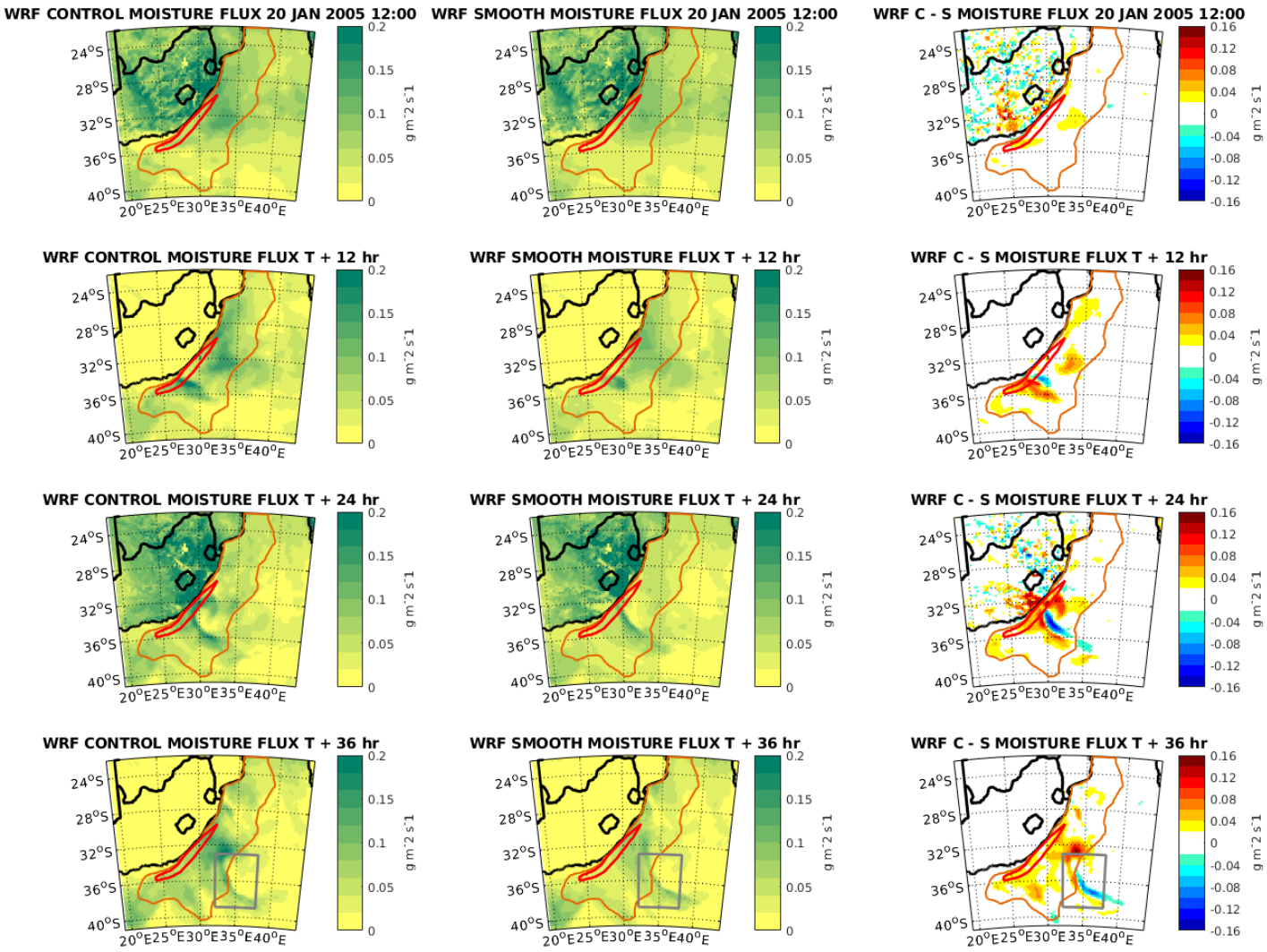

Figure 3.5.18: Storm C3. WRF model surface turbulent moisture flux ($g.m^{-2}.s^{-1}$). From top to bottom: 20 January 12:00; 21 January 00:00; 21 January 12:00 & 22 January 00:00. *(Left)* CTL simulation *(middle)* SMTH simulation & *(right)* Difference (CTL – SMTH). Orange boundary encloses area where SSTs are 0.25 - 1°C warmer in CTL simulation. Red boundary encloses area where SSTs are > 1°C warmer in CTL simulation. *(Bottom)* Grey box encloses developed storm.

Table 3.5.3 shows that a deeper (- 26 ± 2.82 m) developed storm was modelled in the CTL run. Higher rainfall intensity (+ 0.16 ± 2.35 $mm.hr^{-1}$), higher surface wind speeds (+ 3.15 ± 1.540 $m.s^{-1}$), greater storm energy (+ 868 ± 186.8 $m^2.s^{-2}$) and higher surface turbulent moisture fluxes (+ 0.013 ± 0.0065 $g.m^{-2}.s^{-1}$) were all found for the developed storm over the Agulhas Current. Standard deviations are larger than the mean difference for the surface rain variable only.

WRF VARIABLE	AVERAGE DIFFERENCE
850mb geopotential height	**- 26 ± 2.82 m**
Surface rain rate	**+ 0.16 ± 2.35 mm.hr^{-1}**
Surface wind speed	**+ 3.15 ± 1.540 m.s^{-1}**
Eddy kinetic energy (EKE)	**+ 868 ± 186.8 m^2.s^{-2}**
Surface turbulent moisture flux	**+ 0.013 ± 0.0065 g.m^{-2}.s^{-1}**

Table 3.5.3: Storm C3: 20 – 22 January 2005. Average difference (CTL – SMTH) values for five WRF model variables. Values are for developed storm bounded by grey box. Standard deviations for average values are included

Storm C4: 10 – 12 April 2005

The synoptic evolution of the final category C storm is shown in Figure 3.5.19. On 10 April, an interior low is located over the south-western part of South Africa *(Top left).* The following day, this system propagates eastward as the centre surface pressure decreases slightly from 1008 hPa to 1004 hPa *(Top right).* The following day, the cell centre moves southeast offshore over the Agulhas Current with a sustained surface pressure *(Bottom).*

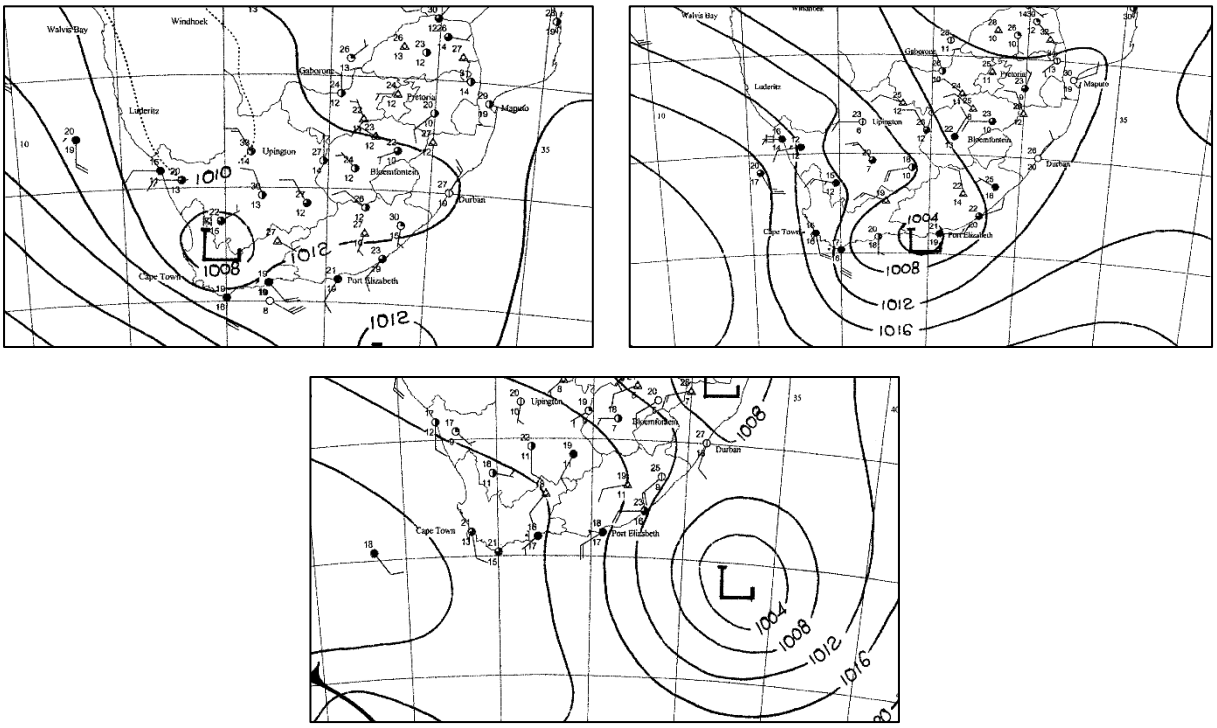

Figure 3.5.19: Storm C4. Surface synoptic conditions for *(Top left)* 10 April 2005 *(Top right)* 11 April 2005 & *(Bottom)* 12 April 2005. Charts are generated at 12h00 UTC.

The system tracks over the southern part of the Agulhas region in both runs as shown in Figure 3.5.20. Deepening of the storm is modelled in both configurations as the storm moves offshore. A similar degree of intensification is found in both runs.

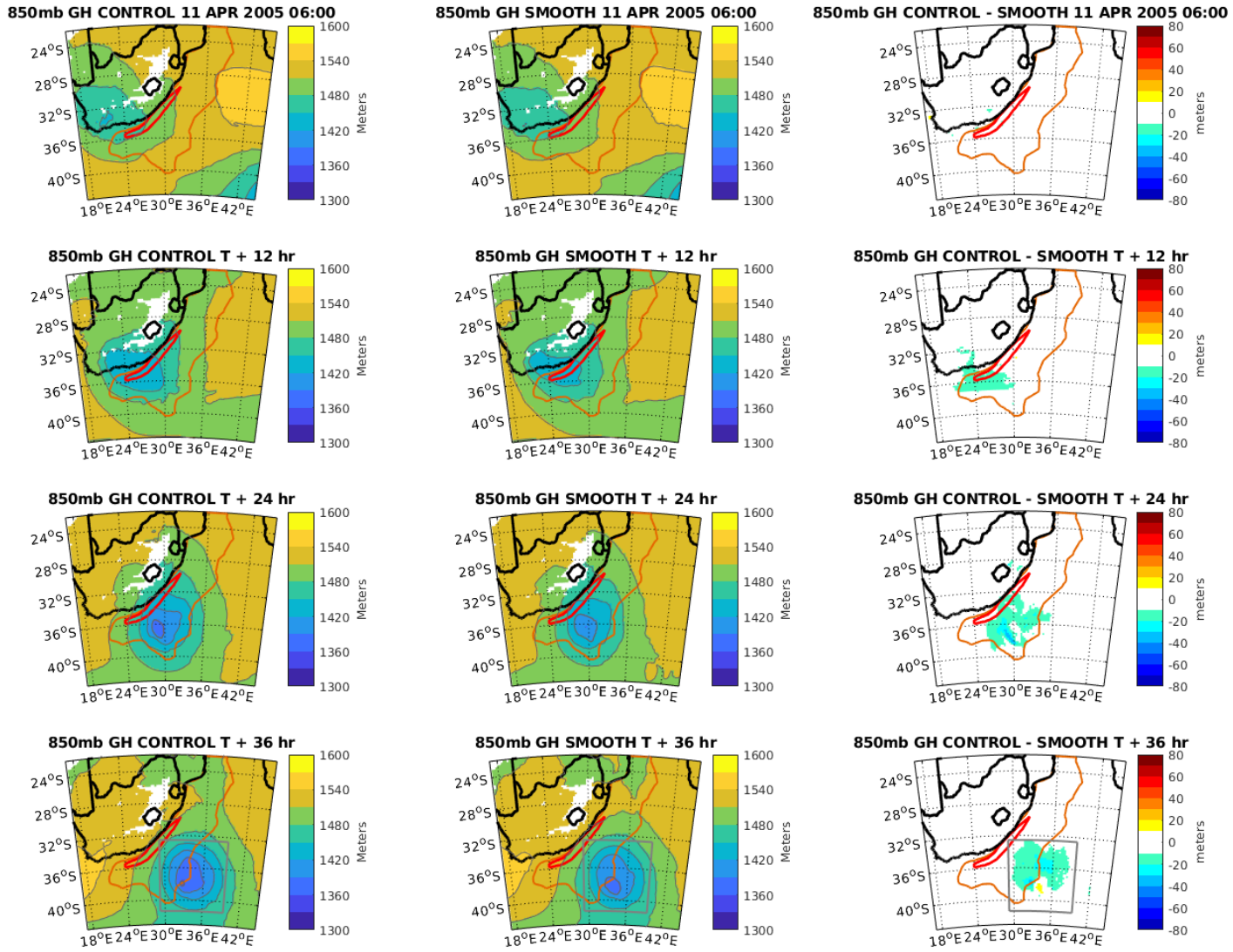

Figure 3.5.20: Storm C4. WRF model 850mb geopotential height (m). From top to bottom: 11 April 06:00; 11 April 18:00; 12 April 06:00 & 12 April 18:00. *(Left)* CTL simulation *(middle)* SMTH simulation & *(right)* Difference (CTL – SMTH). Orange boundary encloses area where SSTs are 0.25 - 1°C warmer in CTL simulation. Red boundary encloses area where SSTs are > 1°C warmer in CTL simulation. *(Bottom)* Grey box encloses developed storm.

Figure 3.5.21 indicates sustained model rain rates when the storm is centred over the Current in both configurations. A slight decrease in rainfall is then found once the system has moved away from the Current region.

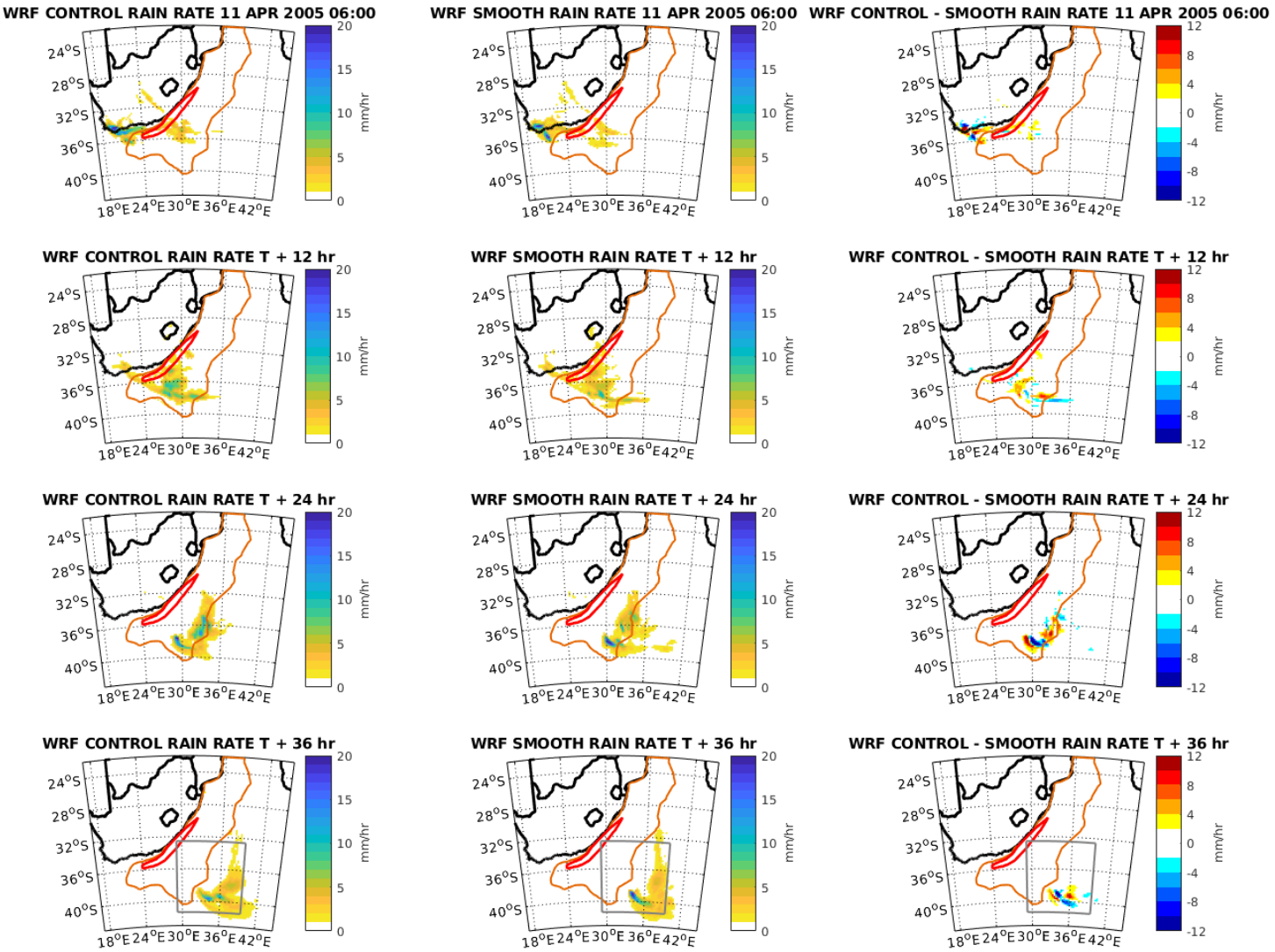

Figure 3.5.21: Storm C4. WRF model surface rain rate (mm.hr^{-1}). From top to bottom: 11 April 06:00; 11 April 18:00; 12 April 06:00 & 12 April 18:00. *(Left)* CTL simulation *(middle)* SMTH simulation & *(right)* Difference (CTL – SMTH). Orange boundary encloses area where SSTs are 0.25 - 1°C warmer in CTL simulation. Red boundary encloses area where SSTs are > 1°C warmer in CTL simulation. *(Bottom)* Grey box encloses developed storm.

Figure 3.5.22 shows that model wind speeds increase in the both runs. The degree of intensification is slightly more severe in the CTL run as higher maximum wind speeds are found for the developed storm.

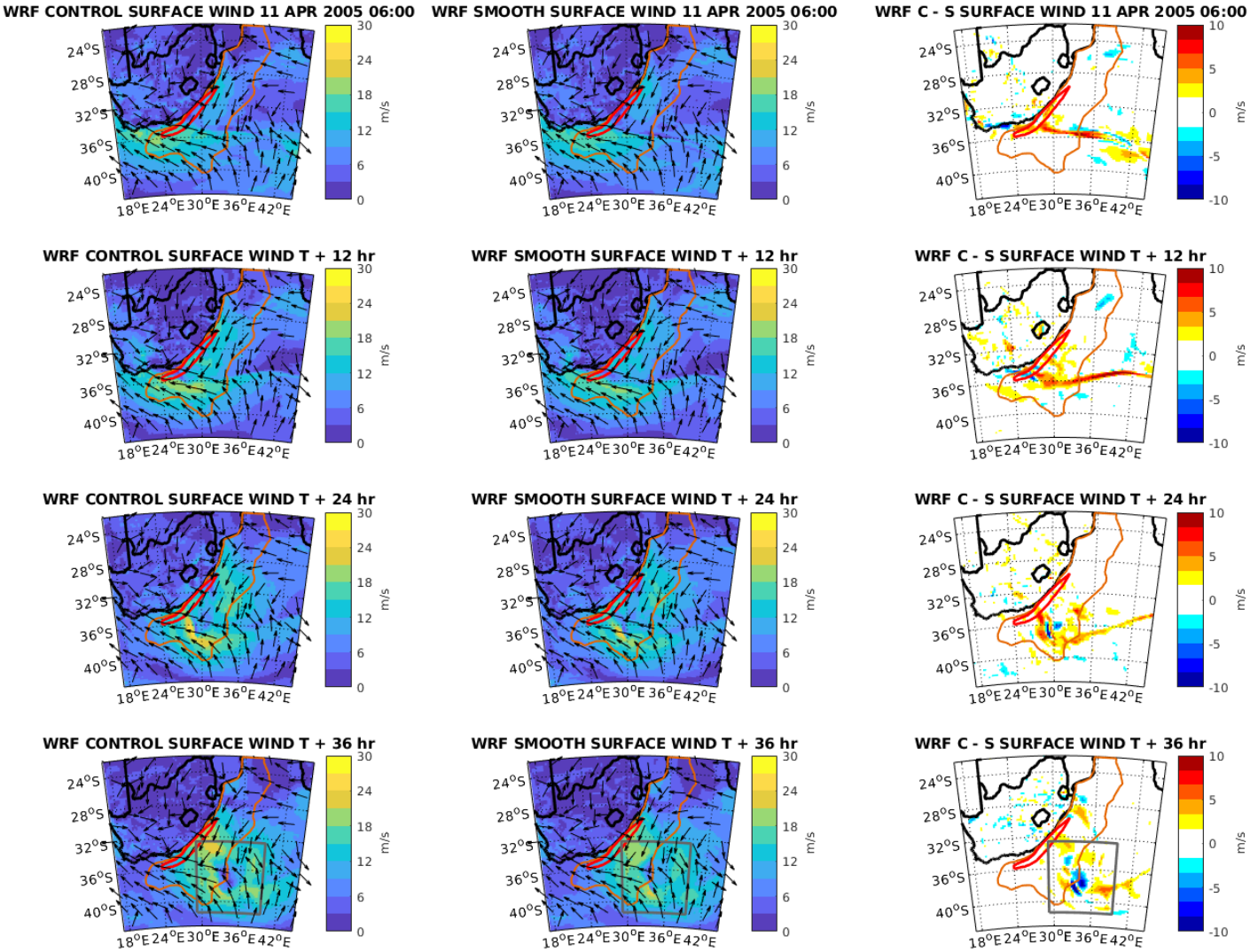

Figure 3.5.22: Storm C4. WRF model surface wind (m.s^{-1}). From top to bottom: 11 April 06:00; 11 April 18:00; 12 April 06:00 & 12 April 18:00. *(Left)* CTL simulation *(middle)* SMTH simulation & *(right)* Difference (CTL – SMTH). Black arrows indicate normalised surface wind vectors. Orange boundary encloses area where SSTs are 0.25 - 1°C warmer in CTL simulation. Red boundary encloses area where SSTs are > 1°C warmer in CTL simulation. *(Bottom)* Grey box encloses developed storm.

Figure 3.5.23 shows storm EKE increases slightly overall in both model runs, however, a sharp rise in storm energy is found close to the Agulhas core despite the storm being located further to the southeast.

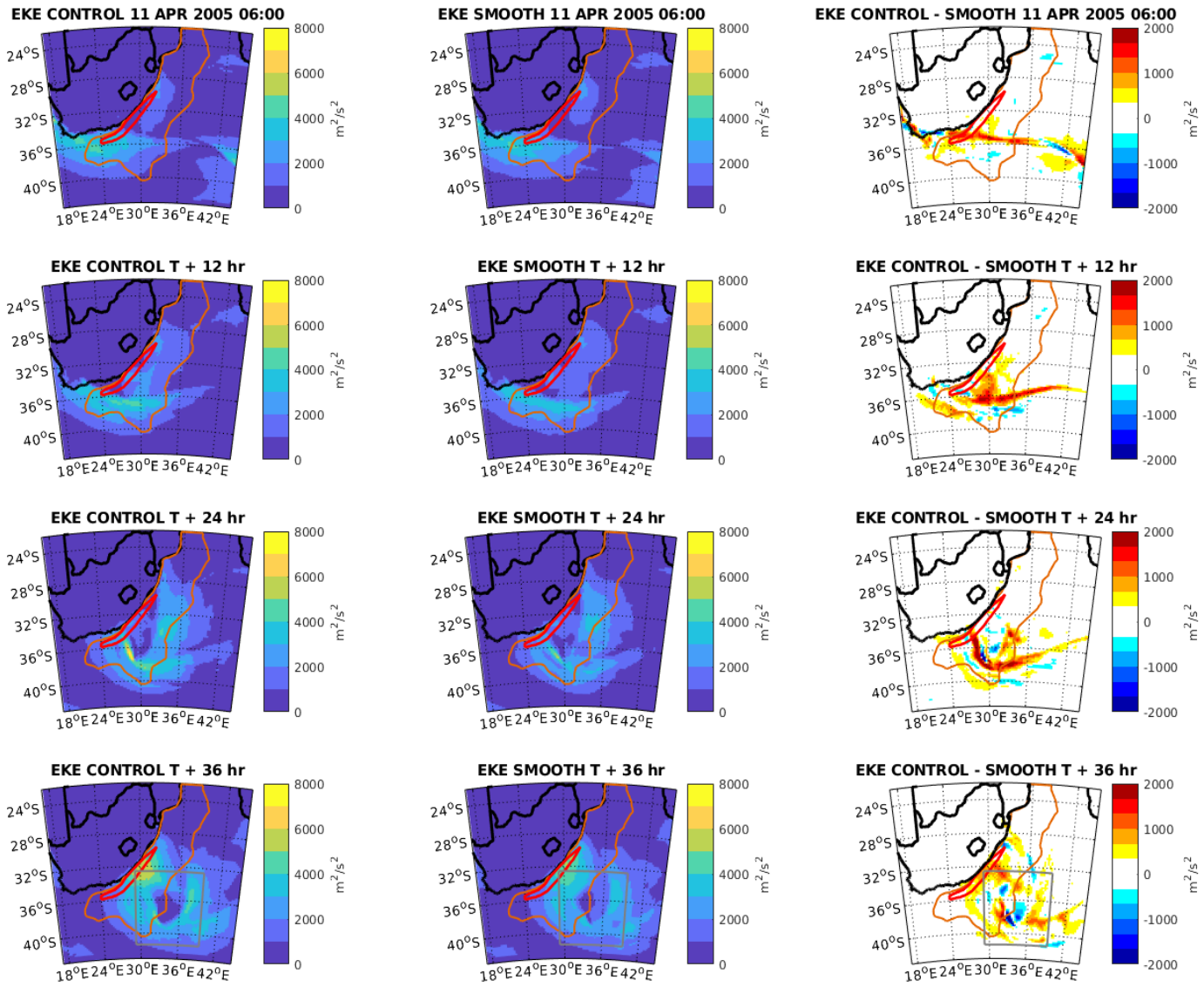

Figure 3.5.23: Storm C4. WRF model eddy kinetic energy up to 850mb level ($m^2.s^{-2}$). From top to bottom: 11 April 06:00; 11 April 18:00; 12 April 06:00 & 12 April 18:00. *(Left)* CTL simulation *(middle)* SMTH simulation & *(right)* Difference (CTL – SMTH). Orange boundary encloses area where SSTs are 0.25 - 1°C warmer in CTL simulation. Red boundary encloses area where SSTs are > 1°C warmer in CTL simulation. *(Bottom)* Grey box encloses developed storm.

Figure 3.5.24 shows sustained high surface turbulent moisture fluxes over the southern region of the Agulhas Current in the vicinity of the storm. However, low fluxes are found at the storm centre. Similar fluxes are modelled in both runs at the storm's location.

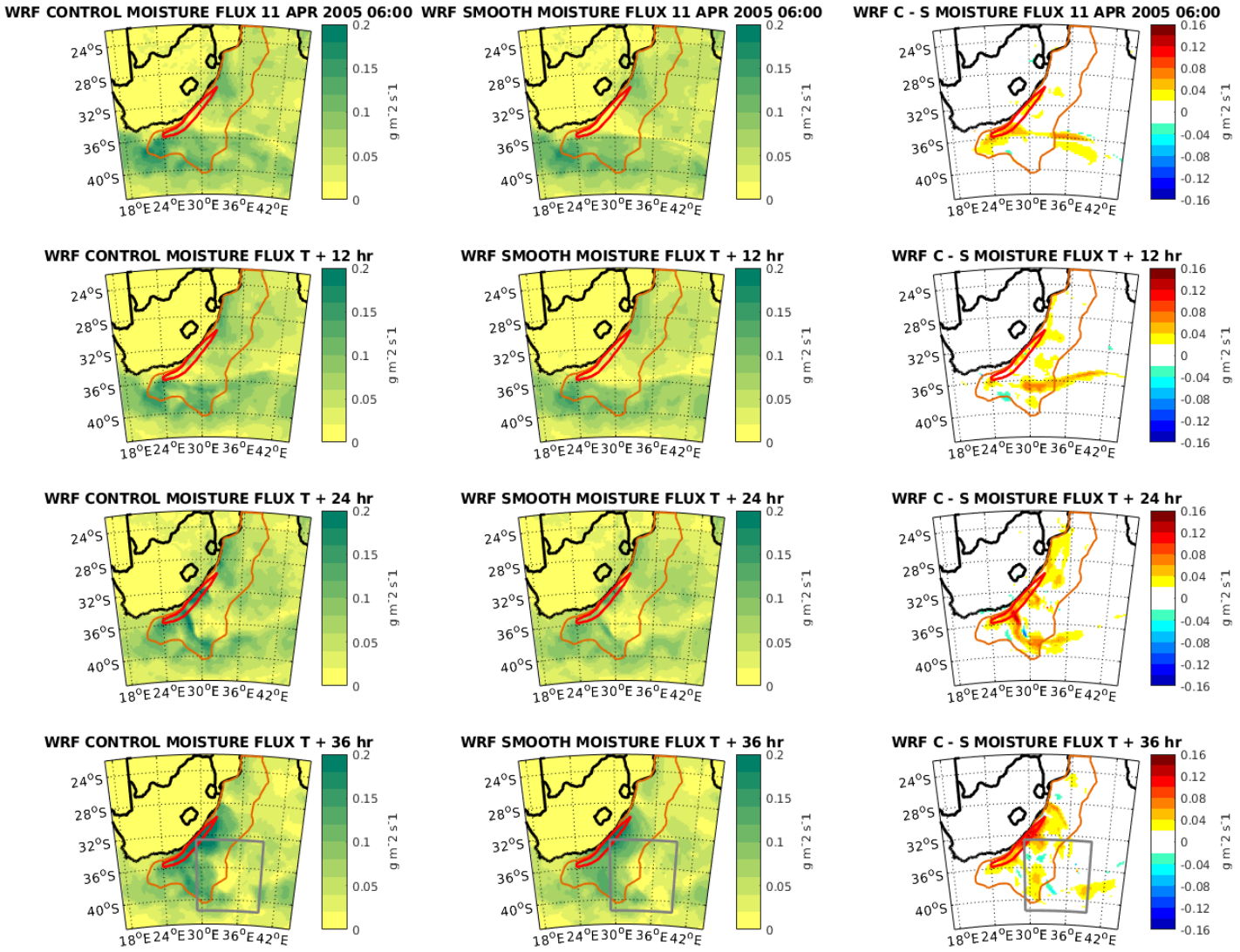

Figure 3.5.24: Storm C4. WRF model surface turbulent moisture flux ($g.m^{-2}.s^{-1}$). From top to bottom: 11 April 06:00; 11 April 18:00; 12 April 06:00 & 12 April 18:00. *(Left)* CTL simulation *(middle)* SMTH simulation & *(right)* Difference (CTL – SMTH). Orange boundary encloses area where SSTs are 0.25 - 1°C warmer in CTL simulation. Red boundary encloses area where SSTs are > 1°C warmer in CTL simulation. *(Bottom)* Grey box encloses developed storm.

Table 3.5.4 indicates that a deeper (- 10.0 ± 2.45 m) developed storm was modelled in the CTL run. Higher rainfall intensity (+ 0.02 ± 1.191 $mm.hr^{-1}$), higher surface wind speeds (+ 0.63 ± 1.021 $m.s^{-1}$), greater storm energy (+ 221 ± 273.8 $m^2.s^{-2}$) and higher surface turbulent moisture fluxes (+ 0.011 ± 0.0621 $g.m^{-2}.s^{-1}$) were all found for the developed storm over the Agulhas Current. The standard deviations are larger than the mean difference for all but one variable.

WRF VARIABLE	AVERAGE DIFFERENCE
850mb geopotential height	**- 10.0 ± 2.45 m**
Surface rain rate	**+ 0.02 ± 1.191 $mm.hr^{-1}$**
Surface wind speed	**+ 0.63 ± 1.021 $m.s^{-1}$**
Eddy kinetic energy (EKE)	**+ 221 ± 273.8 $m^2.s^{-2}$**
Surface turbulent moisture flux	**+ 0.011 ± 0.0621 $g.m^{-2}.s^{-1}$**

Table 3.5.4: Storm C4: 10 -12 April 2005. Average difference (CTL – SMTH) values for five WRF model variables. Values are for developed storm bounded by grey box. Standard deviations for average values are included

Chapter 4: Discussion

Although results of only 10 of the 70 storms passing over the Agulhas Current from 2001 to 2005 are presented in this paper, the general evolution pattern observed in the model output is that storms either intensify or sustain their intensity whilst situated over the Current region. Although there were many (32) cases of small low pressure systems dissipating over the Current, there were 10 cases that showed a clear increase in storm strength. The rest, mostly mid-latitude cyclones, all showed sustained (28) propagations over the Current.

Category A storms

Storm A1 was the only storm amongst all ten to move closer to land as it propagated over the Current, whereas the rest all eventually moved southeast offshore. The geopotential height *(Figure 3.3.2),* surface wind *(Figure 3.3.4)* and EKE *(Figure 3.3.5)* variables all showed discernible patterns of intensification over the Current whereas surface rain *(Figure 3.3.3)* and surface turbulent moisture fluxes *(Figure 3.3.6)* showed no change in storm intensity. However, a large injection of moisture into the atmosphere at the storm's location throughout its evolution over the Current was modelled. Of the variables that were found to intensify, only the geopotential height showed a greater degree of intensification in the CTL run whereas no substantial difference between the CTL and SMTH configurations of the surface wind and EKE variables occurred.

Storm A2 didn't remain near the coastline (as for storm A1) but instead moved southeast offshore as it deepened. This storm also had a lower (1000 hPa) centre surface pressure compared to storm A1 (1012 hPa) after intensifying over the Current. The geopotential height variable shows intensification in both runs however a much deeper system was modelled in the CTL run *(Figure 3.3.8).* In addition, the centre of the storm was found roughly 300km further northeast in the SMTH run and that the centre of the storm in this simulation developed away from the Current region *(east of orange boundary)* as opposed to directly over it in the CTL run. This is the only occurrence amongst these 10 storms where the

geopotential minima in the two runs are located a considerable distance away from each other. Besides the error in the model's accuracy, nothing in the rest of this storm's analysis could explain this discrepancy. Nonetheless, it would be difficult to make a direct comparison between the two runs regarding the effects of the Current considering this discrepancy in the model output. Nonetheless, high rain rates were also found further northeast in the SMTH run. Unexpectedly though, rainfall increased in the SMTH run even though the centre of the storm wasn't located over the Current region *(east of orange boundary)* whereas sustained rain rates occurred in the CTL run over the Current *(Figure 3.3.9).* Slight intensification patterns were observed for the surface wind *(Figure 3.3.10)* and EKE *(Figure 3.3.11)* variables in the CTL run whereas storm intensity remained minimal in the SMTH run. This resulted in the largest difference between the two runs in terms of surface wind and EKE values amongst all three category A storms. Relatively low moisture fluxes were modelled at the storm's location in both runs however slightly higher fluxes were found in the CTL run *(Figure 3.3.12)*. Unlike storm A1, the vorticity of the storm could not be observed, most likely due to the size difference between the two storms.

Storm A3 developed and intensified over the Current within 18 hours. The degree of intensification was greater for this storm relative to the other two category A storms. Although as with both storm A1 & A2, a deeper developed storm was modelled in the CTL run *(Figure 3.3.14).* Increasing rain rates were also modelled in both runs over the Current however again higher maximum rain rates were found in the CTL run *(Figure 3.3.15).* As with storms A1 & A2, intensifying wind speeds were found the CTL run resulting in higher maximum speeds for the developed storm *(Figure 3.3.16).* Like the surface wind, storm EKE increased in both runs over the Current however more so in the CTL run *(Figure 3.3.17).* Surface turbulent moisture fluxes at the storm's centre were sustained in the CTL run as opposed to decreasing fluxes having occurred in the SMTH run. Interestingly though, increasing fluxes were found east of the Agulhas Current boundary in both runs *(Figure 3.3.18).*

Category B storms

Extra-tropical cyclones are important weather features in the mid-latitudes, particularly in the winter when they are at their maximum intensity (Catto et. al 2012). Storm B1 intensified dramatically over the Current as the centre surface pressure decreased from 1004 hPa to 992 hPa over 48 hours *(Figure 3.4.1).* A similar intensification pattern was modelled for the geopotential height variable although no discernible difference in the storm's evolution between the CTL and SMTH runs was found *(Figure 3.4.2).* Change in rainfall along the system's cold front (28°S) was light rainfall over land that then increased once the front was positioned over the northern part of the Current. This rainfall then decreased once the front moved further offshore *(Figure 3.4.3).* Wind speed at the system centre increased sharply from 9 September 2002 18:00 to 10 September 2002 06: 00 in both runs however from then maximum wind speeds were sustained *(Figure 3.4.4).* Unlike the surface wind variable, a more gradual increase in storm energy occurred in both runs although maximum EKE values were found more directly over the Agulhas core. Surface turbulent moisture fluxes at the storm centre remained low in both runs despite fluxes increasing over the Agulhas core and surrounding waters *(Figure 3.4.6).*

Over 24 hours (10 – 11 August 2003), storm B2 intensified considerably from 1008 hPa to 992 hPa *(Figure 3.4.7).* A similar intensification was modelled for the geopotential height variable as the system moved over the Current. Again, minimal difference between the CTL and SMTH runs were found *(Figure 3.4.8).* As with storm B1, the change in rainfall over the Current region is virtually the same in both runs. There was no increase in rainfall along the system's cold front however a slight increase in rainfall at the cyclone's centre was modelled in both configurations *(Figure 3.4.9).* Surface wind speed *(Figure 3.4.10)* in both runs shows a gradual increase in wind speed around the storm centre as opposed to the sharp increase in speed found in storm B1. The same was found for the storm EKE with both configurations showing an increase in storm energy whilst moving over the Current region *(Figure 3.4.11).* Low surface turbulent moisture fluxes were found at 11 August 2003 18:00 & 12 August 2003 00:00 in both runs however a sharp increase in moisture flux at the storm's location over the next 12 hours was then observed. As was the case for storm B1, this storm is characterised by the lack of considerable difference between the CTL and SMTH simulations.

The synoptic strength of storm B3 was relatively lower than the other two category storms as the centre surface pressure was sustained at 1004 hPa over the Current *(Figure 3.4.13).* Similarly, a subtle intensification was modelled in both runs for the geopotential height variable however once more, minimal difference between the two simulations was found *(Figure 3.4.14).* Sustained rain rates occurred along the system's cold front over the Current in both runs however this rain then started to dissipate away from the Current region. Again, virtually no difference between the two simulations was found *(Figure 3.4.15).* Similar evolution patterns were found for the surface wind as increased speeds were found over the Current followed by decreasing speeds away from the Current region *(Figure 3.4.16).* As with the surface wind, an almost identical evolution pattern was modelled for the storm EKE, again showing little difference between the two simulations *(Figure 3.4.17).* Like storm B1, low surface turbulent moisture fluxes were modelled at the storm centre in both runs over the Current despite higher fluxes occurring over the surrounding waters *(Figure 3.4.18).*

Category C storms

Storm C1 was observed to deepen slightly as it moved off land and then over the Current as the centre surface pressure decreased from 1008 hPa to 1004 hPa *(Figure 3.5.1).* Deepening of the storm over the Current was modelled in both runs however the degree of intensification was slightly greater in the CTL configuration *(Figure 3.5.2).* As with the geopotential height variable, a gradual increase in rainfall occurred in both runs however slightly higher maximum rain rates were found for the developed storm in the CTL run *(Figure 3.5.3).* From 17 October 2001 03:00 to 17 October 2001 09:00 no increases in wind speed were found in either run, however over the next 12 hours, speeds intensified in both runs but again more so in the CTL configuration *(Figure 3.5.4).* Similar to the surface rainfall, storm EKE was found to increase gradually in both runs although once more, a more energetic developed storm was modelled in the CTL run *(Figure 3.5.5).* Consistently low surface turbulent moisture fluxes occurred at the storm's location throughout its evolution in both runs and unlike the other variables, little difference between the CTL and SMTH simulations were found *(Figure 3.5.6).*

Two category C storms were identified in January 2005. Both were virtually identical in their synoptic evolution offshore however storm C2 deepened slightly more than storm C3. Moving offshore over the Current, storm C2 deepened slightly from 1008 hPa to 1000 hPa *(Figure 3.5.7).* The geopotential height variable indicated a similar intensification pattern *(Figure 3.5.8)* and like storm C1, and most of the other category C storms, a deeper developed storm was found in the CTL run. Model rainfall increased in both runs over the Current region with higher maximum rain rates found in the CTL run. Rain rates then decreased away from the Current however more so in the CTL run resulting in higher rain rates in the SMTH run for the developed storm *(Figure 3.5.9).* Relative to the geopotential height and surface rain variables, surface winds were modelled to increase only slightly in both runs. Although unlike storm C1, no clear difference between the two configurations were found for surface wind speed *(Figure 3.5.10).* Similarly, storm energy was found to increase only minimally in both runs but with no obvious difference between the CTL and SMTH simulations for the developed storm *(Figure 3.5.11).* Much unlike storm C1, higher surface turbulent moisture fluxes were modelled in both runs at the location of the storm centre although higher fluxes were found at 14 January 2005 15:00 in the CTL run *(Figure 3.5.12).*

Storm C3 was observed to move directly offshore over the Agulhas core however unlike the other nine storms, this storm was found to *weaken* in its synoptic evolution over the Current as the centre surface pressure increased from 1000 hPa to 1004 hPa *(Figure 3.5.13).* The geopotential height variable however illustrated a completely different evolution pattern as the storm deepened gradually in both configurations A substantial difference between the two runs was found with a considerably deeper developed storm being modelled in the CTL run *(Figure 3.5.14)*. Similar rain rates were modelled in both runs as rainfall increased slightly throughout its evolution and unlike the geopotential height variable, higher rain rates were not found in the CTL run *(Figure 3.5.15).* Stronger surface wind speeds were however modelled in the CTL configuration however both runs had light winds intensifying whilst the system was located over the Current region *(Figure 3.5.16).* Storm energy was found to increase slightly in both runs, except for a sharp rise in storm energy reproduced over the Agulhas core in the CTL run at 21 January 2005 12:00 *(Figure 3.5.17).* The highest surface turbulent moisture fluxes modelled over the entire Agulhas region were found at the storm's

location in both runs however virtually no difference in fluxes occurred between the two runs *(Figure 3.5.18).*

A subtle deepening of storm C4 was observed whilst the system tracked offshore over the Current as the surface pressure decreased from 1008 hPa to 1004 hPa *(Figure 3.5.19).* A similar pattern of intensification was modelled for the geopotential height variable in both runs however like the other category C storms, a deeper developed storm was found in the CTL run *(Figure 3.5.20).* Similar to the category A storms, the change in rainfall in both runs was sustained rain rates over the Current region, followed by a decrease in rainfall as the system moved away from the Current region. And as with storm C3, minimal difference between the CTL and SMTH runs was found in terms of rainfall *(Figure 3.5.21)*. A gradual increase in wind speed was modelled in both configurations, and like the surface rainfall, minimal difference between the two runs was found *(Figure 3.5.22)*. A likewise change in storm energy occurred as a slight increase in storm energy was found in both runs. However, similarly to storm C3, a sharp rise in eddy kinetic energy over the Agulhas core, at 12 April 2005 18:00, was observed. As with most category C storms, low turbulent fluxes were modelled at the centre of the storm however relatively higher fluxes were found over the surrounding waters. As with most of the other storms in this study, higher fluxes were found in the CTL run over the Current region. This was mostly due to the relatively higher SSTs present in the CTL run.

Current intensification

Rouault et al. (2002) found the onshore flow of moisture from the Agulhas Current played a crucial role in the evolution of a December 1998 storm that produced severe flooding over the Southern Cape region. In this study though, after scrutinising the evolution of the five atmospheric variables related to storm intensity, there is a strong case supporting the idea that the Agulhas Current intensifies storms that track over despite only 10 out of 70 storms indicating so. For these 10 storms though, the WRF model indicated stronger storm systems by means of either lower 850mb geopotential heights, higher rain rates, stronger surface wind speeds, higher EKE (up to the 850mb level) values and/or higher surface turbulent moisture

fluxes. There were also several cases, most being mid-latitude cyclones, were storm intensity was sustained over the Current.

The most reoccurring pattern with most of these variables in both runs was either an increase or sustained storm intensity over the Current followed by a weakening of storm strength once the system was centred away from the current region *(east of orange boundary).* Interestingly, despite the removal of the sharp SST gradient in the SMTH configuration, intensification was still found in many storm variable evolutions for this configuration. As expected though, there were more cases of intensification in the CTL run. However, in order to measure the degree of intensification of such storm events, statistics of storm variables would need to be recorded before the storm reached the Current and then afterwards once the system had moved over and away. This would be difficult for the category A storms which originate directly over the Current and therefore no prior variable statistics could be measured.

Impact of the Agulhas Current

The effect the sharp SST gradient associated with the Agulhas Current had on the development of these ten storms was quantified by calculating the average of the difference values between the two configurations for each storm once it developed over the Current region. By smoothing out the sharp SST gradients and consequently reducing the latent heat provided to the overlying atmosphere, the impact of the Current could be measured by calculating the difference between the CTL and SMTH simulations. Intensification in the CTL run was found throughout all ten storms however, the SMTH run saw fewer cases of intensified storm strength and instead sustained storm intensity was found.

The Agulhas Current's impact on the 850mb geopotential height variable seems conclusive as all ten storms presented were measured to have a deeper system in the CTL run once the storm had developed over the Current. The impact on rainfall appears slightly less conclusive as only seven developed storms were modelled to have higher rain rates in the CTL run for the developed storm. Nine storms had faster surface wind speeds, eight higher EKE values and nine had higher surface turbulent moisture fluxes at the surface, all in the CTL run. It should be noted however that proper statistical methods were not used to analyse these

storms for several reasons. Small sample size (10), different types of storms (three different categories) and the fact that the 'grey box' used in quantifying the Current's influence is different in each case, made it difficult to implement commonly used statistical methods.

Similarities and differences amongst the category storms were also found. Variable plots for all three of the category B storms indicate that the presence of the Agulhas Current appears to have a minimal influence on the propagation of mid-latitude cyclones (category B storms) over it. This was shown by the lack of difference between the two simulations. This could be due to the size difference between the storm and the width of the Current as most mid-latitude cyclones have a diameter of 1500 km whereas the Agulhas Current is only roughly 100 km wide. The opposite however was found for the category A & C storms where large differences were found between the CTL and SMTH runs for most of the variables. It appears as if the additional latent heat has a greater impact on these smaller low pressure cells compared to the larger mid-latitude cyclones.

WRF rainfall

Many regional atmospheric models continue to struggle to simulate rainfall accurately (Powers et al. 2017) including the WRF model. Model rainfall results in this study show some inconsistency in location of rainfall values. For most storms, where higher rainfall was modelled in the CTL run, this region of higher rainfall was generally located further east compared to the high rainfall region in the SMTH run. An example of this can be observed in storm A3 rainfall plot *(Figure 3.3.15).* There was also a case where most of the rainfall produced by a storm in the CTL run was located at a specific location however the same rainfall region produced in the SMTH run was found considerably further northeast *(Figure 3.3.9).* This figure shows this inconsistency where even the grey box drawn was unable to capture both of the high rainfall regions from both simulations completely.

One of the flaws of this study was the lack of statistical analysis of rainfall whether it be from the TRMM dataset or model output from WRF. Although this study did not primarily use the TRMM data to quantify the rainfall of each system, it is important to provide statistical evidence for the presence of rainfall. In addition, this study fails to define 'rainfall' as rainfall in the TRMM dataset is not the same as rainfall modelled in the WRF output. There are

limitations regarding satellite's ability to sensor rainfall and these limitations should be taken into considerable should this research be continued.

Chapter 5: Conclusion

Results from this study suggest that the impact of the Agulhas Current on storm development is to intensify or sustain storm strength whilst the storm is located over the Current region. Although several cases of flooding along the South African coastline have been recorded, majority of rain-producing weather systems persisting in this region move east or southeast away from the South African landmass. However, there was one storm in the study (*storm A1)* that was modelled to move inland as it intensified over the current and showed considerably more rainfall along the coastline. Nonetheless, the Agulhas Current's influence on these storms and the proximity of its core to the South African coastline should cause enough concern to necessitate further research into this area.

The reader is reminded that the majority of the results presented in this study are model outputs. Although synoptic observations and reanalysis product information were used in the early stages of storm identification, the main outcome of this report is based mostly on simulation output. Although WRF has been described as one of the best regional atmospheric models available, issues with the data output were noticed, mainly with simulated rainfall. Future studies should perhaps use other regional atmospheric model rainfall output in order to better observe potential rainfall patterns associated with these types of weather events.

This study focused more on the variables that can describe storm intensity (geopotential height, wind, rain and EKE) but only one (surface turbulent moisture flux) gave any indication of the moisture input into these storms. It is suggested that more needs to be studied regarding the sensible and latent heat fluxes above the Agulhas Current and how these variables could influence storms. Many studies have recorded moisture increases above the Current (Rouault et al. 1995; Lee-Thorp et. al 1999) however, how this additional moisture impacts the overlying atmosphere, an in particular storm development, is yet to be determined. The Agulhas Current is probably the most important regional oceanic feature impacting the weather and climate of South Africa. Its influence on extreme weather events should be one of the main focuses of academic research as these are the events that really

affect the lives of those living on the South Africa's east coast through flooding, damage to infrastructure and loss of life.

REFERENCE LIST

Beal, L.M. and Bryden, H.L., 1999. The velocity and vorticity structure of the Agulhas Current at 32 S. *Journal of Geophysical Research: Oceans*, *104* (C3), pp.5151-5176.

Catto, J.L., Jakob, C., Berry, G. and Nicholls, N., 2012. Relating global precipitation to atmospheric fronts. *Geophysical Research Letters*, *39*(10).

Chelton, D.B. and Xie, S.P., 2010. Coupled ocean-atmosphere interaction at oceanic mesoscales. *Oceanography*, *23* (4), pp.52-69.

Chen, F. and Dudhia, J., 2001. Coupling an advanced land surface–hydrology model with the Penn State–NCAR MM5 modeling system. Part I: Model implementation and sensitivity. *Monthly Weather Review*, *129* (4), pp.569-585.

Dee, D.P., Uppala, S.M., Simmons, A.J., Berrisford, P., Poli, P., Kobayashi, S., Andrae, U., Balmaseda, M.A., Balsamo, G., Bauer, D.P. and Bechtold, P., 2011. The ERA-Interim reanalysis: Configuration and performance of the data assimilation system. *Quarterly Journal of the royal meteorological society*, *137* (656), pp.553-597.

Dudhia, J., 1989. Numerical study of convection observed during the winter monsoon experiment using a mesoscale two-dimensional model. *Journal of the atmospheric sciences*, *46* (20), pp.3077-3107.

Hong, S.Y. and Lim, J.O.J., 2006. The WRF single-moment 6-class microphysics scheme (WSM6). *J. Korean Meteor. Soc*, *42* (2), pp.129-151.

Hong, S.Y., Noh, Y. and Dudhia, J., 2006. A new vertical diffusion package with an explicit treatment of entrainment processes. *Monthly weather review*, *134* (9), pp.2318-2341.

Huffman, G.J., E.F. Stocker, D.T. Bolvin, E.J. Nelkin, R.F. Adler, 2012, last updated 2019: TRMM Version 7 3B42 and 3B43 Data Sets. NASA/GSFC, Greenbelt, MD. Dataset accessed at 24 September 2019 at https://doi.org/10.5067/TRMM/TMPA/3H/7

Jones, D.A. and Simmonds, I., 1993. A climatology of Southern Hemisphere extratropical cyclones. *Climate Dynamics*, *9* (3), pp.131-145.

Josey, S.A., Kent, E.C. and Taylor, P.K., 1999. New insights into the ocean heat budget closure problem from analysis of the SOC air–sea flux climatology. *Journal of Climate*, *12* (9), pp.2856-2880

Jury, M.R., Valentine, H.R. and Lutjeharms, J.R., 1993. Influence of the Agulhas Current on summer rainfall along the southeast coast of South Africa. *Journal of Applied Meteorology*, *32* (7), pp.1282-1287.

Jury, M., Rouault, M., Weeks, S. and Schormann, M., 1997. Atmospheric boundary-layer fluxes and structure across a land-sea transition zone in south-eastern Africa. *Boundary-Layer Meteorology*, *83* (2), pp.311-330.

Jury, M. and Walker, N., 1988. Marine boundary layer modification across the edge of the Agulhas Current. *Journal of Geophysical Research: Oceans*, *93* (C1), pp.647-654.

Kain, J.S., 2004. The Kain–Fritsch convective parameterization: an update. *Journal of applied meteorology*, *43* (1), pp.170-181.

Kelly, K.A., Small, R.J., Samelson, R.M., Qiu, B., Joyce, T.M., Kwon, Y.O. and Cronin, M.F., 2010. Western boundary currents and frontal air–sea interaction: Gulf Stream and Kuroshio Extension. *Journal of Climate*, *23* (21), pp.5644-5667

Lee-Thorp, A.M., Rouault, M. and Lutjeharms, J.R.E., 1999. Moisture uptake in the boundary layer above the Agulhas Current: A case study. *Journal of Geophysical Research: Oceans*, *104* (C1),pp.1423-1430.

Lutjeharms, J.R.E., 1981. Spatial scales and intensities of circulation in the ocean areas adjacent to South Africa. *Deep Sea Research Part A. Oceanographic Research Papers*, *28* (11), pp.1289-1302.

Lutjeharms, J.R.E., Mey, R.D. and Hunter, I.T., 1986. Cloud lines over the Agulhas Current. *South African Journal of Science*, *82* (11), pp.635-640.

Lutjeharms, J.R.E. and Van Ballegooyen, R.C., 1988. The retroflection of the Agulhas Current. *Journal of Physical Oceanography*, *18* (11), pp.1570-1583.

Minobe, S., Kuwano-Yoshida, A., Komori, N., Xie, S.P. and Small, R.J., 2008. Influence of the Gulf Stream on the troposphere. *Nature*, *452* (7184), p.206.

Nkwinkwa Njouodo, A.S., Koseki, S., Keenlyside, N. and Rouault, M., 2018. Atmospheric signature of the Agulhas Current. Geophysical Research Letters. doi:10.1029/2018GL077042

Mlawer, E.J., Taubman, S.J., Brown, P.D., Iacono, M.J. and Clough, S.A., 1997. Radiative transfer for inhomogeneous atmospheres: RRTM, a validated correlated-k model for the longwave. *Journal of Geophysical Research: Atmospheres*, *102* (D14), pp.16663-16682.

O'Neill, L.W., Chelton, D.B., Esbensen, S.K. and Wentz, F.J., 2005. High-resolution satellite measurements of the atmospheric boundary layer response to SST variations along the Agulhas Return Current. *Journal of Climate*, *18* (14), pp.2706-2723.

Parfitt, R., Czaja, A., Minobe, S. and Kuwano-Yoshida, A., 2016. The atmospheric frontal response to SST perturbations in the Gulf Stream region. *Geophysical Research Letters*, *43* (5), pp.2299-2306.

Parfitt, R. and Czaja, A., 2016. On the contribution of synoptic transients to the mean atmospheric state in the Gulf Stream region. *Quarterly Journal of the Royal Meteorological Society*, *142* (696), pp.1554-1561.

Powers, J.G., Klemp, J.B., Skamarock, W.C., Davis, C.A., Dudhia, J., Gill, D.O., Coen, J.L., Gochis, D.J., Ahmadov, R., Peckham, S.E. and Grell, G.A., 2017. The weather research and forecasting model: Overview, system efforts, and future directions. *Bulletin of the American Meteorological Society*, *98* (8), pp.1717-1737

Preston-Whyte, R.A. and Tyson, P.D., 1988. Atmosphere and weather of southern Africa. Oxford University Press.

Reason, C.J.C., 2001. Evidence for the influence of the Agulhas Current on regional atmospheric circulation patterns. *Journal of Climate*, *14* (12), pp.2769-2778.

Reynolds, R.W., T.M. Smith, C. Liu, D.B. Chelton, K.S. Casey, and M.G. Schlax, 2007: Daily High-Resolution-Blended Analyses for Sea Surface Temperature. J. Climate,20, 5473–5496

Rouault, M., Lee-Thorp, A.M., Ansorge, I. and Lutjeharms, J.R.E., 1995. Agulhas Current air-sea exchange experiment. *South African Journal of Science*, *91*, pp.493-496.

Rouault, M. and Lutjeharms, J.R.E., 2000. Air–sea exchange over an Agulhas eddy at the subtropical convergence. *Global Atmos. Ocean Syst*, *7*, pp.125-150.

Rouault, M., Lee-Thorp, A.M. and Lutjeharms, J.R.E., 2000. The atmospheric boundary layer above the Agulhas Current during along current winds. *Journal of physical oceanography*, *30* (1), pp.40-50.

Rouault, M., White, S.A., Reason, C.J.C., Lutjeharms, J.R.E. and Jobard, I., 2002. Ocean–atmosphere interaction in the Agulhas Current region and a South African extreme weather event. *Weather and Forecasting*, *17* (4), pp.655-669.

Rouault, M., Reason, C.J.C., Lutjeharms, J.R.E. and Beljaars, A.C.M., 2003. Underestimation of latent and sensible heat fluxes above the Agulhas Current in NCEP and ECMWF analyses. *Journal of Climate*, *16* (4), pp.776-782.

Rouault, M.J. and Penven, P., 2011. New perspectives on Natal Pulses from satellite observations. *Journal of Geophysical Research: Oceans*, *116* (C7).

Rouault, M., Roy, S.S. and Balling, R.C., 2013. The diurnal cycle of rainfall in South Africa in the austral summer. *International Journal of Climatology*, *33* (3), pp.770-777.

Rouault, M., Verley, P. and Backeberg, B., 2016. Wind changes above warm Agulhas Current eddies. *Ocean Science*, *12* (2), pp.495-506

Sheldon, L., Czaja, A., Vannière, B., Morcrette, C., Sohet, B., Casado, M. and Smith, D., 2017. A 'warm path' for Gulf Stream–troposphere interactions. *Tellus A: Dynamic Meteorology and Oceanography*, *69* (1), p.1299397.

Simmons, A., 2007. ERA-Interim: New ECMWF reanalysis products from 1989 onwards. *ECMWF newsletter*, *110*, pp.25-36.

Singleton, A.T. and Reason, C.J.C., 2007. A numerical model study of an intense cutoff low pressure system over South Africa. Monthly weather review, 135 (3), pp.1128-1150.

Skamarock, W.C., Klemp, J.B., Dudhia, J., Gill, D.O., Barker, D.M., Wang, W. and Powers, J.G., 2005. *A description of the advanced research WRF version 2* (No. NCAR/TN-468+ STR). National Centre For Atmospheric Research Boulder Co Mesoscale and Microscale Meteorology Div.

Skamarock, W.C., Klemp, J.B., Dudjia, J., Gill, D.O., Barker, D.M., Duda, M.G., Huang, X.Y., Wang, J.G. 2008. A description of the Advanced Research WRF Version 3. NCAR/TN475 STR, NCAR Technical Note, Mesoscale and Microscale Meteorology Division, National Centre for Atmosphere Research, June 2008, 133.

Skamarock, W.C. and Klemp, J.B., 2008. A time-split nonhydrostatic atmospheric model for weather research and forecasting applications. *Journal of Computational Physics*, *227* (7), pp.3465-3485.

Small, R.J., Xie, S.P., O'Neill, L., Seo, H., Song, Q., Cornillon, P., Spall, M. and Minobe, S., 2008. Air–sea interaction over ocean fronts and eddies. Dynamics of Atmospheres and Oceans, 45 (3-4), pp.274-319.

Stramma, L. and Lutjeharms, J.R., 1997. The flow field of the subtropical gyre of the South Indian Ocean. *Journal of Geophysical Research: Oceans*, *102* (C3), pp.5513-5530.

Sutton, R. and Mathieu, P.P., 2002. Response of the atmosphere–ocean mixed-layer system to anomalous ocean heat-flux convergence. *Quarterly Journal of the Royal Meteorological Society: A journal of the atmospheric sciences, applied meteorology and physical oceanography*, *128* (582), pp.1259-1275.

Tyson, P.D. and Preston-Whyte, R. A. 2000. The Weather and Climate of Southern Africa. Oxford University Press Southern Africa, Cape Town, South Africa

Vannière, B., Czaja, A., Dacre, H. and Woollings, T., 2017. A "Cold Path" for the Gulf Stream–Troposphere Connection. *Journal of Climate*, *30* (4), pp.1363-1379.

Xue, H., Bane Jr, J.M. and Goodman, L.M., 1995. Modification of the Gulf Stream through strong air–sea interactions in winter: Observations and numerical simulations. *Journal of physical oceanography*, *25* (4), pp.533-557.

Xu, H., Tokinaga, H. and Xie, S.P., 2010. Atmospheric effects of the Kuroshio large meander during 2004–05. *Journal of Climate*, *23* (17), pp.4704-4715.

Xu, H., Xu, M., Xie, S.P. and Wang, Y., 2011. Deep atmospheric response to the spring Kuroshio over the East China Sea. *Journal of Climate*, *24* (18), pp.4959-4972.